International independent scientific journal

№58 2024

№58 2024
International independent scientific journal

ISSN 3547-2340

Frequency: 12 times a year – every month.
The journal is intended for researches, teachers, students and other members of the scientific community. The journal has formed a competent audience that is constantly growing.

All articles are independently reviewed by leading experts, and then a decision is made on publication of articles or the need to revise them considering comments made by reviewers.

***

Częstotliwość: 12 razy w roku – co miesiąc.
Czasopismo skierowane jest do pracowników instytucji naukowo-badawczych, nauczycieli i studentów, zainteresowanych działaczy naukowych. Czasopismo ma wzrastającą kompetentną publiczność.

Artykuły podlegają niezależnym recenzjom z udziałem czołowych ekspertów, na podstawie których podejmowana jest decyzja o publikacji artykułów lub konieczności ich dopracowania z uwzględnieniem uwag recenzentów.

***

1000 copies
International independent scientific journal
Kazimierza Wielkiego 34, Kraków, Rzeczpospolita Polska, 30-074
email: info@iis-journal.com
site: http://www.iis-journal.com

CONTENT

MATHEMATICAL SCIENCES

Antonov A.
PHYSICAL REALITY OF IMAGINARY NUMBERS AND THEIR PHYSICAL ESSENCE.....3

MEDICAL SCIENCES

Aliyev V.
USING IMPLANTS AS A SUPPORT FOR TEMPORARY DENTURES.....14

Arkhmammadova G., Hasanova V., Piriyev R.
COMPARATIVE CHARACTERISTICS OF CEMENTS FOR FIXING STRUCTURES MADE OF ZIRCONIUM DIOXIDE.....16

Zeynalov H., Aliyev T., Huseynova R.
RELATIONSHIP BETWEEN THE PROGRESSION OF GENERALIZED PERIODONTITIS AND DYSFUNCTION OF THE PERIODONTAL VASCULAR ENDOTHELIUM.....18

Zhanabayeva M., Kaliaskarova K., Imambayeva G.
ANALYZING THE QUALITY OF LIFE OF HEPATITIS C PATIENTS. LITERATURE REVIEW.....21

PHYSICAL SCIENCES

Yurov V., Zhangozin K.
ABOUT THE MECHANISM OF GRAPHITE SPLITTING..29

Yurov V., Zhangozin K.
ON THE QUESTION OF STONE–WELES DEFECTS IN GRAPHENE.....42

VETERINARY SCIENCES

Antipov A., Schmaun S., Tkachenko I., Tkachenko S., Palienko S.
PARASITISES OF SHEEP.....54

MATHEMATICAL SCIENCES

PHYSICAL REALITY OF IMAGINARY NUMBERS AND THEIR PHYSICAL ESSENCE[1]

Antonov A.
PhD, HonDSc, HProf.Sci
Independent researcher, Kiev, Ukraine
https://doi.org/10.5281/zenodo.10491923

Abstract
In the article it is shown that the version of the special theory of relativity (STR), stated in all textbooks of physics, is wrong as the relativistic formulas received in it are wrong, they are incorrectly with use of wrong principle of non-exceeding of speed of light are explained and from them wrong conclusions about physical unreality of imaginary numbers and also about existence in the nature of our only visible universe are made. This generally recognized version of STR is refuted experimentally proved as a result of research of transient processes in linear electric circuits by the general scientific principle of physical reality of imaginary numbers discovered 500 years ago. It is explained that imaginary numbers in astrophysics correspond to the world of invisible parallel universes in other dimensions. Its cognition is the task of future science. However, the neighbouring universes can be seen on the starry sky in portals now. The corrected relativistic formulas are obtained and the corrected version of STR corresponding to them is created.

Keywords: *imaginary numbers, special theory of relativity, invisible universes, hidden Multiverse, invisible Hyperverse.*

1. Introduction

Imaginary numbers were discovered 500 years ago by Scipione Del Ferro, Niccolo Fontana Tartaglia, Gerolamo Cardano, Lodovico Ferrari and Raphael Bombelli [1]. And perhaps even earlier than them such a scientific discovery was made by Paolo Valmes [2], who was burned alive at the stake for this by the verdict of the Spanish inquisitor Thomas de Torquemada. Even Sir Isaac Newton[2] was forced to take into account the opinion of the Inquisition about imaginary numbers, who therefore preferred not to use them in his works.

However, their physical significance remains unknown in science to this day. Indeed, everyone knows what 7 seconds, 12 meters, or 19 grams are, but no one knows what 7*i* seconds, 12*i* meters and 19*i* grams, where $i = \sqrt{-1}$, are. We all know that 7, 12 and 19 are simply numbers having no physical significance outside of their context. However, this knowledge was not enough to understand the STR.

2. The Problem of Understanding Imaginary Numbers

Works of famous mathematicians Abraham de Moivre, Leonhard Euler, Jean le Rond d'Alembert, Caspar Wessel, Pierre-Simon de Laplace, Jean-Robert Argand, Johann Carl Friedrich Gauss, Augustin Louis Cauchy, Karl Theodor Wilhelm Weierstrass, William Rowan Hamilton, Pierre Alphonse Laurent, Georg Friedrich Bernhard Riemann, Oliver Heaviside, Jan Mikusiński and others contributed to creation of a perfect theory of functions of a complex variable. However, the theory neither proves physical reality of imaginary numbers nor explains their physical significance[3].

Imaginary numbers are now widely used in all exact sciences, including radio engineering, electrical engineering, optics, mechanics, acoustics, etc. But in them also the physical reality of imaginary numbers is not proved and their physical meaning is not explained[4].

But in the generally accepted version of the special theory of relativity (STR) [3]-[5], which is rightly considered one of the most outstanding theories created in the 20th century and is therefore currently studied in all physics textbooks, it is even denied, since its creators were unable to explain the relativistic formulas obtained therein.

$$m = \frac{m_0}{\sqrt{1-(v/c)^2}} \quad (1)$$

$$\Delta t = \Delta t_0 \sqrt{1-(v/c)^2} \quad (2)$$

$$l = l_0 \sqrt{1-(v/c)^2} \quad (3)$$

where m_0 is the rest mass of a moving physical body;

[1] This is reprint of the article "Antonov A. A. Proving physical reality and explanation physical nature of imaginary numbers". Norwegian Journal of development of the International Science. 123".

[2] In the atmosphere of the omnipotence of the Inquisition and intolerance of dissent that existed at that time, Newton's friend William Whiston was stripped of his professorship in 1710 for some of his careless statements and expelled from Cambridge University.

[3] Naturally, about physical reality and physical essence of imaginary numbers, as well as real numbers, we can speak only in relation to named numbers, equipped with indications on the used units of measurement of corresponding parameters of physical objects and processes.

[4] More precisely, in radio engineering and electrical engineering it is actually revealed in the process of their practical use, but nothing is written about this in textbooks, so as not to refute physics.

m is the relativistic mass of a moving physical body;

Δt_0 is the rest time of a moving physical body;

Δt is the relativistic time of a moving physical body;

l_0 is the rest length of a moving physical body;

l is the relativistic length of a moving physical body;

v is the velocity of a moving physical body;

c is the speed of light;

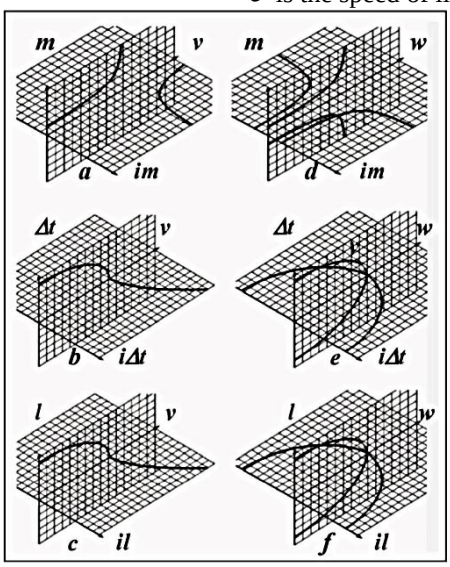

Fig. 1. *Graphs of functions* $m(v)$, $\Delta t(v)$ *and* $l(v)$ *corresponding to the existing and the corrected versions of the STR in the subluminal* $v < c$ *and superluminal* $v > c$ *ranges*

They could not explain physical significance of these formulas for the superluminal velocity range, where, according to these formulas, mass, time, and distance were measured in imaginary numbers (see Fig. 1a, b, c). However, since a theory that could not be explained even by its creators would be useless to anyone, in the STR had to introduce a postulate[5], known as the principle of light speed non-exceedance, the meaning of which is clear from its name.

In relation, for example, to the Lorentz-Einstein formula (1), it was explained as follows. The postulate asserted that since the situation at $v > c$ never occurred anywhere in the early 20th century, it did not need any explanation. Thus, imaginary numbers were unnecessary. i.e. non-existent. Moreover, they were even called imaginary

However, since the existing version of the STR was based solely on a postulate, that is, an unproven assumption, there was no complete certainty that it was correct. Actually, it turned out to be incorrect, since in 2008-2010 (i.e., even before publication of results of the unsuccessful OPERA experiment[6] conducted at the Large Hadron Collider in 2011), it was experimentally proven [6]-[10] that imaginary numbers are physically real.

3. Proof of Physical Reality of Imaginary Numbers

Thus in the 21st century, a Hamlet's question has arisen in physics – is the generally accepted version of the STR correct or not correct? Consequently, does it require correction or not? To address this, it was necessary to answer another question – whether imaginary numbers discovered 500 years ago are physically real or not. And the response to this question required experimental confirmation, even though this issue falls within the realm of mathematics. However, Oliver Heaviside asserted on a similar issue, *"Mathematics is an experimental science."*

Let us further examine electromagnetic transient processes in linear electrical circuits[7] [10]-[15], which allow us to answer this question conclusively using simple experiments[8]. These experiments can be carried out by any engineer in less than a day in any radio engineering laboratory. Such processes in linear electrical LCR circuits are described by linear differential equations (or systems of such equations)

$$a_n \frac{d^n y}{dt^n} + a_{n-1} \frac{d^{n-1} y}{dt^{n-1}} + \ldots + a_0 y = b_m \frac{d^m x}{dt^m} + b_{m-1} \frac{d^{m-1} x}{dt^{m-1}} + \ldots + b_0 x \qquad (4)$$

[5] Since it has never been proven theoretically or confirmed experimentally by anyone.

[6] Which was no longer needed

[7] Unlike the extremely complex and expensive MINOS, ORERA and ICARUS physics experiments, which were no longer needed

[8] In contrast to the extremely expensive physics experiments MINOS, OPEPA and ICARUS, which were no longer needed

where $x(t)$ is the input action (or the input signal);

$y(t)$ is the response (or the output signal);

$a_n, a_{n-1}, ...a_0, b_m, b_{m-1}, ...b_0$ are the constant coefficients;

$n, n-1, ...0, m, m-1, ...0$ is the order of derivatives.

A solution to the equation (5) is known to equal the sum of two components

$$y(t) = y(t)_{forc} + y(t)_{free} \quad (5)$$

where $y(t)_{free}$ is the free component of response, corresponding to the transient process;

$y(t)_{forc}$ is the forced component of response.

They are found in different ways. We are only interested in the free component of response.

Finding a specific type of a free component of response begins with writing and solving the so-called characteristic algebraic equation (usually of the second order) corresponding to the original differential equation (4)

$$a_n p^n + a_{n-1} p^{n-1} + ... + a_0 = 0 \quad (6)$$

where $a_n, a_{n-1}, ...a_0$ are the constant coefficients same as in the equation (4);

$n, n-1, n-2, ...1, 0$ are the degree indices, the magnitude of which is equal to the order of the corresponding derivatives in differential equation (4);

p is the variable, which is often called a complex frequency, when it takes values in the form of complex numbers.

Currently, two algorithms for solving algebraic equations (4) are used in mathematics. According to the first algorithm, solutions are found in the form of real numbers known to everyone. The second algorithm finds solutions to complex numbers that no one understands.

Then, one might assume that no one needs complex numbers because of their incomprehensibility. But, actually, the use of complex numbers greatly simplifies mathematical reasoning and many engineering calculations. Thus, when solving algebraic equations of power n according to the first algorithm, we would receive either n roots or $n-1$ roots or $n-2$ roots ... or even no roots, depending on the value of coefficients. $a_n, a_{n-1}, ...a_0$ And when using the second algorithm to solve the same algebraic equations of power n, we would always receive n roots. Therefore, for some combinations of coefficients $a_n, a_{n-1}, ...a_0$, the algebraic equation (6) might not have any solution within the first algorithm, and would always have n solutions within the second algorithm.

This definitely contradicts common sense and requires an answer to the question – which of the algorithms mentioned above provides the only correct solution in a particular situation? After all, two mutually exclusive statements cannot be simultaneously true. In the formal logics, the Latin aphorism *'Tertium non datur'*, i.e. there is no gap between them that corresponds to this situation.

However, the question is uneasy, otherwise, the answer thereto would have been received long ago. Since humans have a visual thinking, graphical solutions to algebraic equations would be the most helpful in explaining the situation.

For this purpose, we shall convert, for example, the algebraic quadratic equation $a_2 p^2 + a_1 p + a_0 = 0$ as follows

$$\begin{cases} y = a_2 p^2 + a_1 p + a_0 \\ y = 0 \end{cases} \quad (7)$$

Then its solution (see Fig. 2) would correspond to the intersection of the parabola $y = a_2 p^2 + a_1 p + a_0$ and the line $y = 0$, i.e. the abscissa axis p.

As can be seen depending on the parabola position relative to the axis p, which is determined by values of coefficients a_2, a_1, a_0, the parabola $y = a_2 p^2 + a_1 p + a_0$ can cut the axis p either at two or one or none of the points.

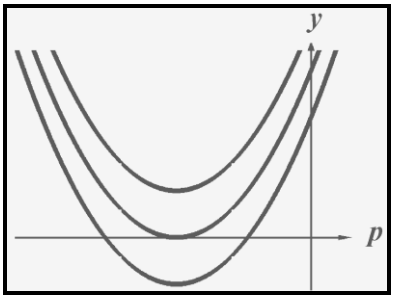

Fig. 2. *Graphical solution to the quadratic equation in the set of real numbers, explaining that the equation can have either or two or one or no solutions*

The result obtained is consistent with the corresponding analytical solution to the quadratic equation. Actually, if a discriminant of the equation $a_2 p^2 + a_1 p + a_0 = 0$ is positive, the equation has two different real roots $p_1 = -\sigma_1$ and $p_2 = -\sigma_2$. If a discriminant is equal to zero, i.e. $a_1^2 - 4a_2 a_0 = 0$, the equation has one real root $p = -\sigma_0$. And if a discriminant is negative, i.e. $a_1^2 - 4a_2 a_0 < 0$, the equation does not have any real root.

The result is so simple and obvious that it would seem to even serve as a proof of existence of the only right solution according to the first algorithm using real numbers. But this is not the case, since a no less clear graphical solution to the quadratic equation can also be obtained within the second algorithm. It looks to be impossible at first sight, since the graph of function , where and are the complex quantities, should be four-dimensional. Humans can neither imagine nor depict four-dimensional graphs. Really, try to imagine and draw, for example, a four-dimensional cube (also referred to as a tesseract or octachoron). But mathematicians can do this.

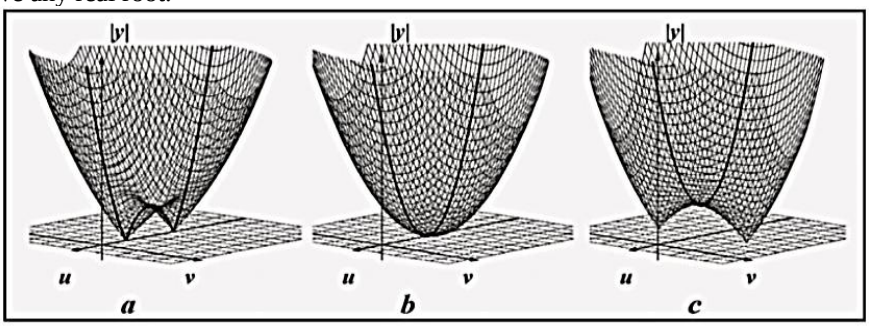

Fig. 3. *Graphical solution to the quadratic equation in the set of complex numbers, explaining that the equation can have two solutions or one double solution*

However, the problem becomes quite solvable if a four-dimensional graph of the function of complex variable $y = f(x)$ is replaced by a three-dimensional graph of function $|y| = |f(x)| = |f(\sigma + i\omega)|$. Thus, within the second solution algorithm, the quadratic equation can be converted into a system of equations, corresponding to the Fig. 3.

$$\begin{cases} |y| = |a_2(\sigma + i\omega)^2 + a_1(\sigma + i\omega) + a_0| \\ |y| = 0 \end{cases} \quad (8)$$

Herewith, Fig. 3a would correspond to the case when a solution to the quadratic equation for $a_1^2 - 4a_2 a_0 > 0$ has two real roots of different values $p_1 = -\sigma_1$ and $p_2 = -\sigma_2$. In this case, the surface $|y| = |f(x)|$ would contact the plane of the complex variable $x = \sigma + i\omega$ at two different points $p_1 = -\sigma_1$ and $p_2 = -\sigma_2$ on the axis of real numbers σ.

Fig. 3b would correspond to the case when a solution to the quadratic equation for $a_1^2 - 4a_2 a_0 = 0$ has one double[9] real root $p_{1,2} = -\sigma_0$. In this case, the surface $|y| = |f(x)|$ would contact the plane of the complex variable $x = \sigma + i\omega$ at one point $p_{1,2} = -\sigma_0$ on the axis of real numbers σ.

Fig. 3c would correspond to the case when a solution to the quadratic equation for $a_1^2 - 4a_2 a_0 < 0$ has two complex conjugate roots $p_{1,2} = -\sigma \pm i\omega$. In this case, the surface $|y| = |f(x)|$ would contact the plane of the complex variable $x = \sigma + i\omega$ at two points that are not on the axis of real numbers σ.

Algebraic equations of the third and higher degrees can be solved graphically in a similar way. Fig. 4 gives an example of a graphical solution to the algebraic cubic equation $a_3 p^3 + a_2 p^2 + a_1 p + a_0 = 0$, which in the set of real numbers is converted as follows

$$\begin{cases} y = a_3 p^3 + a_2 p^2 + a_1 p + a_0 \\ y = 0 \end{cases} \quad (9)$$

[9] For example, for the equation $(x + \sigma_0)^2 = 0$

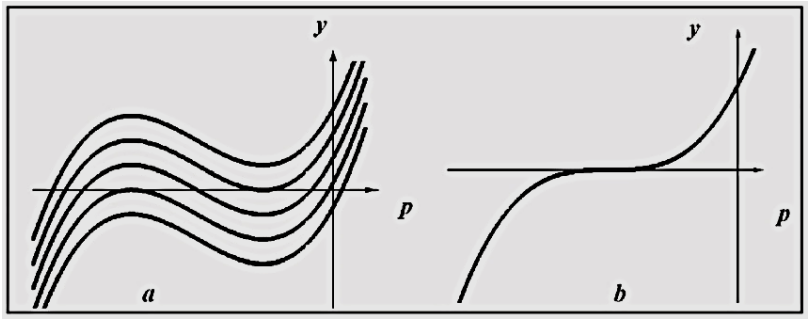

Fig.4. *Graphical solution to the cubic equation in the set of real numbers, explaining that this equation can have either one or two or three solutions*

Apparently, depending on the position of the curve $y = f(x)$ relative to the abscissa axis (i.e. depending on the value of coefficients a_3, a_2, a_1, a_0), the cubic equation can have either one or two or three real solutions within the first algorithm (see Fig. 4a,b). Fig. 5a,b,c,d,e shows graphical solutions to the cubic equation $a_3(\sigma+i\omega)^3+a_2(\sigma+i\omega)^2+a_1(\sigma+i\omega)+a_0=0$ in the set of complex numbers for the same combinations of coefficients a_3, a_2, a_1, a_0, as in Fig. 4, equivalent to the system of equations

$$\begin{cases} |y| = \left|a_3(\sigma+i\omega)^3+a_2(\sigma+i\omega)^2+a_1(\sigma+i\omega)+a_0\right| \\ |y| = 0 \end{cases} \tag{10}$$

As can be seen, a solution to the equation $a_3p^3+a_2p^2+a_1p+a_0=0$ has always three roots when using the second algorithm. But some roots can be double as in Fig. 4a, 5b, 5d, and even triple[10] as in Fig. 4b and 5f. In the latter case, in Fig. 3b, the graph is somewhat different, looking like a tangentoid (or cotangentoid).

And while the points of intersection of the curve $y = a_3p^3+a_2p^2+a_1p+a_0$ and the abscissa axis p correspond to solutions to the equation $a_3p^3+a_2p^2+a_1p+a_0=0$ in Fig. 4, the points of contact of the surface $|y| = \left|a_3(\sigma+i\omega)^3+a_2(\sigma+i\omega)^2+a_1(\sigma+i\omega)+a_0\right|$ of the complex plane $x=\sigma+i\omega$ correspond to solutions to the same equation $a_3p^3+a_2p^2+a_1p+a_0=0$ in Fig. 5. Moreover, both figures show the same particular cases of the situations mentioned. Consequently, equally convincing graphical solutions can also be proposed to the cubic equations (and equations of higher degrees) in the set of both real (Fig. 4) and complex (Fig. 5) numbers.

Thus, purely mathematical reasoning above do not allow us to make an indisputable conclusion about the truth of one and the falsity of another algorithm for solving algebraic equations; or, in other words, to draw a conclusion about physical reality or unreality of their solution expressed in the form of complex numbers.

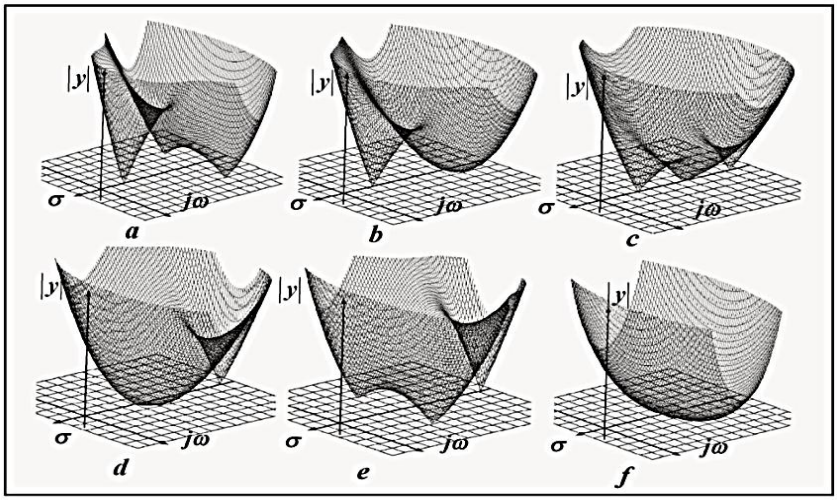

Fig. 5. *Graphical solution to the cubic equation in the set of complex numbers, explaining that in this case it has either three solutions or two solutions, one of which is double, or one triple solution, i.e. having always three solutions*

[10] For example, for the equation $(x+\sigma_0)^3=0$

It is clear that then the choice from the mentioned two algorithms for solving algebraic methods could be made differently - in accordance with the general scientific criterion called "Occam's razor" [11]. According to this criterion, the theory that has the simpler explanation[12] must be accepted as true. And in accordance with this criterion, in all likelihood, sooner or later the second recognized algorithm would be true.

But the trouble is that this choice would require explaining physical significance of complex numbers. Physicists do not have an explanation. And, what is worse, instead of admitting this, they state without evidence that imaginary (and, consequently, complex and hyper-complex) numbers have no physical content, referring to the principle of light speed non-exceedance. Authority of the STR actually hinders the study of this important problem. Such a point of view turned out to be even terminologically[13] fixed in science, since one of components of complex numbers is called imaginary, i.e. supposedly non-existent, numbers.

That is why mathematics still uses both algorithms for solving algebraic equations, even despite the fact that

- solutions there often mutually exclude each other;
- the STR considers one of these solutions (in the form of complex numbers) to be physically non-existent[14].

So what is the answer to the question whether solutions to algebraic equations physically exist in the form of complex numbers? Since, as has just been shown, the use of purely mathematical[15] means cannot answer the question, let us try to figure it out relying solely on common sense.

For this purpose we try to understand what meaning the words 'solution exists' or 'solution does not exist' should have. Where does it exist? On paper? In computer? On a blackboard in a university classroom? We could say so, but "in nature, in the physical world we live in" would apparently be more correct answer.

Therefore, we should talk about existence of a solution as a physical reality. And it would be logical to conclude that answering the question requires physical experiments. What kind of experiments are these? And it turns out that such experiments have been done for a long time by both humans and nature. We meet them everywhere. They are well known to everyone. These are shock oscillations. In any form. In the form of sound of a piano or a tuning fork, in the form of tsunami or 'Indian summer', in the form of children's swing[16] rocking after being pushed by parents, etc.

In this regard, let us recall that only solutions in the form of complex numbers are always used in solving characteristic algebraic equations (6) while studying transient processes (for example, in electrical circuits). The first algorithm for solving algebraic equations using real numbers is never applied in relation to characteristic equations.

Why? The answer to this question is extremely important. Therefore, let us consider in more detail how this question is covered, for example, in the electrical circuit theory. It states that if a characteristic algebraic equation of the second degree has two different real roots $p_1 = -\sigma_1$ and $p_2 = -\sigma_2$, then an aperiodic transient process exists in an electrical circuit and is described by the time function

$$y(t)_{free} = Ae^{-\sigma_1 t} + Be^{-\sigma_2 t} \quad (11)$$

If roots of a characteristic equation of the second degree are real and multiple of $p_{1,2} = -\sigma_0$, then the so-called critical transient process exists in an electrical circuit and is described by the time function

$$y(t)_{free} = (A + Bt)e^{-\sigma_0 t} \quad (12)$$

And, finally, if roots of a characteristic equation of the second power are complex conjugate numbers $p_{1,2} = -\sigma \pm i\omega$, then an oscillatory transient process corresponding to them exists in an electrical circuit, and the quantities p_1 and p_2 are the complex frequencies of free oscillations. This transient process is described by the time function

$$y(t)_{free} = e^{-\sigma t}[A\cos(\omega t) + B\sin(\omega t)] \quad (13)$$

Herewith, integration constants A and B are determined from the initial conditions $y(0)$ and $y'(0)$ in all particular cases.

Solutions to characteristic algebraic equations of higher powers can include aperiodic, critical and oscillatory components. This is covered in detail in textbooks. However, they neither explain nor substantiate why characteristic equations are solved only using the second algorithm, which allows finding their roots in the form of complex numbers And, it turns out, because only in such a case the transient can also exist in the form of shock oscillations (13). The use of the first algorithm would necessitate arguing that shock oscillations should not have existed. However, they do exist.

Thus, the point is that oscillatory transition processes exist in nature. And they can exist only if the

[11] 'Occam's Razor' is a principle formulated in the 14th century by the English monk William of Ockham: "More things should not be used than are necessary".

[12] As, for example, in astronomy the Copernican heliocentric system was recognized as true and the Ptolemaic geocentric system was recognized as false.

[13] Actually, long before the STR was created.

[14] Consequently, mathematicians have not recognized the principle of light speed non-exceedance postulated in the STR as scientifically sound.

[15] But we must not forget that names such as mathematics, physics, radio electronics, etc. were given by people specializing in some narrow research area subject to their limited intellectual capabilities. However, when it comes to Nature, all these names are replaced by the only name of Science.

[16] It is interesting to note that children's swing, on which children are rocking without the help of their parents, refutes another scientific misconception, which, according to information on the Internet, is shared by many authoritative scientists. The misconception suggests that unsupported motion devices, the so-called inertioids, cannot exist, and their existence is therefore denied by modern science, as it contradicts the law of conservation of momentum.

characteristic algebraic equations corresponding to them have solutions in the form of complex numbers. And only for this reason the unsolvable in pure mathematics question about which of the two mutually exclusive algorithms of solving algebraic equations is correct, turned out to be quite solvable with the help of simple physical experiments. And common sense.

It follows from the above that it is necessary to recognise solutions of algebraic equations[17] using complex numbers as the only correct and corresponding to physically real existing processes in the world around us. Therefore, complex frequencies $p_{1,2} = -\sigma \pm i\omega$ of free oscillations are physically real, including their imaginary components. And not only complex frequencies, but also any other imaginary and complex numbers. And as this statement is true for transients not only in the theory of linear electric circuits, but also for transients studied by all other sciences, i.e. it is general scientific, so we will call it the principle of physical reality of imaginary numbers.

And this experimentally provable principle of the physical reality of imaginary numbers naturally refutes the postulated principle of non-exceeding the speed of light, asserting from the unreality,

4. Explanation of Physical Essence of Imaginary Numbers

Hence, for relativistic formulas of STR (1)-(3) the results of calculations on them not only in the form of real, but also in the form of imaginary numbers should be explainable. Nevertheless, these formulas still cannot be explained for one more reason - as can be seen (see Fig. 1a,b,c) their graphs in sub light and hyper light ranges have essentially different form. Moreover, they correspond to physically unstable processes, which cannot exist in Nature. Therefore relativistic formulas (1)-(3) are still incorrect.

And so that the same patterns took place in nature in the subluminal $V < C$ and superluminal $V > C$ speed ranges, and, therefore, formulas describing the corresponding processes could be explained, the graphs $m(v)$, $\Delta t(v)$ and $l(v)$ should be as depicted in Fig. 1d,e,f. For this purpose, the function i^q should be introduced into the corrected relativistic formulas of the STR corresponding to them.

$$m(q) = \frac{m_0 i^q}{\sqrt{1-(v/c-q)^2}} = \frac{m_0 i^q}{\sqrt{1-(w/c)^2}} \quad (14)$$

$$\Delta t(q) = \Delta t_0 i^q \sqrt{1-(v/c-q)^2} = \Delta t_0 i^q \sqrt{1-(w/c)^2} \quad (15)$$

$$l(q) = l_0 i^q \sqrt{1-(v/c-q)^2} = l_0 i^q \sqrt{1-(w/c)^2} \quad (16)$$

where $q(v) = \lfloor v/c \rfloor$ is the "floor" discrete function of the argument v/c;

$w = v - qc$ is the local velocity of each universe.

This is the function convenient for explaining, as for integer values of the argument *0,1,2,3,4,5,…* it takes the required alternating values *+1,+i,-1,-i,+1,+i,…* corresponding to four types of universes alternating in space. Herewith local velocity $w = v - qc$ (Fig. 1d,e,f) of each universe takes finite values only in the range $0 \le w < c$.

But it's not hard to notice that Euler's formula takes the same values +1, +i, -1, -i, +1, +i..., corresponding to the integer values 0, 1, 2, 3, 4, 5,... of the argument q. And the right side of Euler's formula allows determining the values of this function also for non-integer values of the argument q. Therefore, considering this circumstance, we can conclude that the function i^q takes the form

$$i^q = \cos(q\pi/2) + i\sin(q\pi/2) \quad (17)$$

for both integer and non-integer values of the argument q.

The new formula thus obtained has an important advantage - it introduces into the mathematics of complex and hyper complex numbers the mathematical operation of raising imaginary numbers to a non-integer degree, which has been absent in it until now. In astrophysics, it therefore allows us to assert that the integer values of the quantity in formula (17) correspond to mutually invisible parallel universes[18], since they are relative to each other beyond the event horizon, and its non-integer values correspond to portals between such neighbouring universes. And the invisible Multiverse containing these parallel universes has a spiral structure.

In other cases, described by other mathematical formulas containing imaginary numbers, other objects of the invisible world will correspond to them, Determining the specific nature of these objects will require further specialized research. The research will significantly define the content of future science.

5. Conclusion

In the article by simple researches of transients in linear electric circuits, carried out before publication of results of extremely difficult and expensive, but unsuccessful experiment OPERA, the physical reality of imaginary numbers is proved and, consequently, the fundamental principle of non-exceeding the speed of light in the generally recognised version of STR is refuted. And therefore it is asserted that the version of STR stated in all physics textbooks used in the educational process of even the most prestigious universities is incorrect [16]-[72].

The existence of physically real imaginary numbers, discovered 500 years ago, shows that besides our visible world there is also a bigger, but invisible and unknown to us world. And cognition of physical essence of this invisible world will become the main problem of science of the future [73]-[96]. Moreover this problem is now in relativistic physics astrophysics, overcoming the resistance of opponents, is already

[17] And not only characteristic ones.

[18] Since, despite their boundlessness, they do not overlap anywhere, but they do dip slightly into each other in many places, forming portals.

solved. And that's fine. One of the most authoritative philosophers of science of the 20th century Sir Karl Raimund Popper [97] wrote on this occasion that *"...the struggle of opinions in scientific theories is inevitable and is a necessary condition for the development of science"*. I.e., the development of science is possible only as a result of identifying incorrect statements in existing theories and their subsequent refutations [98]-[104].

This article identifies such false statements and ***demonstrates how the incorrect (due to the use of the erroneous postulate of light speed non-exceedance) version of the STR can be corrected.***

Acknowledgments

The author gratefully acknowledges the insights, comments, and assistance of Olga Ilyinichna Antonova

References:

1. Weisstein E.W. 2005. The CRC Concise Enciclopedia of Mathematics. 3-rd ed. CRS Press. Roca Raton. FL.

2. Beckmann P. 1976. A History of π. 3-rd edition. St. Martin's Press. NY.

3. Einstein A. 1920. Relativity: The Special and General Theory. H. Holt and Company. NY.

4. Bohm D. 2006. The Special Theory of Relativity. Routledge, Abingdon on Thames.

5. Penrose R. 2010. The Nature of Space and Time. Princeton University Press. Princeton.

6. Antonov A. A. 2008. Physical Reality of Resonance on Complex Frequencies. European Journal of Scientific Research. 21(4). 627-641.
http://www.eurojournals.com/ejsr.htm

7. Antonov A. A. 2009. Resonance on Real and Complex Frequencies. European Journal of Scientific Research. 28(2). 193-204.
http://www.eurojournals.com/ejsr.htm

8. Antonov A. A. 2010. New Interpretation of Resonance. International Journal of Pure and Applied Sciences and Technology. 1(2). 1-12. http://doi.org/10.17686/sced_rusnauka_ 2010-888

9. Antonov A. A. 2010. Oscillation processes as a tool of physics cognition. American Journal of Scientific and Industrial Research. 1(2). 342-349. doi:10.5251/ajsir.2010.1.2.342.349

10. Antonov A. A. 2010. Solution of algebraic quadratic equations taking into account transitional processes in oscillation systems. General Mathematics Notes. 1(9). 11-16. http://doi.org/10.17686/sced_rusnauka_2010-887

11. Antonov A. A. 2013. Physical Reality of Complex Numbers. International Journal of Management, IT and Engineering. 3(4). 219-230.
http://doi.org/10.17686/sced_rusnauka_2013-898

12. Antonov A.A. 2015. Principle of physical reality of imaginary and complex numbers in modern cosmology: the nature of dark matter and dark energy. Journal of the Russian physico-chemical society. 87(1). 328-355. (In Russian). http://doi.org/10.17686/sced_rusnauka_2015-1119

13. Antonov A. A. 2016. Physical Reality and Nature of Imaginary, Complex and Hypercomplex Numbers. General Mathematics Notes. 35(2). 40-63.
http://www.geman.in/yahoo_site_admin/assets/docs/4_GMN-10932-V35N2.31895146. pdf

14. Antonov A.A. 2017. The physical reality and essence of imaginary numbers. Norwegian Journal of development of the International Science. 6. 50-63. http://www.njd-iscience.com

15. Antonov A. A. 2018. Physical Reality and Essence of Imaginary Numbers in Astrophysics: Dark Matter, Dark Energy, Dark Space. Natural Science. 10(1). 11-30. doi:10.4236/ns.2018.101002.

16. Antonov A.A. 2021. The special theory of relativity stated in physics textbooks is incorrect. 77th International Scientific Conference of the Eurasian Scientific Association "Theoretical and practical issues of modern science". Moscow. ESA. 11-15. (Im Russian)

17. Antonov A. A. 2021). Special theory of relativity presented in physics textbooks is wrong. Norwegian Journal of development of the International Science. 68(1). 3-7. DOI: 10.24412/3453-9875-2021-68-3-7.

18. Antonov A. A. 2021. Version of the special theory of relativity that is studied in all physics textbooks is incorrect. Österreichisches Multiscience Journal. (Insbruck, Austria). 43(1). 17-22.http://osterr-science.com

19. Antonov A. A. 2021. Generally accepted version of the special theory of relativity contained in physics textbooks is incorrect. The scientific heritage. (Budapest, Hungary). 73(2). 39-43.
DOI: 19.24412/9215-0365-2021-73-2-39-43

20. Antonov A. A. 2021. Special theory of relativity, which is studied in physics textbooks, is incorrect. German International Journal of Modern Science. 16, 49-53. DOI: 10.24412/2701-8369-2021-16-49-53

21. Antonov A. A. 2021. Special theory of relativity, which is studied in all physics textbooks, is incorrect. Danish Scientific Journal. 51(1). 31-35.
http://www.danish-journal.com

22. Antonov A. A. 2021. Special theory of relativity taught in all physics textbooks is incorrect. Annali d'Italia. 22(1). 39-44. https://www.anditalia.com/

23. Antonov A. A. 2021. In all physics textbooks an erroneous version of special theory of relativity is given. International independent scientific journal. 31. 34-39. http://www.iis-journal.com

24. Antonov A. A. 2021. Special theory of relativity taught in physics textbooks is wrong. Journal of science. Lyon. 23. 47-52.https://www.joslyon.com/

25. Antonov A. A. 2021. All physics textbooks study incorrect special theory of relativity. Sciences of Europe. (Praha, Czech Republic). 79(1). 30-35.
DOI: 10/24412/3162-2364-2021-79-30-35

26. Antonov A. A. 2021. Experimental proofs of infidelity of the version of the special theory of relativity studied in physics textbooks and the truth of its alternative version. 80th International Scientific Conference of the Eurasian Scientific Association "Development of science and education in the conditions of world instability". Moscow. ESA. 8-17. (In Russian)
https://esa-conference.ru/sborniki/?y=2021

27. Antonov A. A. 2021. The incorrectness of the STR version presented in physics textbooks proven

experimentally. Norwegian Journal of development of the International Science. 74(1). 3-7.

DOI: 10.24412/2453-9875-2021-74-53-62.

28. Antonov A. A. 2021. The fallacy of the STR version studied in physics textbooks proved experimentally. Österreichisches Multiscience Journal (Innsbruck, Austria). 45(1). 17-26. http://osterr-science.com

29. Antonov A. A. 2021. Experimental evidences for the fallacy of the STR version in the physics textbooks. European Journal of Applied Sciences. Services for Science and Education. UK. 9(6). 349-364. DOI:10.14738/aivp.96.11304.

30. Antonov A. A. 2021. If the STR version in physics textbooks were true, we would never have heard the music of the piano and the bell ringing, there would be no television, no cellular telephony, no radar or GPS navigation, we would not even be aware of the existence of resonance and Ohm's law as interpreted by Steinmetz, and our children could not swing on the swings. The scientific heritage (Budapest, Hungary). 78(2). 41-50.

DOI: 10.24412/9215-0365-2021-78-2-41-50

31. Antonov A. A. 2021. Experimental refutations of the STR version contained in physics textbooks and confirmations of the truth of its alternative version. German International Journal of Modern Science. 22. 52-61.

DOI: 10.24412/2701-8369-2021-22-52-61

32. Antonov A. A. 2021. The STR version in physics textbooks must be corrected, because if it were true, there would be no tsunamis or indian summer in nature, we would be never have heard piano music, engineers would be not have been able to create television, cell phones, GPS trackers, and even children would not be able to swing on swings. Danish Scientific Journal. 54(1). 29-38. http://www.danish-journal.com

33. Antonov A. A. 2021. Experimental evidence of the incorrectness of the STR version studied in physics textbooks. Annali d'Italia. 25(1). 32-41.

https://www.anditalia.com/

34. Antonov A. A. 2021. Experimental refutations of the generally accepted version of the SRT studied in physics textbooks. International independent scientific journal. 34(1). 23-32. http://www.iis-journal.com

35. Antonov A. A. 2021. Experimental refutations of the SRT version in the physics textbooks. Journal of science. Lyon. 26(1). 29-37.

https://www.joslyon.com/

36. Antonov A. A. 2021. Experimental evidences for the fallacy of the STR version in phisics textbooks. Sciences of Europe (Praha, Czech Republic). 82(2). 19-28. DOI: 10.24412/3162-2364-2021-82-2-19-28

37. Antonov A. A. 2020. How to discover invisible universes. Norwegian Journal of development of the International Science. 42(1). 36-48. (In Russian)

http://www.njd-iscience.com

38. Antonov A. A. 2020. How to See Invisible Universes. Journal of Modern Physics. 11(05), 593-607. DOI: 10.4236/jmp.2020.115039

39. Antonov A. A. 2020. Can invisible universes be seen? International independent scientific journal. 21(2). 51-60. http://www.iis-journal.com

40. Antonov A. A. 2020. Universes Being Invisible on Earth outside the Portals Are Visible in Portals. Natural Science. 12(8). 569-587.

https://doi.org/10.4236/ns.2020.128044

41. Antonov A. A. 2021. Invisible universes can be seen in anomalous zones. International independent scientific journal. 23(1). 28-44.

http://www.iis-journal.com

42. Antonov A. A. 2020. Invisible universes can be seen in anomalous zones. Danish Scientific Journal. 43(1). 9-24. http://www.danish-journal.com

43. Антонов А. А. 2023. Geophysical exploration of portals will provide new knowledge about space. Proceedings of the III International Scientific Conference. Philadelphia. USA. "The modern vector of the development of science". Philadelphia, USA. 85-101.

DOI https://doi.org/10.5281/zenodo.7709801

44. Antonov A.A. 2023. Why geophysical researches of portals are necessary. Norwegian Journal of development of the International Science. 105. 83-96.

https://doi.org/10.5281/zenodo.7779019

45. Antonov A.A. 2023. Geophysical researches of portals will allow to discover invisible universes and to explore them. European Journal of Applied Sciences. Services for Sciences and education. UK. 11(2). 370-391

46. Antonov A.A. 2023. The necessity of geophysical researches of portals. The scientific heritage. (Budapest, Hungary). 110. 77-90.

47. Antonov A.A. 2023. Geophysical researches of portals will allow to prove the existence of invisible universes and to explore them. German International Journal of Modern Science. 53. 64-78

48. Antonov A.A. 2023. The relevance of geophysical researches of portals. Danish Scientific Journal. 70. 75-89.

49. Antonov A.A. 2023. Geophysical researches of portals will allow to prove the existence of hidden Multiverse and to research it. Annali d'Italia. 42. 71-85.

50. Antonov A.A. 2023. Geophysical researches of portals will allow toprove the existence of hidden Multiverse and to research it. International independent scientific jornal. 49. 23-37.

51. Antonov A.A. 2023. Geophysical researches of portals will allow to discover invisible universes. Journal of science. Lyon. 41. 26-38.

52. Antonov A.A. 2023. Geophysical researches of portals will allow to prove the existence of hidden Multiverse and to research it. Sciences of Europe. 114. 76- 90

53. Antonov A. A. 2021. The version of STO stated in physics textbooks is incorrect, as it denies the existence of radio engineering. 82nd International Scientific Conference of the Eurasian Scientific Association "Scientific results in theory and practice". Moscow. ESA. 11-15.

https://esa-conference.ru/sborniki/?y=2021

54. Antonov A.A. 2022. The version of STR stated in physics textbooks is refuted by the existence of radio engineering. Norwegian Journal of development of the International Science. 78(1). 63-67.

DOI: 10.24412/3453-9875-2022-78-63-66.

55. Antonov A. A. 2022. The version of STR presented in physics textbooks is incorrect, since it follows from it that radio engineering should not exist. European Journal of Applied Sciences. Services for Science and Education. UK. 10(1). 440-445. DOI://doi.org/10.14738/aivp.101.2022

56. Antonov A. A. 2022. The existence of radio engineering refutes the physics textbooks' version of STR. The scientific heritage. (Budapest, Hungary). 83(1). 19-22. DOI: 10.24412/9215-0365-2022-83-1-19-22

57. Antonov A.A. 2022. The fundamental Ohm's law in radio engineering as interpreted by Steinmetz, which proves the physical reality on imaginary capacitive and inductive reactances, refuted the version of the STR presented in physics textbooks even before its creation. German International Journal of Modern Science. 26. 50-53. DOI: 10.24412/2701-8369-2022-26-50-63

58. Antonov A.A. 2022. The version of STR stated in physics textbooks is refuted by the existence of radio engineering. Danish Scientific Journal. 56. 56-59.

http://www.danish-journal.com

59. Antonov A.A. 2022. The version of STR presented in physics textbooks is incorrect because it denies the possibility of the existence of Ohm's law as interpreted by Steinmetz and, consequently, the existence of radio engineering. Annali d'Italia 28(1), 43-47. https://www.anditalia.com/

60. Antonov A.A. 2022. If the physics textbook version of STR were true, then Ohm's law should not exist in nature, and therefore all radio engineering would not exist. International independent scientific journal. 36. 16-19.

http://www.iis-journal.com

61. Antonov A.A. (2022). If the version of STR in physics textbooks were true, then there would be no radar, no television, no radio navigation, no telecommunication and many other things. Journal of science. Lyon. 28. 76-79.

https://www.joslyon.com/

62. Antonov A.A. (2022). The version of STR set out in physics textbooks is incorrect because it states that Ohm's law as interpreted by Steinmetz does not really exist, and therefore radio engineering does not exist either. Sciences of Europe (Praha, Czech Republic). 87(1). 54-57.

DOI: 10.24412/3162-2364-2022-1-54-57

63. Antonov A.A. 2022. Why the physics textbooks teach an incorrect version of the special theory of relativity which denies the existence of radio- and electrical engineering. III international scientific conference "Challenges and problems of modern science." London. Great Britain. 78-86.

DOI: https: //doi/org/10.528/zenodo.7486814

64. Antonov A. A. 2023. Why is the incorrect version of the special theory of relativity being studied in physics textbooks, refuted the existence of radio and electrical engeneering even before its creation? The scientific heritage. (Budapest, Hungary) 105. 83-89. DOI: 10.5281/zenodo.7560145

65. Antonov A.A. 2023. Why is incorrect version of the special theory of relativity that denies the possibility of the existence of radio and electrical engineering being studied in textbooks of physics? Norwegian Journal of development of the International Science. 100. 27-33.

https://doi.org/10.5281/zenodo.7528512

66. Antonov A.A. 2023. Why is an incorrect version of the special theory of relativity that denies the possibility of the existence radio and electrical engineerng being studied in physics textbooks? German International Journal of Modern Science. 48. 23-29. DOI: https://doi.org/10.5281/zenodo.7541137

67. Antonov A.A. 2023. Who needs the incorrect version of special relativity taught in physics textbooks despite all its experimental refutations? Annali d'Italia. 39, 64-70. DOI: 10.5281/zenodo.7568916

68. Antonov A.A. 2023. Why is incorrect version of the special theory of relativity, refuted by the existence of radio and electrical engineering, is still studies in all university physics textbooks? Danish Scientific Journal. 69. 66-72.

https://doi.org/10.5281/zenodo.7692053

69. Antonov A.A. 2023. Why is incorrect version of the special relativity still being studied in physics textbooks, which denies Ohm's law for alternating current used worldwide by millions of radio and electrical engineers? International independent scientific journal. 46. 38-44.

https://doi.org/10.5281/zenodo.7525751.

70. Antonov A.A. 2023. Why is the generally accepted version of STR, which denies the possibility of the existence of radio engineering and electrical engineering, tsunamis and bell ringing, the physical phenomenon of resonance and Ohm's physical law for alternating current, music created by the piano and even swing swings on the playground, nevertheless is still considered correct and studied in physics textbooks? Sciences of Europe (Praha, Czech Republic). 112. 44-50.

71. Antonov A.A. 2023. Why is the incorrect version of the special theory of relativity still being studied in physics textbooks, despite all its experimental refutations. European Journal of Applied Sciences. Services for Science and Education. UK. 11(2). 61-71. DOI: https://doi.org/10.14738/aivp.112.14128

72. Antonov A.A. 2023. Why the incorrect version of the special theory of relativity, which denies the possibility of the existence of radio engineering and electrical engineering, has not yet been refuted. Journal of science. Lyon 40. 19-25. https://doi.org/10.5281/zenodo.7704392

73. Antonov A. A. 2021. Antimatter, Anti-Space, Anti-Time. Journal of Modern Physics, 12(05), 646-660. DOI: 10.4236/jmp.2021.125042.

74. Antonov A. A. 2021. Antimatter, anti-space, anti-time. 75th International Conference of the Eurasian Scientific Association "Strategies of Sustainable Development of World Science". Moscow. ESA. 1-4.

DOI: 10.5281/zenodo.4926585

75. Antonov A. A. 2021. From the alternative version of the SRT it follows that there is not only antimatter, but also anti-space and anti-time. Norwegian

Journal of Development of the International Science. 62(1). 41-51. DOI: 10.24412/3453-9875-2021-62-1-41-51

76. Antonov A. A. 2021. Do antimatter, anti-time and anti-space exist in nature. Annali d'Italia. 20(1). 14-24. https://www.anditalia.com/

77. Antonov A. A. 2021. Antipodes in space. German International Journal of Modern Science. 11(1). 15-25. DOI: 10.24412/2701-8369-2021-11-1-15-25

78. Antonov A. A. 2021. There is not only antimatter, but also anti-space and anti-time. Journal of science. Lyon. 21. 22-30. https://www.joslyon.com/

79. Antonov A. A. 2021. Where are antimatter, anti-space and anti-time? Österreichisches Multiscience Journal. (Insbruck, Austria). 40(1). 34-44.

http://osterr-science.com

80. Antonov A. A. 2021. Do antmatter, anti-time and anti-space exist in nature? Danish Scientific Journal. 48(1). 64-74. http://www.danish-journal.com

81. Antonov A. A. 2021. Antipodes in space. International independent scientific journal. 28. 50-61. http://www.iis-journal.com

82. Antonov A. A. 2021. How alternative version of SRT explains the existence of antimatter, anti-space and anti-time? The scientific heritage (Budapest, Hungary). 67(1). 11-21. DOI: 10.24412/9215-0365-2021-67-1-11-21

83. Antonov A. A. 2011. Realisation of Human Super-Intelligence (Developmental Learning). WSEAS transactions on advances in engineering education. 4(8): 109-119.

http://www.wseas.us/e-library/transactions/education/2011/55-269.pdf

84. Antonov A. A. 2011. Human Super Intelligence. International Journal of Emerging Sciences. 1(2): 164-173.

https://pdfs.semanticscholar.org/c8cb/b9e7202fcc15e89bb62ecf31b4c3af7d8f05.pdf

85. Antonov A. A. 2010. Human-computer superintelligence. American Journal of Scientific and Industrial Research. 1(2): 96-104.

doi:10.5251/ajsir.2010.1.2.96.104

86. Antonov A. A. 2011. From Artificial Intelligence to Human Super Intelligence. International Journal of Computer Information Systems. 2(6): 1-6.

https://www.researchgate.net/publication/267992073_From_Artificial_Intelligence_to_Human_Super-Intelligence

87. Antonov A. A. 2011. Realisation of Human Super-Intelligence (Developmental Learning). WSEAS transactions on advances in engineering education. 4(8): 109-119.

http://www.wseas.us/e-library/transactions/education/2011/55-269.pdf

88. Antonov A. A. 2011. Human Super Intelligence. International Journal of Emerging Sciences. 1(2): 164-173.

https://pdfs.semanticscholar.org/c8cb/b9e7202fcc15e89bb62ecf31b4c3af7d8f05.pdf

89. Antonov A. A. 2010. Human-computer superintelligence. American Journal of Scientific and Industrial Research. 1(2): 96-104.

doi:10.5251/ajsir.2010.1.2.96.104

90. Antonov A. A. 2021. How to turn human civilisation into a supercivilisation. 72 International Scientific Conference of the Eurasian Scientific Association "Modern concepts of scientific research". Moscow. ESA. 3-15. (Im Russian) https://esa-conference.ru/sborniki/?y=2021

91. Antonov A. A. 2021. Human super civilization. Österreichisches Multiscience Journal. (Insbruck, Austria). 38(1). 34-46.http://osterr-science.com

92. Antonov A. A. 2021. Emergence of human super civilization. International independent scientific journal. 25(1). 30-43.http://www.iis-journal.com

93. Antonov A. A. 2021. Formation of human supercivilization. The scientific heritage (Budapest, Hungary). 63(3) 39-51.

94. Antonov A. A. 2021. Human civilization will soon become a super civilization. German International Journal of Modern Science. 6(1). 15-28.

DOI: 10.24412/2701-8369-2021-6-1-15-28

95. Antonov A. A. 2021. How to create a human super civilization. Sciences of Europe. (Praha, Czech Republic). 66(2). 38-50.

DOI: 10.24412/3162-2364-2021-66-2-38-50

96. Antonov A. A. 2021. Creation of human super civilization. Danish Scientific Journal. 45(1). 44-57. http://www.danish-journal.com

97. Popper K. R. 2002. Conjectures and Refutations. The Growth of Scienrific Knowledge. Routledge. London.

98. Antonov A. A. 2023. The Corrected Version of the Special Theory of Relativity. Norwegian Journal of development of the International Science. 118. 40-49. https://doi.org/10.5281/zenodo.10009500

99. Antonov A. A. 2023. The Corrected Version of the Special Theory of Relativity. European Journal of Applied Sciences. Services for Science and Education. UK. 11(5). 68-83.

100. Antonov A. A. 2023. The Corrected Version of the Special Theory of Relativity. The scientific heritage. (Budapest, Hungary). 123. 72-81,

101. Antonov A. A. 2023. Alternative Version of the Special Theory of Relativity. Sciences of Europe. (Praha, Czech Republic). 128. 62-71.

102. Antonov A. A. 2023. Special Theory of Relativity. German International Journal of Modern Science. 67. 64-73. DOI: 10.5281/zenodo.10966458

103. Antonov A. A. 2023. Antonov A. A. (2023). Corrected Version of the Special Theory of Relativity. Danish Scientific Journal. 77. 88-97.

https://doi.org/10.5281/zenodo.10054677

104. Antonov A. A. 2023. Alternative Version of the Special Theory of Relativity. International independent scientific journal. 57. 18-103.

https://doi.org/10.5281/zenodo.10353074

MEDICAL SCIENCES

USING IMPLANTS AS A SUPPORT FOR TEMPORARY DENTURES

Aliyev V.
Doctor of Philosophy in Medicine,
Department of Dentistry Faculty of Medicine, teacher
Nakhchivan State University
Nakhichvan. Azerbaijan
https://doi.org/10.5281/zenodo.10492061

Abstract

The use of intraosseous dental implants is one of the most distinctive features of modern dentistry. The designs of dentures on implants are more physiological compared to traditional prosthetic methods because transfer the chewing load directly to the bone of the alveolar process of the jaw, in addition, they do not require preparation of adjacent teeth.

Management of patients using dental implantation methods requires the use of temporary prostheses at almost all clinical stages, starting from the moment of tooth extraction, the period of osseointegration, and up to the manufacture of permanent prostheses

Keywords: *intraosseous implants, temporary prostheses.*

Temporary dentures are used to clarify the final shape of the future permanent denture structure, correct occlusal relationships, and the vertical size (height) of fixed dentures. On temporary dentures, progressive loading of the bone tissue in the implantation area is carried out, soft tissues are formed, including interdental papillae. [2]

In our work, we did not conduct studies regarding temporary prostheses supported by permanent implants (immediate loading).

In the literature studied, there is a small amount of data on the optimal placement of temporary (transit) implants as supports for temporary structures of fixed dentures, which led to our study.

Removal of temporary implants is carried out, as a rule, after the completion of the process of osseointegration of permanent implants (after 3-6 months) at the second surgical stage. In some cases, at this stage, it is possible to leave temporary implants and transitional dentures after their preliminary correction in the area of installation of the gum formers and remove them in parallel with the installation of abutments and fixation of new temporary dentures on them. However, in most cases, temporary implants interfere with the installation of healing abutments. Thus, due to the loss of supports during the period of gum formation, a period of two weeks without any prostheses begins. This problem has been highlighted by some authors who have said that the ability to maintain fixed temporary prostheses throughout all stages of implant treatment is a very difficult task.[1]

However, in some cases, despite the wishes of the doctor and the patient, temporary rehabilitation can be only partial due to insufficient bone tissue to install the required number of temporary implants. Providing temporary rehabilitation in such cases is crucial, because the presence of a prosthesis in the frontal area not only relieves psycho-emotional stress in the patient, but also ensures relative chewing function. The need for temporary rehabilitation may also exist when replacing one to three teeth, and the methods for solving it with the help of temporary implants depend on the volume of bone tissue after the installation of permanent implants or preserving the bone septum of the socket of an extracted tooth during bone grafting without implantation.[4]

With significant atrophy of the jaw bone tissue and unfavorable anatomical conditions, such cases currently most often cannot be considered as contraindications to implantation. Modern methods and means of reconstructive surgery used in dental implantology make it possible to carry out implantation under almost any clinical conditions. Therefore, the question of the possibility or impossibility of implantation when there is insufficient bone volume is more of a professional problem than a contraindication.[3]

Thus, the use of temporary (transit) implants creates the opportunity to avoid the problem of a long period of lack of aesthetic, phonetic and masticatory function of lost teeth from the moment of removal, bone grafting, osseointegration of permanent implants until the final fixation of a permanent fixed dental prosthesis; neutralize the risk of excessive transmucosal influence by abandoning removable dentures and increase the level of patient comfort, which, according to some foreign authors, determines the quality of life during the treatment period.[5]

In connection with the above, we set the following objectives in our study: 1) to study the possibilities of the combined use of temporary and two-stage dental implantation techniques, using the principles of computer design and computed tomography data to plan the rehabilitation of patients with dentition defects; 2) systematize the indications for the use of temporary fixed dentures supported by temporary dental implants for the period of osseointegration of two-stage intraosseous implants; 3) using mathematical modeling and, of course, elemental analysis, theoretically substantiate the possibility of using temporary fixed dentures sup-

ported by temporary implants; 4) analyze existing options for fixed denture structures for temporary replacement of a dentition defect with a length of 3 teeth and develop an improved design and method for manufacturing a temporary denture supported by temporary dental implants.

In the course of our research, we found that the influence of the vertical (occlusal) force acting on a temporary implant on the field of deformation in the bone is quite limited. At the same time, the action of the load in the bucco-lingual direction, as well as the action of the moment in the mesiodistal direction, causes deformations affecting the areas of bone tissue located directly next to the permanent implants. Minimizing the moment acting on each temporary implant can be achieved by shifting the axes of the temporary implants relative to the central axis of the alveolar process. Such displacements have limitations associated with the anatomical characteristics of the jaw of each patient. We have developed several options that display possible installation schemes for temporary implants with displacement in the bucco-lingual direction, which allows you to create a certain shoulder for forces in the occlusal direction and with their help minimize moments in the mesiodistal direction.

To study the effectiveness of moment perception in the mesiodistal direction, two options for displacement of temporary implants have been proposed - staggered displacement and U-shaped displacement of implants.

Based on the analysis of the results of calculating the stress-strain state of the bridge-temporary implants-bone tissue structure, the optimal scheme for installing temporary implants was determined.

The total height of the structure of a temporary fixed dental prosthesis on an implant should not exceed its length.

The proposed method, with known data on the strength properties of certain standard sizes of implants, makes it easier for orthopedic dentists to make informed decisions about the choice and implementation of a particular prosthesis design in a specific clinical situation. The clinical situation refers to the anatomical features of the patient: first of all, the topography and extent of the defect, the height of the artificial crown in the prosthesis replacing the dentition defect, the condition of the antagonist teeth and masticatory muscles, age, etc.

Temporary dental implants are subject to large complex loads of varying magnitude, duration and direction. The action of the prosthesis is closely related to the transfer of load on the surface of the dental implant and between the components of the implant-temporary prosthesis system.

The results of this study make it possible to increase the effectiveness of orthopedic treatment of patients using dental implants through a scientifically based choice of the design of a temporary fixed denture installed on temporary implants.

The created temporary fixed denture design supported by temporary implants that replace the defect in the dentition located in the projection of installed two-stage dental implants eliminates the load in this area and promotes effective osseointegration of the main dental implants.

References:

1. (Podorvanova S.V., 2003; Adilkhanyan V.A., 2007; Babbush C., 2001; Weinberg L., 2003).

2. (Olesova V.N. i soavt., 2000; Zhdanov E.V. i soavt., 2007; Arutyunov S.D. i soavt., 2012; Zoller J., Neugebauer J., 2008).

3. Shirokov I.Yu. Povyshenie kachestva stomatologicheskogo lecheniya s ispol'zovaniem vremennykh implantatov. // Dental Forum (Sbornik statei XXXIII itogovoi nauchnoi konferentsii molodykh uchenykh MGMSU). -M.,-2011.-№3. -S.141.

4. Agapov B.C. Eksperimental'no-klinicheskoe obosnovanie nemedlennoi dental'noi implantatsii // Sovremennye voprosy stomatologii. 2000. -№3 - S.109-110.

5. Babush Ch.-A. Vremennye implantaty: khirurgicheskie i ortopedicheskie etapy. // Mezhdunarodnyi zhurnal Chikagskogo tsentra sovremennoi stomatologii. 2004. - № 1. S. 31 - 37.

COMPARATIVE CHARACTERISTICS OF CEMENTS FOR FIXING STRUCTURES MADE OF ZIRCONIUM DIOXIDE

Arkhmammadova G.,
Department of Orthopedic Dentistry.Assistent
Hasanova V.,
Department of Orthopedic Dentistry assistant
Piriyev R.
Doctor of Philosophy in Medicine, Assistant
Department of Pediatrik Dentistry
Azerbaijan Medical University
Baku, Azerbaijan

Abstract

The effectiveness of orthopedic treatment of patients using fixed prosthetic structures depends on their high-quality fixation on the supporting teeth. In order to improve the adhesion of the material to the tooth tissues, in recent years, special attention has been paid to adhesive fixation systems that improve the fixation of dentures not only to enamel, but also to dentin. Adhesion of dental materials to dentin is difficult due to its heterogeneity. With the development of adhesive dentistry, all-ceramic restorations have become more widely used. The development and introduction into practice of composite cements has led to a change in the technique of fixing ceramic restorations using adhesive systems. Thus, the problem of choosing a material for fixing all-ceramic prostheses remains relevant. Clinical practice dictates the need for a clear differentiated approach when using modern composite cements, depending on the type of restoration.

Keywords: *zirconium prostheses, adhesion of composite cements, glass ionomer and composite cements.*

In recent years, patients' demands for the aesthetics of dental structures have increased significantly, which was one of the reasons for the widespread use of metal-free prostheses based on zirconium dioxide (zirconia), which has high mechanical and optical properties and low thermal conductivity. Due to the high resistance of the material to fracture and its chemical inertness, the use of these dentures is extremely promising in dental practice. Over time, such designs, apparently, can constitute an alternative to metal-ceramic products.[1/3]

One of the most common complications, according to domestic and foreign authors, is a violation of the fixation of structures made of zirconium dioxide, therefore one of the most important in dental practice is the issue of choosing optimal fixing materials, which will help increase the effectiveness of orthopedic dental treatment.[2.4]

The purpose of the study is a primary analysis of the results of using certain cements for fixation of structures based on zirconium dioxide.

Material and methods.

An experimental study was carried out on the adhesion strength of materials based on phosphate and glass ionomer cement with zirconium dioxide samples under conditions identical to those in the oral cavity. 16 standard templates based on dioxide and 5 standard samples of fixing materials based on phosphate (visphate, viscin) and glass ionomer cements used to fix the templates were used. The samples were incubated in a humid environment simulating oral conditions for three days. The bond strength of the zirconia-based structure and fixing materials was tested in a universal testing machine. The rupture zone of a metal-free structure based on zirconium dioxide and a fixing material was tested using a light-optical microscope.

Results.

Two series of experimental studies of the adhesion strength of twenty standard templates based on zirconium dioxide were carried out using standard samples of fixing materials based on phosphate and glass ionomer cements used for fixing templates. The time for complete hardening of the cements was determined. For zinc-phosphate cement visphate it was 6.13±0.35 minutes; for zinc-phosphate cement viscin it was 6.43±0.41 minutes. For glass ionomer cements fuji-1 and fuji-2, the curing time was 5.83 ± 0.94 min and 6.05 ± 0.82 min, respectively, however, for the final "ripening" of the cements, the samples were kept for 24 hours before testing. The ranges of indicators in general corresponded to the literature data.

When studying the adhesion strength when using zinc phosphate cement for fixation of both samples, it was shown that minimal force is required to break the bonds between the fixing material and zirconium dioxide. To destroy the adhesive strength when using both samples of glass ionomer cements in the "fixing material—zirconium dioxide" system, the required force was less than 1.0 N/mm2.

Conclusion.

An experimental study showed the insufficient strength of the fixing bonds of standard templates based on zirconium dioxide when using fixing materials based on phosphate and glass ionomer cements. Cements used without adhesive systems cause the formation of localized stress concentration points along the surface of the treatment at the moment the load is applied. The use of zinc phosphate or glass ionomer cement samples for fixation of structures based on zirconium dioxide under prolonged exposure to a humid environment leads to the formation of weak adhesion, which is insufficient for practical use. The results of the

study indicate the need to continue studying the strength of the fixing bonds of zirconium dioxide with samples of other fixing materials. It is expected that, based on the research carried out, the choice of materials for fixing metal-free structures based on zirconium dioxide will be scientifically justified.

References:

1. Dadabaeva M. U., Habilov N. L., S. S. Sharipovich, Madrahimova M. KRITERIJ OPTIMIZACIJa FIKSACII CEL"NOKERAMIChESKIH KORONOK JOURNAL OF NEW CENTURY INNOVATIONS

2. Dadabaeva M.U., Normurodova R. Z., Nijazov H. Z., Komilova N. K. Vlijanie s#emnogo protezirovanija u bol'nyh saharnym diabetom 2 tipa. Journal of Biomedicine and Practice 2018 vol. 1, issue 4, pp. 60-67.

3. Sostojanie mikrocirkuljacii v tkanjah parodonta pri protezirovanii iskusstvennymi koronkami iz raznyh konstrukcionnyh materialov. N.L. Habilov., F.H. Irsalieva 39(2.2), 268-274.

4. Pulatov B., Alieva N., Dadabaeva M. Sovremennye metody monitoringa osteointegracii //Medicina i innovacii. – 2021. – T. 1. – №. 1. – S. 45-49.

RELATIONSHIP BETWEEN THE PROGRESSION OF GENERALIZED PERIODONTITIS AND DYSFUNCTION OF THE PERIODONTAL VASCULAR ENDOTHELIUM

Zeynalov H.,
Doctor of Philosophy in Medicine,assistent
Department of Pediatric Dentistry
Aliyev T.,
Doctor of Philosophy in Medicine,assistant
Department of Pediatric Dentistry
Huseynova R.
Department of Therapeutic c Dentistry
Assistent
Azerbaijan Medical University
Baku, Azerbaijan
https://doi.org/10.5281/zenodo.10492244

Abstract
Periodontitis is a common chronic inflammatory disease characterized by the destruction of the tissues that contain the teeth. According to epidemiological studies, moderate periodontitis affects 40–60% of the adult population, while severe disease affects up to 10–15% [3]. The mutual influence between somatic diseases and dental pathology is associated with hemodynamic, metabolic, immunological and neurohumoral disorders in the body [4, 5, 6, 7]. A disease that directly affects the condition of periodontal tissues is diabetes mellitus (DM), which is one of the pressing problems of modern medicine.

Keywords: *generalized periodontitis, diabetes mellitus, endothelial dysfunction.*

This is explained by its significant prevalence, the severity of its course, and the seriousness of complications arising from it. As of 2016, the prevalence of diabetes mellitus in Ukraine averaged 9.1% (men – 8.3%, women – 9.7%) [8]. The prevalence of severe periodontitis is significantly higher in adults with HbA1c levels >9% compared to people without diabetes [11]. There is also a relationship between the degree of hyperglycemia and the severity of periodontitis. One of the early, frequent and prognostically unfavorable manifestations of diabetes is diabetic angiopathy, which develops as a result of long-term relative or absolute deficiency of insulin in the body [6, 14]. The most common idea is that periodontal pathology in patients with diabetes is a local manifestation of microangiopathy specific to diabetes. An important achievement in solving the pathogenesis of generalized periodontitis (GP) against the background of CD was the study of endothelial dysfunction (ED). Endothelial dysfunction is characterized by an imbalance between vasoconstriction and vasodilation factors in blood vessels and plays an important role in pathogenesis. is a 21-amino acid peptide that is a powerful vasoconstrictor produced by endothelial cells. It plays a role in the development of diseases such as hypertension and atherosclerosis. Preliminary studies identified ET-1 in gingival tissues of patients with HP [15]. Increased levels of circulating endothelin-1 (ET-1) have been identified in patients with diabetes, and a positive correlation has been demonstrated between plasma ET-1 levels and microangiopathy in patients with type II diabetes. envelope effect on nitric oxide (NO). Vascular DE may precede insulin resistance, although features of the insulin resistance syndrome include factors that have a negative impact on endothelial function. In addition, ET-1 induces a decrease in insulin sensitivity and may be involved in the development of metabolic syndrome [16]. An important fact is that signs of DE increase with increasing duration of diabetes, which manifests itself in debilitation. reducing the dilating properties of the endothelium. Despite the variety of studies of endothelial functions in recent years, the mechanisms of development of DE in HP against the background of diabetes have not been sufficiently studied [12, 17]. The purpose of the study was to study the correlation between the clinical manifestations of HP, functional changes in its vascular system in patients with diabetes mellitus II and the severity of the disease.

Material and methods

A clinical and laboratory study was carried out on 34 patients with type II diabetes aged 40-65 years and 10 people without somatic pathology with clinically intact periodontium (comparison group). According to the taxonomy of periodontal diseases and M.F. Danilevsky, 16 patients were diagnosed with GP of initial and 1st degree, 11 patients – GP of 2nd degree, 7 people – GP of 3rd degree. Depending on the course of HP, 15 patients with chronic HP were examined, in whom diabetes was in the stage of compensation, and 19 patients with HP in the acute stage, in whom diabetes was in the stage of decompensation. The duration of diabetes averaged 12.5±2.42 years. Decompensation of diabetes was diagnosed in 19 (58.9%) patients, subcompensation in 15 (41.1%) patients. During diagnosis, generally accepted clinical methods were used, taking into account the results of the examination, in particular the presence of dental plaque, determination of the depth of periodontal pockets, the degree of recession, pathological mobility of teeth and traumatic occlusion.

To assess the prevalence and intensity of periodontal inflammatory processes, the PMA index (C. Parma, 1960), the dental plaque registration index

(O'Leary T., Drake R., Naylor J., 1972), as well as the BOP bleeding index (Ainamo, Bay) were used , 1975). graphy and intraoral contact radiography. The object of immunological studies was rotovaridine (RR). Oral fluid was collected in the morning on an empty stomach by spitting into sterile tubes. The resulting substrates were centrifuged at 3000 rpm. within 15 min. For the studies, we used the supernatant liquid, which was stored in a freezer at -70°C. Supernatants were examined after thawing using STAT FAX 303 plus enzyme immunoassay analyzers. The concentration of ET-1 was determined using the Endothelin-1 ELISA sys-tem reagent kit produced by Biomedica (Austria). Patients with decompensated diabetes were treated as inpatients in the endocrinology departments of the 1st and 4th clinical hospitals in Lvov. Disorders of carbohydrate metabolism were determined by the level of fasting glycemia. The diagnosis of diabetes is considered established if the level of fasting glucose in the blood plasma increases by more than 7.0 mmol/l, and in the capillary blood plasma by more than 6.1 mmol/l[12]. Diabetes compensation was considered good when fasting glycemia was up to 9.0 mmol/l, subcompensation – at 9.0–12.0 mmol/l, decompensation – more than 12.0 mmol/l. The stability of long-term compensation of diabetes was assessed by the content of glycosylated hemoglobin (HbA1c). Its value in healthy individuals is 4–6% of total hemoglobin [12]. When HbA1c was 4–6%, compensation was considered good, 6–8.9% – subcompensation, 9% and above – decompensation. Statistical processing of the results was carried out using the Microsoft OfficeExel application package. The probability indicator was assessed using Student's t-test

Research results

The results of a clinical instrumental examination of 34 patients with HP against the background of diabetes revealed significant changes in the indicators of the index assessment of the condition of periodontal tissues, which correlated with the severity, course of HD and greater HD and compensation of stage I. development up to 2.9±0.06 mm, with stage II GP. up to 4.6±0.05 mm, with stage III GP. – 7.2±0.06 mm, most often with serous-purulent exudate. RMA index for HP and st. was 50.3±2.5%, with stage II HP. 56.3±3.1%, with stage III HP. –67.7±2.9%. Dental plaque index (O'Leary et al., 1972) for stage I HP. development up to 34.9±4.2%, with stage II HP. up to 59.8±4.5%, with stage III GP. – 90.3±7.2%. Bleeding index BOP in HP and art. development up to 41.5±3.8%, with stage II HP. up to 62.7±6.1%, with stage III HP. – 88.3±5.5%. X-rays revealed osteoporosis and destruction of interdental membranes, a decrease in their height, and a mixed type of resorption predominated. tissues. An increase in the level of ET-1 in the examined patients indicates increased vasoconstriction, which is caused by increased secretion of endothelial-dependent constrictor factors. times higher than its level compared to the control group (0.42 ± 0.03; $p < 0.001$). Thus, a direct correlation is revealed between the level of ET-1, the severity of HP (Table 1) and the degree of compensation for diabetes (Table 2). Conclusion 1. In case of HP against the background of diabetes, a disturbance of endothelium-dependent vascular relaxation and an increase in endothelial adhesiveness are observed in periodontal vessels. This encourages the development of severe vasoconstriction and a decrease in the intensity of local blood flow, which can cause increased platelet aggregation. The increase in the severity of the process in periodontal tissues during exacerbation of HP in patients with diabetes is accompanied by the development of DE, which is manifested by increased synthesis and release of the powerful vasoconstrictor ET-1 by the mendothelium. ah periodontal. Determining the level of ET-1, a marker of endothelial dysfunction, can serve as a diagnostic test for the course of the pathological process and assess the effectiveness of treatment in patients with HP.2. As a result of the studies, the hygienic condition of the oral cavity in patients with type 2 diabetes corresponds to an unsatisfactory assessment, which contributes to the development of pathogenic microflora of the oral cavity and support of the inflammatory process. Therefore, all patients need effective prevention and treatment

Conclusions.

Determining the level of endothelin-1 in oral fluid can be a diagnostically significant factor for establishing the severity of the pathological process and the effectiveness of treatment in patients with generalized periodontitis against the background of diabetes mellitus.

References:

1. Fox CH New considerations in prevalence of periodontal disease. Curr OpinDent. 1992, 2:5-11

2. Foks CH, Dzhett AM, McGuire SM, Feldman HA, Douglass CW Periodontal diseaseamong New England elders. J Periodontol. 1994, 65: 676-684

3. Kelly M, Steele J, Nuttall N et al. (2000). V: Walker A, Cooper I. (eds.) Otdel'naja dental'naja zdravoohranenie: oral health in United Kingdom, 1998. The Stationery Office, London, p. 123-146

4. Volf GF, Ratejchak ZM, Ratejchak K, Barer GM, editor. Parodontologija. Moskva: MEDpress-inform, 2008; p. 542 [v Russian]

5. Mamedova L.A., Podojnikova MN. Istoricheskie aspekty jetiologii i patogenezazabolevaniya parodonta. Rossijskij stomatologicheskij zhurnal. 2006 (4): 42-4 [v Russian]

6. Cepov LM, Nikolaev AI, Miheeva EA, Novikov VI. Osobennosti patogenezavospalitelnych zabolevaniya parodonta i vrachebnoj taktiki pri saharnom diabete. Parodontologija, 2002, 3 (24): 15–23 [v Russian]

7. Jarovaja SP, Mozhova NV. Rol' sosudistyh min pri pererabotke generalized par-odontyta. V: M. F. Danilevskij, editir. Materialy IX zizda stomatologov Ukrainy: Kiev, 2004,p. 216 [In Russian]

8. World Health Organization. Diabetes globally [Internet]. Diabetes country profiles.ACT: Diabetes Ukraine; 2016 g. [Internet]. Available from: https://www.who.int/diabetes/country-profiles/rus_en.pdf?ua=1

9. Mealey BL, Ocampo GL. (2007) Diabetes mellitus and periodontal disease. Peri-odontol. – 2000 44: 127–153. DOI: 10.1111/j.1600-0757.2006.00193.x

10. Ide R, Hoshuyama T, Uilson D, Takahashi K, Higashi T. (2011) Periodontal disease andincident diabetes:a seven-year study. J Dent Res 90: 41-6. DOI:10.1177/0022034510381902

11. Tsai C, Hayes C, Taylor GW. (2002) Glycemic control of typ II diabetes and severoperiodontal disease v US adult population. Community Dent Oral Epidemiol. 30: 182-192

12. Kravchuk NO, Alekseev II. Dosmyslenie revnija jendotin-1 u hvoryk nacukrovoj diabet 2 tipa ta ego korrekcija pri pomoshhi diabetona MR. Problemy endokrynolo-hichnoy patolohii. – 2004 (4): 3–7 [In Russian]

13. Pankiv VI. Cukrovyj diabet, peridediabet i sercevo-sudinnoe jekologichestvo. Prak-tehnicheskaja anhiolohiia. – 2007, 3 (08): 5–10 [In Russian]

14. Horuzha Riu, Komarevskaja OV. Vyvedenie paradodontal'nogo sostojanija kompleksa tainshykh organiv rotovoj porozzhny u khvorykh na tsukrovyy diabet. Ukrainskie stomatologicheskie animanii. – 2003 (3): 26-8 [In Russian]

15. Khalid W, Vargheese SS, Lakshmanan R, Sankari M, Jayakumar ND. Rol' ofendothelin-1 v periodantal'nyh uslovijah: A structured review. Indian J Dent Res. – 2016, May-Jun; 27 (3): 323-33. DOI:10.4103/0970-9290.186247

16. Kalani M Vazhnost' jendotelina-1 dlja microvascular dysfunction in diabetesVasc Health Risk Manag. – 2008; 4 (5): 1061-8

17. Korkushko O.V., Lishnevskaja V.Ju. Jendotelial'naja disfunkcija. Klinicheskie aspektyproblemy. Krovoobyg ta gemostaz. 2003, 2: 4–15 [In

ANALYZING THE QUALITY OF LIFE OF HEPATITIS C PATIENTS. LITERATURE REVIEW

Zhanabayeva M.,
2nd year master's student in the specialty "Medicine", NJSC "Astana Medical University", Astana, Republic of Kazakhstan
Kaliaskarova K.,
doctor of medical sciences, Professor, National Scientific Oncology Center, Astana, Republic of Kazakhstan
Imambayeva G.
candidate of medical sciences, associate professor of the Department of Internal Medicine with courses in gastroenterology, endocrinology, pulmonology, NJSC "Astana Medical University", Astana, Republic of Kazakhstan
https://doi.org/10.5281/zenodo.10492302

Abstract

A literature review was conducted on the study of quality of life in patients with hepatitis C in global clinical practice based on data published to date. Viral hepatitis C is a serious global health problem that affects millions of people worldwide. In addition to physical symptoms, the disease can significantly affect the overall well-being and quality of life of patients. A number of studies are now available to shed light on various aspects of hepatitis C patients' lives that affect their physical health, psychological well-being and life satisfaction. The key point emphasized by most researchers is the need for a comprehensive approach to the treatment of patients, focusing not only on virus elimination, physical aspects of the disease, but also on adequate emotional support, disease awareness and the possibility of social integration to mitigate the negative impact on people's quality of life. Therefore, assessment of long-term quality of life in patients with hepatitis C at different stages of treatment and after virus elimination remains relevant at present.

Keywords: *quality of life, viral hepatitis C, interferon-free therapy.*

Introduction

According to the World Health Organization (WHO), today one third of the world's population is infected with hepatitis viruses [1].

Hepatitis C, along with HIV infection, tuberculosis, hepatitis B and a number of other infectious diseases, is a global medical and social problem [2].

The number of patients with chronic hepatitis C worldwide is about 58 million. About 1.5 million new cases of infection are reported annually. According to the WHO estimates, in 2019, approximately 290 000 people died from liver cirrhosis and hepatocellular carcinoma as a result of hepatitis C virus infection [1, 3].

The all-round spread of infection and the uneven territorial distribution of morbidity, the latent course of the infectious process and the high frequency of its chronicity, as well as the active involvement of persons of reproductive and working age in the epidemic process determine the high socio-economic significance of hepatitis C [4, 5].

Over the last 5-6 years, serious progress has been made in the treatment of chronic hepatitis C, the main goal of which is to eliminate the virus. Today, according to various estimates, the effectiveness of therapy for chronic viral hepatitis C is 95-97%. However, taking into account the long-term chronic course of viral liver damage, combined with the negative impact of numerous psychological and social aspects, the study of the quality of life in this category of patients in the long term remains relevant at the present stage [6, 7, 8].

Purpose of the study

Analysis of literature data on the influence of modern methods of antiviral therapy for chronic hepatitis C on the quality of life of patients.

Materials and methods

A literature search was conducted in the electronic databases of PubMed, The Cichrane Library, Scopus. Inclusion criteria: reports on randomized and cohort studies, meta-analyses and systematic reviews; articles in the English and Russian languages. Exclusion criteria: materials with no evidence base, newspaper articles.

Results and discussions

Studying the quality of life in various diseases allows us to evaluate ongoing treatment and rehabilitation measures from the patient's perspective. According to WHO experts, quality of life is "an individual ratio of one's position in the life of society in the context of the culture and value systems of this society to the goals of a given individual, his plans, capabilities and the degree of general disorder" [1]. According to other definitions, quality of life is "a subjective indicator of the satisfaction of human needs, the degree of comfort of a person both within himself and within his society" [9].

Outpatient care for patients with hepatitis C affects various aspects of life, which determines the relevance of studying the quality of life in this category of patients [10]. To assess the impact of CHC (chronic hepatitis C) on QL (quality of life) and related socially significant problems, general tools and methods specific to this disease are used: the short form health survey 36 (SF-36); the European quality of life - 5 dimensions (EQ-5D-5L); the liver disease life quality assessment tool (LDQOL), etc. [11]. New approaches to measure fatigue as one of the main symptoms of manifestation of viral hepatitis C were described in their study by Gerber L.H. and his colleagues (2019). This group studying

chronic liver disease concluded that a number of questionnaires could be used to assess quality of life, such as: Chronic Liver Disease Questionnaire (CLDQ), SF-36, Fatigue Assessment Scale (FAS) [12].

According to numerous studies, it has been shown that the quality of life of patients with chronic viral hepatitis is significantly reduced in terms of physical and psychological components of health [13-16]. The same conclusion was reached by the authors of the study of quality of life of patients with chronic hepatitis using the EQ-5D-5L questionnaire. In the course of data collection and processing involving 100 patients on the basis of 2 polyclinics in Moscow and Tula with a confirmed diagnosis of CHC, Maksimova L.V. and Vorobyeva P.A. (2013) concluded that the majority of respondents (79%) have health disorders, with moderate pain or discomfort, mild anxiety or depression being the most common [17].

Honrubia López R. and colleagues (2020), evaluating the QL in 86 asymptomatic CHC patients and the control group, found no statistically significant differences in physical and psychological state as measured by the EQ-5D-5L (Table 1). It is worth noting that there was a positive dynamics in all the questionnaire indicators at the stages of treatment in the group of studied patients with CHC [18].

Using a similar questionnaire EQ-5D-5L (Table 1) and VAS (visual analogue scale), Spanish scientists Silvia Goñi-Esarte and his colleagues (2019) assessed the quality of life of 199 patients with CHC at weeks 12 and 48 after achieving sustained virological response (SVR) [19]. Analyzing the results, the researchers noted a gradual improvement in the quality of life in patients receiving interferon-free therapy. Thus, there was an improvement in 4 of 5 indicators of quality of life (mobility, daily activities, pain/discomfort, anxiety/depression) at week 48, in contrast to small changes in 3 indicators after week 12, which indicates the need for longer follow-up of patients with CHC. Improvements were more often observed in patients under 48 years of age, with fibrosis levels F2-F4, supporting the view that patients with F0-F1 have better QL data at baseline and require longer follow-up, as shown in several other studies [20, 21].

At the same time, the results of the study conducted by Canadian scientists (2023) show improvement in all EQ-5D-5L indicators (Table 1) between baseline, during the treatment phase (6 weeks from the start of therapy) and 12, 48 weeks after the completion of the course of direct-acting antiviral drugs in patients without cirrhosis (n=161). In the cohort of patients with cirrhosis (n=48), there were no statistically significant changes between baseline (pre-treatment) and 1 year after the antiviral therapy [22].

Table 1.

Descriptive results of the EQ-5D-5L questionnaire at different therapy stages

QL questionnaire	Authors/year	Number of patients / average age	Indicator	Before treatment	After treatment
EQ-5D-5L (Questionnaire of life quality assessment of the European life quality group)	GoñiEsarte S., Juanbeltz R., Martínez-Baz I., Castilla J., San Miguel R., Herrero J.I., Zozaya J.M., 2019	199 (52.3 (9))	mobility	35% (p = 0.002)	21%
			daily activities	26% (p<0.001)	11%
			pain/discomfort	60% (p < 0.001)	35%
			daily activities	4%	5%
			anxiety/depression	57% (p < 0.001)	35%
			VAS	70%	90%
	Honrubia López R., Madejón Seiz A., Romero Portales M., García Sánchez A., Castillo Grau P., Erdozain Sosa J.C., Olveira Martín A., Robles A., García-Samaniego Rey J., 2020	86 (57.24 (11.52))	mobility	77.4% (p = 0.045)	86.1%
			daily activities	73.8% (p=0.61)	83.3%
			pain/discomfort	56.0% (p =0.19)	80.6%
			daily activities	73.8% (p= 0.66)	83.3%
			anxiety/depression	58.3% (p=0.35)	77.1%
			VAS	72.4%	82,7%
	Wong W.W.L., Wong J., Bremner K.E., Saeed Y., Mason K., Phoon A., Martel-Laferrière V., Bruneau J., Feld J.J., Feng Z., Baguley E., Lee S.S., Powis J., Krahn M.D., 2023	209 (53.4 ± 11.6)	Cohort without cirrhosis (n=161)	0.79 ±0.17	0.84 ±0.15
			Cohort with cirrhosis (n=48)	0.69 ±0.28	0.71 ±0.23

One of the first studies to assess quality of life in the long term (more than 6 months after treatment) is "Direct antiviral agents for chronic hepatitis C virus infection improve health-related quality of life significantly in the long term" (2021). In their work, Mahmoud Atamla, Johad Khoury [24], studied the quality of life of hepatitis C patients using "The Liver Disease Symptom Index 2.0" (LDSI) life quality index questionnaire [25] in the period from January 2015 to August 2018 with more than 100 patients. The authors concluded that 7 of 9 parameters assessed, including itching, right upper abdominal pain, sleepiness during the day, anxiety about marital status, decreased appetite, depression, and anxiety about complications of liver disease showed significant improvement in the long term. The 2 assessed indicators such as joint pain and jaundice remained unchanged (Table 2).

Using a similar questionnaire, Egyptian scientists Youssef N.F., El Kassas M., Farag A., Shepherd A. (2017), assessed the quality of life in patients with CHC, having previously divided them into 2 identical groups with different therapy regimens (1 - sofosbuvir 400 mg + ribavirin 1000 mg /1200 mg, 2 - with the addition of peg-IFN for 24 weeks). There was a decrease in the QL indicators at the treatment stage in the group receiving triple therapy, which was probably due to the effect of the drug (peg-IFN), in contrast to the group with a dual treatment regimen, where positive dynamics was observed (Table 2). However, after the therapy completion, all indicators returned to the baseline level and no significant differences between the two groups were found [26].

Table 2.

LDSI 2.0 questionnaire results

QL questionnaire	Authors/year	Number of patients / average age	Before treatment	After treatment
LDSI 2.0 (The Liver Disease Symptom Index 2.0)	Mahmoud Atamla, Johad Khoury, Ihab Dabbah, Rimma Kramsky, Afif Yaacob, Ella Veitsmanand Tarek Saadi, 2021	100 (58.1±13.3)	1.22±0.95	0.29±0.47
	Youssef N.F., El Kassas M., Farag A., Shepherd A., 2017	62 (54.06 ± 10.41)	Dual therapy n=31(sofosbuvir 400 mg + ribavirin 1000 mg /1200 mg) 32.54 ± 21.23	26.60±17.01
			Triple therapy n=31 (+peg-IFN) 30.74 ± 17.67	37.53 ± 20.47

Kaminskaya S.N. (2014) in her study came to the conclusion that despite the fact that CHC is characterized by a low-symptom but progressive course, manifestations from the psycho-emotional sphere often become leading in the clinical picture. In her work, the author demonstrated various methods of psychological testing, depression assessment scales, as well as quality of life. Changes in the psycho-emotional sphere and a decrease in life quality (Table 3) were more pronounced in patients infected with 1B virus genotype. However, the use of modern combined antiviral therapy as part of the general complex treatment of CHC patients significantly reduced the identified psychopathological manifestations and improved the quality of life of this category of individuals [23].

A study aimed at assessing the long-term impact (1 year after the sustained virological response) of direct-acting antiviral drugs in the treatment of HCV on the quality of life of patients was conducted by Japanese scientists Akio Miyasaka, Yuichi Yoshida, Akiko Suzuki, Yasuhiro Takikawa (2021). The instrument for studying QL in patients after HCV treatment was the short form eight-item questionnaire (SF-8). As a result of a survey of 109 patients with CHC, none of the SF-8 indicators differed significantly between baseline and 1 year after SVR24 (Table 3). Regarding age, sex, liver status and treatment regimen, only age influenced SF-8 scores 1 year after SVR24. In multivariable analysis, only age ≥ 65 years was significantly associated with physical component effects 1 year after SVR24. However, no significant factors were identified for assessing the mental component [27].

Similar studies using a different questionnaire (Short-Form-36) were conducted by Silvia Nardelli, Oliviero Riggio, Davide Rosati, Stefania Gioia (2019) and concluded that symptoms of depression and anxiety had a negative impact on the quality of life in patients with CHCV (Table 3). Treatment with direct-acting antiviral drugs to eradicate hepatitis C virus significantly improved neuropsychological symptoms [28].

Table 3.

Scores of patients with CHC according to the SF-36, SF-8 questionnaires. Baseline QL data and those after achieving SVR

QL questionnaire	Authors/year	Number of patients / average age	Physical component		Psychological component	
			Before	After	Before	After
SF-36 (Medical Outcomes Study Short Form-36)	Kaminskaya S.N., 2014	62 (19-59 years)	69.2 ± 2.8	83.7 ± 4.7	50.6 ± 1.2	56.4 ± 1.4
	Wong W.W.L., Wong J., Bremner K.E., Saeed Y., Mason K., Phoon A., Martel-Laferrière V., Bruneau J., Feld J.J., Feng Z., Baguley E., Lee S.S., Powis J., Krahn M.D., 2023	209 (53.4 ± 11.6 years)	45.92 ± 10.54	48.35 ± 10.32	46.12 ± 12.82	49.66 ± 11.58
	Fagundes R.N., Ferreira L.E.V.V.C., Pace F.H.L., 2020	113 (58.69 ± 9.88)	47.77 (p<0.001)	57.10	48.27 (p = 0.04)	50.41
	Silvia Nardelli, Oliviero Riggio, Davide Rosati, Stefania Gioia, Alessio Farcomeni, Lorenzo Ridola, 2019	39 (59.8 ± 14.2)	62.8 ± 22.7	71.6 ± 21.2	59.8 ± 21.9	71.8 ± 19.1
	Ng X., Nwankwo C., Arduino J.M., Corman S., Lasch K.E., Lustrino J.M., Patel S., Platt H.L., Qiu J., Sperl J., 2018	255 (48)	53.34 ± 7.39		43.01 ± 8.61	
	Siqueira F.M., Ferreira V.L., Borba H.H.L., Pontarolo R., 2018	56 (57.4 ± 11.4)	56 (±66.4)	71.7 (±28.7)	59.9 (±24.5)	67.1 (±22.1)
	Ohlendorf V., Schäfer A., Christensen S., Heyne R., Naumann U., Link R., Herold C., Schiffelholz W., Günther R., Cornberg M., Serfert Y., Maasoumy B., Wedemeyer H., Kraus M.R., 2021	1180 (53.4)	48 (p<0.001)	50	40 (p<0.001)	45
	Kracht PAM, Lieveld F.I., Amelung L.M., 2018	68 (57)	43.2 ± 11.9	44.7 ± 10.9	49.2 ± 11.9	49.9 ± 12.6
SF-8	Akio Miyasaka, Yuichi Yoshida, Akiko Suzuki, Yasuhiro Takikawa, 2021	109 (67)	47.31 ± 7.94	46.96 ± 8.31	49.43 ± 6.88	49.72 ± 6.29

Several studies have examined QL in patients treated with direct-acting antiviral drugs and interferon-based regimens [29-31]. In particular, a study conducted by Ng X. et al. (2018) [32] demonstrated that interferon-free treatment regimens (elbasvir/grazoprevir) for CHC resulted in a significant improvement in QL indicators (Table 3) according to the questionnaire (SF-36), compared with the sofosbuvir/peg-IFN/ribavirin regimen.

A Brazilian study by Antoher (2018) assessed changes in QL using the SF-36 and CLDQ in a cohort of 56 patients with CHC treated exclusively with direct-acting antiviral drugs and found significant improvement in both tests after viral eradication [33].

At the same time, scientists Fagundes R.N., Ferreira L.E.V.V.C., Pace F.H.L. (2020) conducted a study to assess quality of life in 113 patients with CHC at different stages of therapy (Table 3). Results obtained 12 weeks after treatment were significantly better compared to baseline, weeks 6 and 12 of treatment. Among the 6 CLDQ domains assessed, 5 showed statistically significant increases: abdominal symptoms ($p = 0.02$), fatigue ($p < 0.001$), systemic symptoms ($p < 0.001$), activity ($p < 0.001$), and anxiety ($p < 0.001$) (Table 4). The emotional function did not reveal a significant difference ($p>0.05$) [34].

Table 4

CLDQ questionnaire scores depending on therapy regimen and fibrosis stage

QL questionnaire	Authors/year	Number of patients / average age	Indicator	Before treatment		After treatment	
CLDQ (Chronic Liver Disease Questionnaire)	Siqueira F.M., Ferreira V.L., Borba H.H.L., Pontarolo R., 2018	56	abdominal pain	4.04 (± 1.78)		4.14 (± 1.74)	
			activity	4.26 (± 1.7)		4.32 (± 1.65)	
			fatigue	3.35 (± 1.65)		3.75 (± 1.64)	
			systemic symptoms	4.05 (± 1.33)		4.42 (± 1.14)	
			emotionality	3.55 (± 1.62)		4.01 (± 1.44)	
			anxiety	3.58 (± 1.65)		4.85 (±1.31)	
			Total	3.81 (±1.31)		4.25 (± 1.13)	
	Fagundes R.N., Ferreira L.E.V.V.C., Pace F.H.L., 2020	113 (58.69 ±9.88)	abdominal pain	6.17		6.48	
			activity	6.24		6.84	
			fatigue	5.86		6.81	
			systemic symptoms	5.88		6.55	
			emotionality	5.52		5.88	
			anxiety	6.39		6.83	
			Total	5.99 (p<0.001)		6.63 (p<0.001)	
	Younossi Z.M., Racila A., Muir A., Bourliere M., Mangia A., Esteban R., Zeuzem S., Colombo M., Manns M., Papatheodoridis G.V., Buti M., Chokkalingam A., Gaggar A., Nader F., Younossi I., Henry L., Stepanova M., 2022	854	Cirrhosis	Compensated (n = 730)	Decompensation (n = 124)	Compensated (n = 730)	Decompensation (n = 124)
			activity	4.95 ± 1.45	4.22 ± 1.34	5.43 ± 1.33	4.74 ± 1.40
			systemic symptoms	4.63 ± 1.33	4.06 ± 1.29	5.03 ± 1.33	4.42 ± 1.48
			emotionality	5.18 ± 1.29	5.00 ± 1.31	5.76 ± 1.16	5.34 ± 1.45
			anxiety	4.99 ± 1.38	4.51 ± 1.50	6.08 ± 1.11	5.68 ± 1.44
			Total	4.94 ± 1.21	4.45 ± 1.19	5.58 ± 1.11	5.05 ± 1.32
	Vyas B.H., Darji N.H., Rana D.A., Vyas K.Y., Malhotra S.D., 2021 [41]	31 (49.83 ± 13.81)	Regimen 1: sofosbuvir + daclatasvir	64.1 ± 25.00		65.86 ± 24.1	
			sofosbuvir + velpatasvir	64,1 ± 25.00		77.5 ± 20.5	
			sofosbuvir + ledipasvir	64.1 ± 25.00		68 ± 0	
			ribavirin + sofosbuvir + daclatasvir	64.1 ± 25.00		49.34 ± 29.9	
			ribavirin + sofosbuvir + velpatasvir	64.1 ± 25.00		86 ± 0	

A study of quality of life in 854 patients with liver cirrhosis as a result of CHC (730 - compensated, 124 - decompensated), conducted by Zobair M. Younoss and his colleagues (2021) for 3.5 years, shows improvement in all indicators according to CLDQ and SF- 36 scores (Table 3, 4), with the exception of the psychological component in decompensated patients after the antiviral therapy. The gains in QL indicators were largely maintained at later time points in patients with compensated cirrhosis; however, starting at week 120, a decreasing trend was observed in the decompensated group. In addition, QL scores remained consistently lower in patients with decompensated cirrhosis compared to the compensated patients group [35].

Jean-Michel Pawlotsky, Christian B. Ramers (2020) used the same tool to assess the quality of life in patients with hepatitis C in their study, where they studied the effect of treatment on the improvement of patients' mental state before treatment and on average six months after. The results of the study prove that after successful treatment with direct-acting antiviral drugs, emotional well-being improved by 14%, while physical well-being did not change [36].

The results of the study conducted in a real cohort of patients (more than 1000) suffering not only from CHC infection (HIV co-infection, hepatocellular carcinoma (HCC), active injecting drug users, cardiovascular diseases, depression, etc.) were ambiguous. In their work Ohlendorf V., Schäfer A., Christensen S. "Only partial improvement in health-related quality of life after treatment of chronic hepatitis C virus infection with direct acting antivirals in areal-world setting-results from the German Hepatitis C-Registry (DHC-R)" (2021) studied the impact of modern treatment regimens on clinically important aspects of quality of life and confirmed that direct-acting antiviral drugs therapy leads to an overall improvement in quality of life in patients infected with hepatitis C. However, half of the patients did not achieve clinically significant improvement, and some of them even experienced a significant decrease in quality of life. In particular, the benefit of CHC treatment was particularly high in patients with initially critical life quality indicators (Table 3). The results may also indicate a greater impact of CHC treatment on mental health than on physical health. As an explanation, the authors suggest that the diagnosis of CHC itself leads to the development of mental health disorders due to stigmatization, isolation and discrimination, or the need to combat a potentially fatal infectious disease, uncertainty about the future. When the infection is cured, these concerns may disappear, which is likely to lead to an improvement in the mental aspect of QL [37, 38].

Authors from the Netherlands (2018) came to similar conclusions in their work, assessing the quality of life of 68 patients with HCV who underwent direct-acting antiviral drugs therapy immediately after treatment and 12 weeks after, and confirming that one of the predictors of a decrease in the mental aspect of QL (Table 3) is the use of different treatment regimens (ribavirin), obesity [39].

Thus, quality of life is a multidimensional concept; therefore, when identifying a decrease in QL, additional causes should be taken into account (chronic viral hepatitis B, D, HIV co-infection, alcoholic liver disease, etc.), possible therapeutic concepts and the level of QL before treatment. Direct-acting antivirals have revolutionized treatment with high rates of viral elimination and reduced health outcomes. A number of authors believe that further studies with longer follow-up are needed to optimize the quality of life of patients, which can contribute to increase their responsibility for their own health and the health of others, adequate perception of their own disease and optimal coexistence with it, prevention of social isolation and the best adaptation of patients in the conditions of modern society.

Conclusions

1. Analysis of the literature shows that viral hepatitis C has a significant impact on the quality of life of patients, including physical, psychological and social spheres. Changes in the psycho-emotional sphere and a decrease in quality of life were more pronounced in patients infected with 1B virus genotype.

2. Direct-acting antiviral drugs have revolutionized treatment by providing high rates of virus elimination and reducing health outcomes.

3. Improvement in indicators was more often observed in patients under 48 years of age, with fibrosis level of F2-F4, confirming the opinion that patients with F0-F1 initially have better QL data. The gains in QL were largely maintained at later time points in patients with compensated cirrhosis; however, starting at week 120, there was a decreasing trend in the decompensated group.

4. A number of authors believe that further studies with longer follow-up are needed to optimize the quality of life of patients, which can contribute to increasing their responsibility for their own health and the health of others, adequate perception of their own disease and optimal coexistence with it, prevention of social isolation and the best adaptation of patients in the conditions of modern society.

References:

1. World Health Organization. Global progress report on HIV, viral hepatitis and sexually transmitted infections, 2021. Available at: https://www.who.int/publications/i/item/9789240027077

2. Kozhevnikova G.M., Alikeeva G.K., Shamov A.S., Yushchuk N.D. Risk factors for contracting viral hepatitis in drug users. Epidemiology and infectious diseases. 1998; 3:47-48.

3. Sukhoruk A.A. abstract. Determination of tactics for managing patients with chronic hepatitis C with outcome in liver cirrhosis based on their clinical and laboratory characteristics, 2015.

4. Pimenov N.N. abstract. Current manifestations of the hepatitis C epidemic process in Russia and ways to improve epidemiological surveillance, 2019.

5. Gower, E. Global epidemiology and genotype distribution of the hepatitis C virus infection / E.

Gower, C. Estes, S. Blach, K. Razavi-Shearer, H. Razavi // Journal of Hepatology. - 2014. - V.61. - P. 45-57.

6. Viral hepatitis in the Russian Federation. Analytical review. Ed. Pokrovsky V.I., Zhebrun A.B. St. Petersburg; 2013.

7. Enaleeva D. Sh., Fazylov V. Kh., Sozinov A. S. Chronic viral hepatitis B, C and D: a guide for doctors. V.: GEOTAR-Media; 2015. 192 p.

8. Younossi Z.M., Boparai N., Price L.L., et al. Health-related quality of life in chronic liver disease: the impact of type and severity of disease. Am J Gastroenterol 2001; 96 (7):2199-205. DOI: 10.1111/j.1572-0241.2001.03956.x

9. Baygaliev A.A. Pavlodar branch of State Medical University of Semey, Kazakhstan. Study of the quality of life in patients with chronic hepatitis C, 2010

10. Golubeva M. D., Dorofeeva K. V. Assessing the impact of chronic liver diseases on the presence of fatigue in patients, 2020.

11. Ishinuki T., Ota S., Harada K., Kawamoto M., Meguro M., Kutomi G., Tatsumi H., Harada K., Miyanishi K., Kato T., Ohyanagi T., Hui T.T., Mizuguchi T. Current standard values of health utility scores for evaluating cost-effectiveness in liver disease: A meta-analysis. World J Gastroenterol. 2022 Aug 21; 28(31):4442-4455. doi: 10.3748/wjg.v28.i31.4442. PMID: 36159009; PMCID: PMC9453766.

12. Importance of fatigue and its measurement in chronic liver disease / Gerber L. H., Younossi Z.M. [et al.] // World J Gastroenterol. – 2019. – Vol. 25 (28). – P. 3669-3683.

13. Rozina V.L., Sitnikov I.G., Bokhonov M.S. Changes in the quality of life of patients during combined antiviral therapy for chronic hepatitis C //Children's infections. 2019 - 18 (4). - P. 38-42.

14. Horváth G. et al. Effect of hepatitis C infection on the quality of life //Perspectives in psychiatric care. 2018; 54 (3). - P. 386–390.

15. Jean-Michel Pawlotsky, Christian B. Ramers, John F. Dillon, Jordan J. Feld, Jeffrey V. Lazarus - Simplification of Care for Chronic Hepatitis C Virus Infection. Semin Liver Dis. 2020 Nov; 40(4):392-402. doi: 10.1055/s-0040-1713657. Epub 2020 Jul 28.

16. Josep Mallolas, Adriana Ahumada, Javier Ampuero, José Ramón Blanco, Álvaro Hidalgo, Maria-Carlota Londoño, Esther Molina, Salvador Ruiz - Quality of life in patients with hepatitis C. Importance of treatment. Gastroenterol Hepatol. 2019 Sep; 42 Suppl 1:20-25.

17. Maksimova L.V., Vorobyov P.A. Determination of the quality of life of patients with chronic hepatitis B (C) using the euroqol 5d questionnaire. - Problems of standardization in healthcare, 5-6, 2013

18. Honrubia López R., Madejón Seiz A., Romero Portales M., García Sánchez A., Castillo Grau P., Erdozain Sosa J.C., Olveira Martín A., Robles A., García-Samaniego Rey J. Quality of life study in asymptomatic patients with hepatitis C. Rev Esp Enferm Dig. 2020 Jul;112(7):520-524. doi: 10.17235/reed.2019.6339/2019. PMID: 31617364.

19. GoñiEsarte S, Juanbeltz R, Martínez-Baz I, Castilla J, San Miguel R, Herrero JI, Zozaya JM. Long-term changes on health-related quality of life in patients with chronic hepatitis C after viral clearance with direct-acting antiviral agents. Rev EspEnferm Dig. 2019 Jun;111(6):445-452. doi: 10.17235/reed.2019.6063/2018. PMID: 31066286.

20. Juanbeltz R, Martínez-Baz I, San Miguel R, et al. Impact of successful treatment with direct-acting antiviral agents on health-related quality of life in chronic hepatitis C patients. PLoS One 2018;13(10):e0205277. DOI:10.1371/journal.pone.0205277

21. Marcellin F, Roux P, Protopopescu C, et al. Patient-reported outcomes with direct-acting antivirals for the treatment of chronic hepatitis C: current knowledge and outstanding issues. Expert Rev Gastroenterol Hepatol 2017;11(3):259-68. DOI: 10.1080/17474124.2017.1285227

22. Wong WWL, Wong J, Bremner KE, Saeed Y, Mason K, Phoon A, Martel-Laferrière V, Bruneau J, Feld JJ, Feng Z, Baguley E, Lee SS, Powis J, Krahn MD. Impact of direct-acting antiviral treatment on health utility in patients with chronic hepatitis C in hospital and community settings. Liver Int. 2023 Apr;43(4):805-818. doi: 10.1111/liv.15518. Epub 2023 Feb 5. PMID: 36606706.

23. Kaminskaya S. N. Clinical and psychological characteristics and quality of life of patients with chronic viral hepatitis C, 2014.

24. Atamla M., Khoury J., Dabbah I., Kramsky R., Yaacob A., Veitsman E., Saadi T. Direct antiviral agents for chronic hepatitis C virus infection improve health-related quality of life significantly in the long term. Clin Exp Hepatol. 2021 Sep; 7(3):258-263. doi: 10.5114/ceh.2021.109192. Epub 2021 Sep 20. PMID: 34712826; PMCID: PMC8527337.

25. van der Plas S.M., Hansen B.E., de Boer J.B., Stijnen T., Passchier J., de Man R.A., Schalm S.W. The Liver Disease Symptom Index 2.0; validation of a disease-specific questionnaire. Qual Life Res. 2004 Oct; 13(8):1469-81. doi: 10.1023/B:QURE.0000040797.17449.c0. PMID: 15503842.

26. Youssef N.F., El Kassas M., Farag A., Shepherd A. Health-related quality of Life in patients with chronic hepatitis C receiving Sofosbuvir-based treatment, with and without Interferon: a prospective observational study in Egypt. BMC Gastroenterol. 2017 Jan 21; 17(1):18. doi: 10.1186/s12876-017-0581-1. PMID: 28109264; PMCID: PMC5251342

27. Akio Miyasaka, Yuichi Yoshida, Akiko Suzuki, Yasuhiro Takikawa - Health-related quality of life in patients with chronic hepatitis C treated with sofosbuvir-based treatment at 1-year post-sustained virological response. 2021 Dec; 30(12):3501-3509. doi: 10.1007/s11136-021-02874-6. Epub 2021 May 19.

28. Silvia Nardelli, Oliviero Riggio, Davide Rosati, Stefania Gioia, Alessio Farcomeni, Lorenzo Ridola - Hepatitis C virus eradication with directly acting antivirals improves health-related quality of life and psychological symptoms. World J Gastroenterol. 2019 Dec 28; 25(48): 6928–6938

29. Suzuki M., Ishikawa T., Sakuma A., Abe S., Abe H., Koyama F., et al. Evaluation of the health-related quality of life using the 36-item short form health

survey in patients with chronic hepatitis C receiving pegylated interferon/ribavirin/telaprevir triple treatment. Exp Ther Med. 2016; 12:3353–3358.

30. Shahid I., AL Malki W.H., Hafeez M.H., Hassan S. Hepatitis C virus infection treatment: an era of game changer direct acting antivirals and novel treatment strategies. CritRevMicrobiol. 2016; 42:535–547.

31. Perlin C.M., Ferreira V.L., Borba H.H., Wiens A., Ivantes C.A., Lenzi L., et al. Quality of life in Brazilian patients with treated or untreated chronic hepatitis C. Rev Inst Med Trop Sao Paulo. 2017; 59:e81

32. Ng X., Nwankwo C., Arduino J.M., Corman S., Lasch K.E., Lustrino J.M., Patel S., Platt H.L., Qiu J., Sperl J. Patient-reported outcomes in individuals with hepatitis C virus infection treated with elbasvir/grazoprevir. Patient Prefer Adherence. 2018; 12:2631–2638

33. Siqueira F.M., Ferreira V.L., Borba H.H.L., Pontarolo R. Quality of life of Brazilian chronic hepatitis C patients treated with interferon-free therapies. Rev Inst Med Trop Sao Paulo. 2018; 60:e72.

34. Fagundes R.N., Ferreira L.E.V.V.C., Pace F.H.L. Health-related quality of life and fatigue in patients with chronic hepatitis C with therapy with direct-acting antivirals agents interferon-free. PLoS One. 2020 Aug 19; 15(8):e0237005. doi: 10.1371/journal.pone.0237005. PMID: 32813740; PMCID: PMC7437906.

35. Younossi Z.M., Racila A., Muir A., Bourliere M., Mangia A., Esteban R., Zeuzem S., Colombo M., Manns M., Papatheodoridis G.V., Buti M., Chokkalingam A., Gaggar A., Nader F., Younossi I., Henry L., Stepanova M. Long-term Patient-Centered Outcomes in Cirrhotic Patients With Chronic Hepatitis C After Achieving Sustained Virologic Response. Clin Gastroenterol Hepatol. 2022 Feb;20(2):438-446. doi: 10.1016/j.cgh.2021.01.026. Epub 2021 Jan 22. PMID: 33493697.

36. Jean-Michel Pawlotsky, Christian B Ramers, John F. Dillon, Jordan J. Feld, Jeffrey V. Lazarus - Simplification of Care for Chronic Hepatitis C Virus Infection. Semin Liver Dis. 2020 Nov; 40(4):392-402. doi: 10.1055/s-0040-1713657. Epub 2020 Jul 28.

37. Ohlendorf V., Schäfer A., Christensen S., Heyne R., Naumann U., Link R., Herold C., Schiffelholz W., Günther R., Cornberg M., Serfert Y., Maasoumy B., Wedemeyer H., Kraus M.R. Only partial improvement in health-related quality of life after treatment of chronic hepatitis C virus infection with direct acting antivirals in a real-world setting-results from the German Hepatitis C-Registry (DHC-R). J Viral Hepat. 2021 Aug; 28(8):1206-1218. doi: 10.1111/jvh.13546. Epub 2021 Jun 8. PMID: 34003549.

38. Marcellin F., Roux P., Protopopescu C., Duracinsky M., Spire B., Carrieri M.P. Patient-reported outcomes with direct-acting antivirals for the treatment of chronic hepatitis C: current knowledge and outstanding issues. Expert RevGastroenterolHepatol. 2017 Mar; 11(3):259-268. doi: 10.1080/17474124.2017.1285227. Epub 2017 Jan 31. PMID: 28116926.

39. Kracht P.A.M., Lieveld F.I., Amelung L.M., et al. The impact of hepatitis C virus direct-acting antivirals on patient-reported outcomes: A Dutch prospective cohort study. Infect Dis Ther. 2018; 7:373-385.

40. Vyas B.H., Darji N.H., Rana D.A., Vyas K.Y., Malhotra S.D. Impact of newer direct-acting antiviral drugs based on quality-adjusted life years: A prospective pharmacoeconomic study in hepatitis C patients. Perspect Clin Res. 2021 Apr-Jun; 12(2):76-82. doi: 10.4103/picr.PICR_123_19. Epub 2020 May 7. PMID: 34012903; PMCID: PMC8112329.

PHYSICAL SCIENCES

ABOUT THE MECHANISM OF GRAPHITE SPLITTING

Yurov V.,
Karaganda Technical University, candidate of phys.-mat. sciences, associate professor, Kazakhstan, Karaganda
Zhangozin K.
TSK Vostok LLP, candidate of phys.-mat. sciences, associate professor, Kazakhstan, Ust-Kamenogorsk
https://doi.org/10.5281/zenodo.10492416

Abstract

The article provides a review of experimental work on the production of graphene by processing graphite and a review of mathematical models for the splitting of layered structures. Next, the surface layer of graphite, from where the splitting of layered materials begins, is examined for the first time. The graphite layer, which we denote as R(I), its thickness according to our model is $R(I)_a$ = 1.07 nm and $R(I)_c$ = 2.92 nm, that is, it is a nanostructure. This layer contains 4 sheets of graphene. This means that the R(I) layer will more easily move along the cleavage plane. Moreover, at the stages of easy sliding, linear and parabolic strain hardening, as well as at the stage of preliminary destruction, the observed localization patterns are different types of wave processes. At the boundary of the R(I) layer with the bulk phase, internal stresses arise due to relaxation or reconstruction of the surface. Next, we will build a theoretical model of graphite, presenting it in the form of a cylinder of finite dimensions, and use our modified work, supplementing it with homogeneous boundary conditions. The model we obtained for the splitting of graphite mathematically coincides with Stefan's fourth problem, where the freezing of ice is considered, and the movement of phase boundaries $\beta(t) = \beta_0\sqrt{t}$ is called the self-similar law of motion. We have shown that to split graphite into graphene sheets, it is necessary to expend work that exceeds the adhesion energy of the R(I) layer from the rest of the volume. It has also been shown that it is much easier to obtain graphene mechanically (including ultrasonic splitting) than by changing the temperature gradient. However, graphene-like structures can be obtained using a pulsed picosecond laser for heating.

Keywords: *graphite, graphene, surface layer, nanostructure, Stefan problem, surface, splitting, delamination, crystal.*

Introduction

Graphene is a two-dimensional single-layer sheet of sp^2-hybridized carbon atoms arranged in hexagonal shapes. The presence of strong covalent C-C σ-bonds in the plane of the graphene sheet in combination with π-electrons outside it determines the unique physical and chemical properties of graphene, such as a large theoretical specific surface area (~ 2600 m^2/g) [1], high mobility of charge carriers (~ 200000 cm^2/V s) [2], high Young's modulus (~ 1000 GPa) [3], thermal conductivity (~ 5000 W/m K) [4], optical transparency (~ 97.7%) [5], mechanical strength, chemical stability, etc. To obtain graphene from graphite, there are several methods, which we will briefly review below.

The purpose of this article is a theoretical model of the splitting of graphite, with the aim of obtaining graphene and graphene-like structures from it.

Methods for obtaining graphene structures

Mechanical splitting. This is the first method for synthesizing graphene, a method in which longitudinal or transverse stress is created on the surface of materials with a layered structure. Graphite is a layered material consisting of many layers of graphene, which are interconnected by relatively weak van der Waals forces (VDVs). Therefore, if you apply longitudinal or transverse stress to it, thereby breaking weak airborne forces, you can obtain individual sheets or stacks of graphene-like structures (Figure 1a). Highly oriented pyrolytic graphite, single-crystalline graphite or natural graphite are used as the starting material in this method [6-8]. Cleavage can be performed using various means, such as the Scotch-tape method [9], ultrasonic treatment [10], electrochemical synthesis [11], transfer printing method [12] and many others.

Thermal splitting. Thermal decomposition also makes it possible to obtain few-layer graphene structures (MLS). The process is carried out at high (more than 1000 °C) and low (about 100 °C) temperatures, at different heating rates, in the environment of various gases (hydrogen, argon, etc.) and in vacuum, using graphite or its derivatives, thereby obtaining most graphene structures of various shapes and sizes.

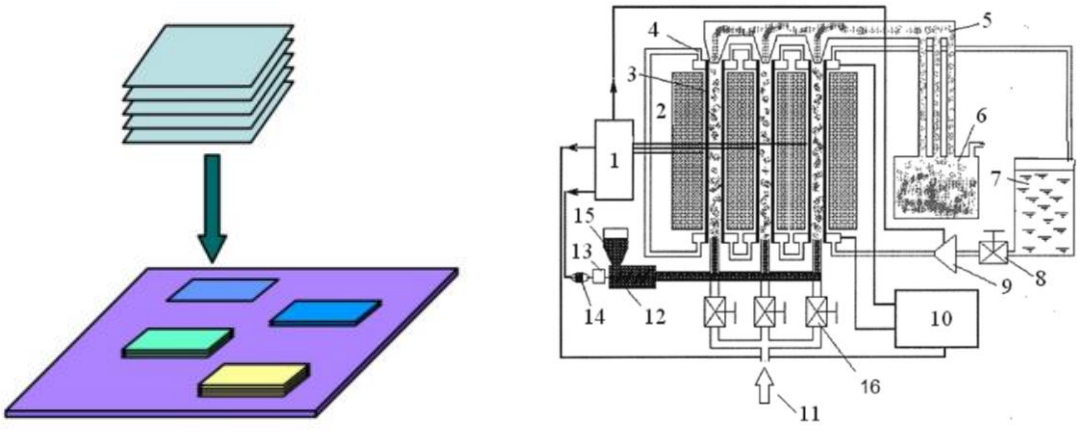

a) *b)*

Figure 1. Scheme for obtaining graphene samples by micromechanical splitting (a); device for thermal splitting (see text) (b).

The device (Figure 1b) is illustrated by a circuit diagram from the Patent [13]. Control panel 1 includes controls and devices for monitoring the operating mode of the device. The splitting unit 2 contains three reactor pipes 3. To supply electrical supply voltage to the end sections of the reactor pipes 3, copper water-cooled current leads 4 are used. The TRG entering the cavity of the heaters 3 in the ascending air flow through three pipelines 5 settles in the receiving hopper 6. To ensure For water cooling of the reactor pipes of the device, a ballast tank 7 with water is used, from which coolant is circulated through valve 8 by means of pump 9. The three-phase power supply unit10 contains three step-down furnace transformers and three groups of thyristors with fuses and RC filters. At the bottom of the splitting unit 2 there is a centrifugal fan 11 for air supply. Continuous supply of initial oxidized graphite is carried out by block 12 of three parallel screw feeders driven through gear 13 by an electric motor 14. Oxidized graphite powder is periodically added by the operator to the supply hopper 15. To smoothly regulate air flow, three ball valves 16 are used. For example, when using high-temperature splitting processes can occur in seconds [14]. Graphite oxide or intercalated graphite compounds are used as starting materials for thermal decomposition instead of pure graphite.

Ultrasonic splitting. The first successful decomposition of graphite by ultrasonic treatment was achieved in the organic solvent N-methylpyrrolidone [15]. The exfoliation of graphite by ultrasonic treatment in the presence of surfactants has also been proposed. This was first reported in [16], in which dodecylbenzenesulfonate was used as a surfactant. Works [17, 18] show that graphene structures obtained by ultrasonic processing of graphite and its derivatives contain a lot of oxygen. In [19], multilayer graphene was obtained by ultrasonic splitting of graphite microparticles in a surface-active solvent, a mixture of nonane and water, and a surface-active surfactant was selected that ensures the dispersion of graphene in hydrophilic systems. In [20], a technology was developed for producing polymers modified with graphene structures using ultrasonic dispersion (Fig. 2).

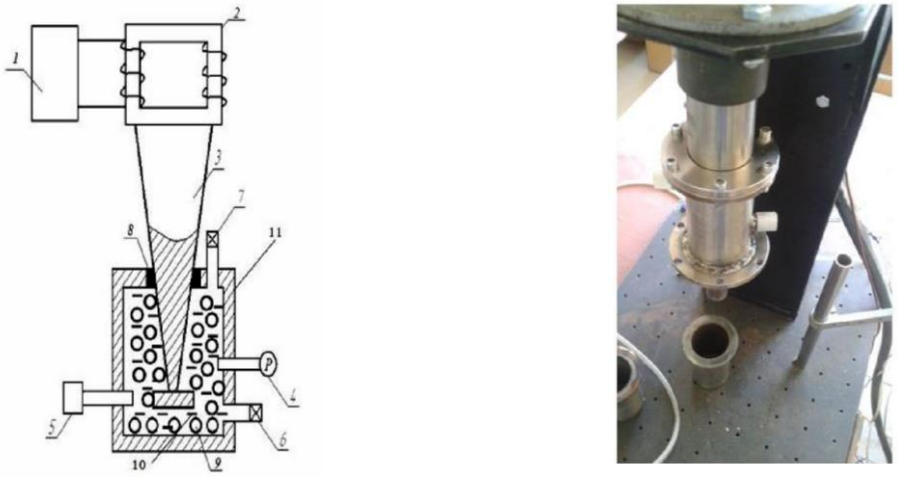

a) *b)*

Figure 2. Diagram (a) and appearance (b) of the ultrasonic unit of the installation for liquid-phase stratification of graphite [20]: 1 – ultrasonic generator; 2 – magnetostrictive transducer; 3 – waveguide; 4 – pressure gauge; 5 – cavitometer; 6 – drain hole; 7 – overpressure valve; 8 – sealing gasket; 9 – finely dispersed graphite; 10 – solvent; 11 – pressure chamber.

Chemical degradation. Chemical digestion is a multi-step process. At the first stage, intercalated graphite compounds are obtained [21].

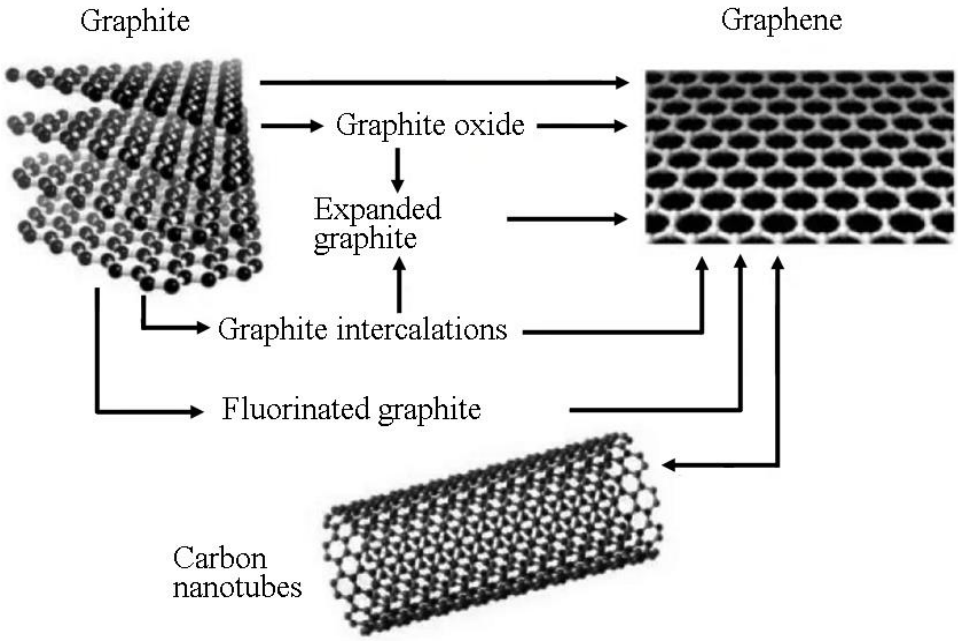

Figure 3. Routes to obtain graphene through the cleavage of various precursors

The Hummers method [22] involves the oxidation of graphite powder with strong oxidizing agents such as $KMnO_4$ and $NaNO_3$ into H_2SO_4 or H_3PO_4 [22, 23]. This leads to oxidation of the internal layers of graphite and, as a consequence, to an increase in the interlayer distance in the crystal and, accordingly, to a decrease in the interaction energy between the layers. The chemical method implies several possible options for preparing graphene-containing suspensions (Fig. 3). At the second stage, the resulting graphene oxide is reduced to obtain MGS [24].

Chemical vapor deposition (CVD). Already in 1976, it was known about the synthesis of graphite on nickel. It was shown that at a temperature of 900 °C on a metal substrate it is possible to form a graphite film with a thickness of 400 Å [25-30]. The mechanism of formation of a graphite-like film is very simple (Fig. 4).

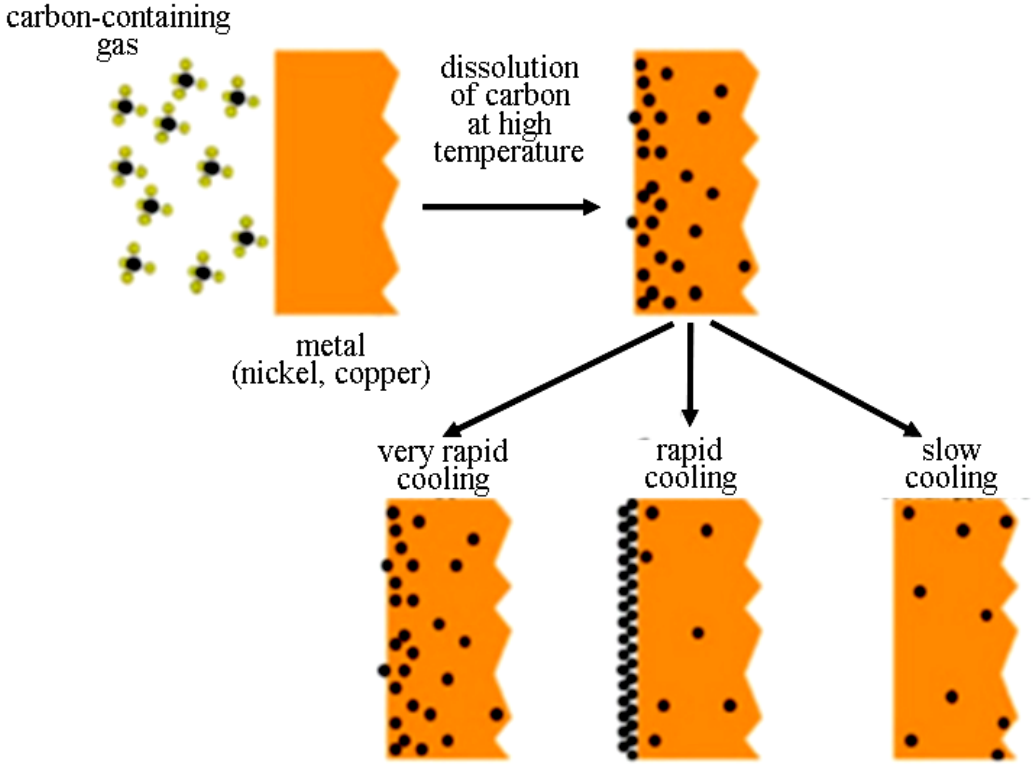

Figure 4. Scheme of the formation of a graphene film on the surface of nickel or copper using the chemical vapor deposition method.

In a mixture of carbon-containing gas, hydrogen and argon at various pressures (from several fractions of a millitorr to atmospheric pressure), upon heating, decomposition into carbon and components occurs at temperatures below 400 °C. Further, as the temperature increases, carbon atoms are deposited onto the nickel substrate, starting at 650 °C. At temperatures above 800 °C they begin to diffuse into the bulk of nickel. Heating stops at temperatures of 950-1000 °C, and then, when the sample is cooled to room temperature, the crystal lattice of the metal (due to thermal compression) squeezes carbon atoms onto the surface, where they form a graphite-like structure, since the lattice constant of nickel is very close to the lattice constant of graphite . By selecting certain synthesis parameters, such as the thickness of the nickel film, the maximum synthesis temperature, the synthesis time and the cooling rate of the sample, it is possible to achieve the formation of a thin graphene film - up to obtaining a graphene monolayer.

Epitaxial growth. Epitaxial growth of graphene on metal surfaces of crystals such as ruthenium, iridium, platinum, palladium, nickel, etc. [31-33]. This method is based on the increasing nature of the temperature dependence of carbon solubility in transition metals. At temperatures exceeding 1000 °C, in the presence of any carbon source, metal saturation occurs as a result of chemical deposition of carbon from the gas phase. Further, in a high or ultra-high vacuum at a pressure of 10-10 millibars and a decrease in the substrate temperature, the solubility of carbon in the metal drops significantly, and due to thermal compression of the crystal lattice, carbon comes to the surface, forming graphene domains of a large area (Fig. 5a). Sublimation of silicon from a SiC substrate at high temperature (~1000 °C), leading to graphitization of the silicon carbide surface (Fig. 5b), is also one of the promising methods for obtaining high-quality graphene samples (from single-layer graphene to graphene containing several layers) with a size of ~100 mm (with a crystallite size of up to 50 μm) [34, 35].

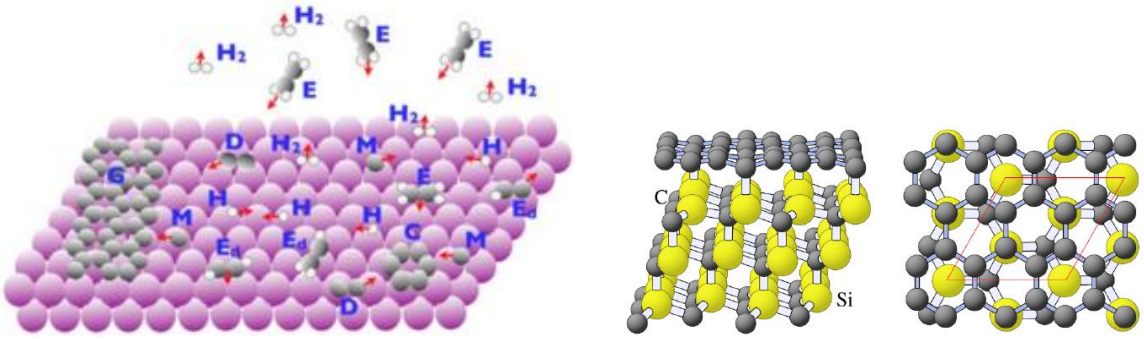

a) *b)*

Figure 5. Schematic representation of the main processes occurring during the epitaxial growth of graphene from hydrocarbon molecules E. They are deposited on the surface, undergoing decomposition through a series of dehydrogenation reactions leading to different types of C_xH_y, shown as E and H atoms. New species diffuse through the surface. The smaller forms of carbon M and D do not diffuse, but stick together into larger clusters of C atoms. The H atoms of the parent molecule migrate from the surface and form a hydrogen molecule, which evaporates from the surface. And finally, some of the forms such as M and D, or even their large clusters C, may attach to the island of G at its edge (a); A type of epitaxial growth of graphene is the thermal decomposition of silicon carbide. When SiC is heated to 1300 °C in an ultra-high vacuum, silicon sublimation occurs, resulting in the formation of graphene layers on the surface of the crystal (b).

Other methods for producing graphene. Let's list some of them. In [36], the possibility of electrochemical intercalation of the tetrafluoroborate anion into graphite from a supercritical electrolyte based on carbon dioxide, acetonitrile as a cosolvent, and tetrabutylammonium tetrafluoroborate salt was shown for the first time.

In [37], the task was set: to develop a technology for producing graphene films using the method of dissociative evaporation (sublimation) of the SiC surface and to study the possibility of instrumental applications of the resulting structures.

In [38], the task was set: to develop a method of plasma-electrochemical splitting of graphite to obtain nanocomposites, which are few-layer graphene structures doped with nitrogen atoms and decorated with transition metal oxides, which have a set of necessary characteristics for their use as effective platinum-free catalysts for the reduction of oxygen in fuel cathodes elements.

As a result: the synthesis of graphene and graphene-like materials is based on increasing the interplanar distance, weakening the van der Waals interaction forces between graphene layers with subsequent delamination of graphite.

Theory of splitting or delamination of layered structures

Classification of layered inorganic compounds [39].

The layered structure of the substance is characterized by strong interactions in two orthogonal directions and several orders of magnitude weaker interactions in the third orthogonal direction. The most famous example of substances with a layered structure is graphite (see above), in which layers formed by covalently bonded carbon atoms in sp2 hybridization (with a binding energy of ≈ 524 kJ/mol) are connected by van der

Waals forces (with a binding energy of ≈ 7 kJ/mol) [26]. Table 1 shows the classification of layered materials according to the presence and absence of charge in their constituent layers.

Layered materials can be classified by comparing the forces that hold the layers together. These are, first of all, electrostatic, hydrogen and van der Waals interactions.

Table 1.

Classification of layered inorganic materials by type of layers [39].

Uncharged layers	Chemical composition
Non-conducting layers (dielectrics)	
clay	
kaolinite	$Al_2Si_2O_5(OH)_4$
serpentine	$Mg_3Si_2O_5(OH)$
Nickel cyanide	Ni(CN)2
hexagonal boron nitride	h-BN
Electrically conductive layers	
graphite	C
transition metal dichalcogenides	MX_2 (M = Ti, Zr, Hf, V, Nb, Ta, Bi, Mo, W; X = S, Se, Te)
Metal carbides and nitrides, MAX and MXene phases	$M_{n+1}(A)_mX_n$ (n=1-3; m= 0,1; M – Ti, Zr, Hf, V, Nb, Ta, Bi, Mo, W; A – Si, Ge, Al, S, Sn; X – C, N)
metal oxyphosphates	$MOPO_4$ (M = V, Nb, Ta)
Charged layers	
Negatively charged layers	
clay	
montmorillonite	$Na_x(Al_{2-x}Mg_x)(Si_4O_{10})(OH)_2$
saponite	$Ca_{x/2}Mg_3(Al_xSi_{4-x}O_{10})(OH)_2$
vermiculite	$(Na,Ca)_x(Mg_{3-x}Li_xSi_4O_{10})(OH)_2$
muscovite	$KAl_2(AlSi_3O_{10})(OH)_2$
β-alumina	$NaAl_{11}O_{17}$
complex oxides of transition and alkali metals	M^IXO_2 (M^I – alkali metal; X = Ti, V, Cr, Mn, Co, Ni)
layered perovskites Ruddlesden–Popper phases	$M_{n+1}X_nO_{3n+1}$ (M - elements I-III групп; X – transition elements)
Dion–Jacobson phases	$M^ILn_{n-1}X_nO_{3n+1}$ (M^I - alkali metal; Ln = РЗЭ; X = Nb, Ta)
Aurivillius phases	$(Bi_2O_2)M_{n-11}X_nO_{3n+1}$ (M – elements I-III; X – transition elements)
Positively charged layers	
layered double hydroxides	$[M^{2+}_{1-x}M^{3+}_x(OH)_2]A_{n-x/n\cdot m}H_2O$
layered transition hydroxides metals	$M_2(OH)_3X$ (M^{II} = Co, Cu, Ni, Mn, Zn и X^- = NO^{3-}, $CH_3CO_2^-$, Cl^-)
layered REE hydroxides class LREH-I	$Ln_2(OH)_5(A^{m-})_{1/m}\cdot nH_2O$ (Ln = REE, A = anion, n = 1-2)
class LREH-II	$Ln(OH)_2(A^{m-})_{1/m}\cdot nH_2O$ (n = 0-2)
class LREH-III	$Ln_2(OH)_{5-x}(A^{m-})_{(1+x)/m}\cdot nH_2O$ (n = 0-2; 0<x<1)
boehmite	AlOOH
antimony oxohydroxide	$[Sb_4O_4(OH)_2](O_3SCH_2CH_2SO_3)\cdot H_2O$

The layered structure is characteristic not only of inorganic substances (Table 1), but also of many other materials. Laminated rods and slabs are essential elements of many modern structures. They play one of the leading roles in rocket, space and aviation technology, automobile and shipbuilding, chemical and power engineering, industrial and housing construction [40]. Deformable layered structures made of polymer composite materials are widely used in technology as elements of load-bearing structures [41].

Mathematical models of splitting layered structures. In [40, 42], a new method was developed for solving problems in the spatial theory of elasticity in the Saint-Venant formulation - the asymptotic splitting method. The application of the asymptotic splitting method to problems of longitudinal-transverse bending of layered slabs with an arbitrary arrangement and number of layers is substantiated. It has been established that for surface loads that are m-harmonic functions, the method provides an exact analytical solution. The application of the asymptotic splitting method to the study of the edge effect in layered orthotropic composites is justified. Moreover, previously known analytical solutions for homogeneous single-layer structures, obtained either using Airy functions or the symbolic Lurie method, are also obtained using the asymptotic splitting method. In terms of historical con-

tinuity, the method of asymptotic splitting is a development of the ideas laid down by Navier, Poisson, Cauchy and Saint-Venant, and then by Mitchell and Almanzi.

In [41, 43], a method of regularization of the incorrect according to A.N. Tikhonov problem on the deformation of a volumetric incompressible medium, in which the limit of the solution of the regularized problem is explicitly calculated. A mathematical model of static deformation of axisymmetric layered structures containing elastic orthotropic and elastic volumetrically incompressible layers has been constructed using a developed regularization method. The sensitivity of the numerical solution to changes in the initial value of Poisson's ratio and the dimensions of the finite elements has been studied. It is shown that with the same number of iterations and with sequential refinement of the mesh, the solution converges faster to the analytical one when choosing the initial Poisson's ratio in the range of 0.3-0.35 than with values close to 0.5. The following characteristics of graphite are given in [44]: apparent density 1860-1960 kg/m3, tensile strength 14.7 MPa, compressive strength 67 MPa, elastic modulus 8.8 GPa, thermal conductivity 130 W/(m K) at 20 °C, LTLE 6.6 10^{-6} 1/K, electrical resistivity 5-8 μOhm m, emissivity at 2300 °C 0.85. Poisson's ratio μ = 14.7/67 = 0.22.

In [38], for the first time, in a one-stage process with a bipolar supply of potential, various nanocomposites of few-layer graphene structures with transition metal oxides were simultaneously obtained in two electrochemical reactors isolated from each other. For pulsed action, a phenomenological model of one-stage plasma-electrochemical splitting of graphite with the formation of few-layer graphene structures was proposed for the first time. In [38, 40, 41], a detailed literature review of mathematical models of splitting layered structures was carried out, but we will limit ourselves only to work [45].

The scientific value of the work [45] lies in the construction of methods for mathematical modeling of the process of chemical pressing of oxidized graphite, the development and testing of methods for solving emerging boundary value problems with a moving interface between regions (Stefan type problems). Numerical experiments show the influence of the thermophysical parameters of thermally expanded graphite on the characteristics of the foaming process, such as the process time and the propagation of phase interfaces over time - a typical Stefan problem. Let us note the following: from a mathematical point of view, Stefan boundary value problems are fundamentally different from classical problems of heat conduction or diffusion. Due to the time dependence of the size of the flow transfer region, the classical methods of separation of variables and integral Fourier transforms are not applicable to this type of problem, since, while remaining within the framework of the methods of mathematical physics, it is not possible to coordinate the solution of the heat equation with the motion of the phase boundary. Stefan's problem has been treated both analytically and numerically since the end of the 19th century. A review of these works can be found in monographs [46–52], and especially in [53].

Our model of graphite splitting

Let us consider the surface layer of graphite, from where the splitting of layered materials begins. In general, there are two approaches: the Gibbs approach [54], in which the surface layer is conventionally considered as a geometric surface without thickness; the approach of Van der Wals, Guggenheim, Rusanov, in which the surface layer is considered as a layer of finite thickness [55]. According to modern concepts [56, 57], the surface phase γ_1 is understood as an ultrathin film (surface layer) that is in equilibrium with the crystalline base, the properties and structure of which are different from the bulk properties of γ_2. However, the question of the theoretical "thickness" of this surface layer for various substances remained open until 2018. Only after our work [58-60] it became clear how the thickness of the surface layer, which plays a big role in nanotechnology, can be theoretically determined [61]. Thus, the surface layer, which we denote as R(I), its thickness is equal according to our model [58-60]:

$$R(I) = 0{,}17 \cdot 10^{-9} \upsilon = 0{,}17 \cdot 10^{-9} \cdot \grave{I} / \ \rho\,(m). \qquad (1)$$

Equation (1) shows that the layer R(I) is determined by the parameter – the molar (atomic) volume of the metal (υ = M/ρ, M – molar mass, ρ – density).

Its diagram is shown in Fig. 6a, and in Fig. 6b shows table D.I. Mendeleev with a periodic dependence of volume υ on Z.

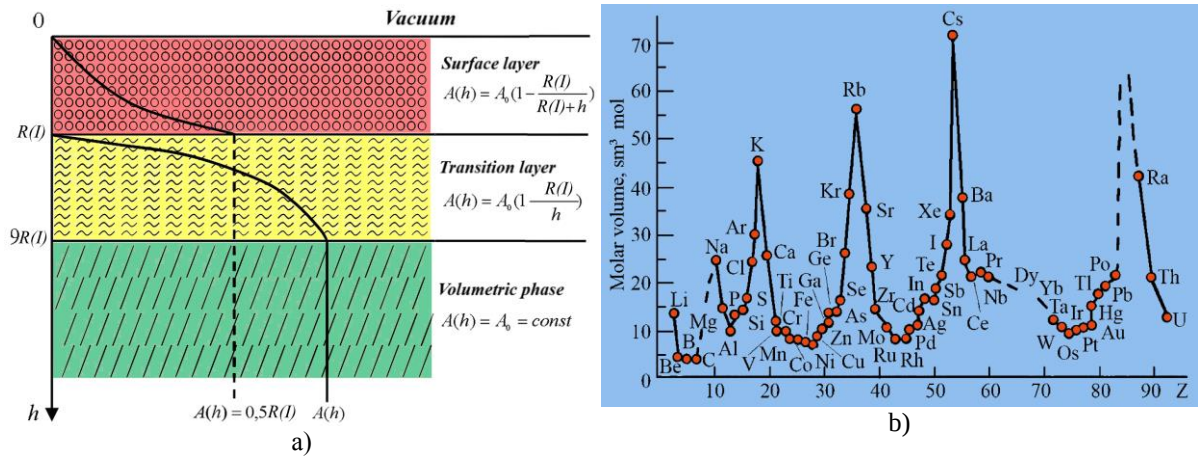

Figure 6. Schematic representation of the surface layer (a), periodic change in the atomic volume of elements (b)

From Fig. 6b carbon is at the beginning of the periodic table next to boron. Using formula (1), we calculate R(I) (Table 2) for graphite parallel to the plane (where the carbon hexagon lies) x = a = b and perpendicular to this plane x = c.

Table 2.

Graphite parameters.

Graphite	ρ, g/sm^3	T_m, K	$R(I)_a$, nm	$R(I)_c$, nm	γ_a, mJ/m^2	γ_c, mJ/m^2
C	1,91	3970 K	1,07 (4)	2,92 (4)	2779	591

The anisotropy of graphite was determined using our formula [60]:

$$R(I) = 0{,}17\cdot 10^{-9}\cdot \text{Ì}/\ \rho,$$
$$R(I)_{\text{õ=à}} = 0{,}4\cdot 10^{-11}\cdot \text{õ(à)}^3,$$
$$R(I)_{y=b} = 0{,}4\cdot 10^{-11}\cdot y(b)^3,$$
$$R(I)_{z=c} = 0{,}4\cdot 10^{-11}\cdot z(c)^3, \quad (2)$$
$$\gamma_{\text{à}} = 0{,}7\cdot 10^{-3}\cdot \text{Ò}_m\cdot R(I)_{\text{à}}/R(I),$$
$$\gamma_b = 0{,}7\cdot 10^{-3}\cdot \text{Ò}_m\cdot R(I)_b/R(I),$$
$$\gamma_c = 0{,}7\cdot 10^{-3}\cdot \text{Ò}_m\cdot R(I)_{\text{ñ}}/R(I).$$

In formula (2), γ is the surface energy of graphite faces, which is equal, according to the empirical formula [62]:

$$\gamma = 0{,}70\cdot 10^{-3}\cdot T_m\ \ [\text{J/m}^2], \quad (3)$$

In Table 2, the number in brackets n = R(I)/a,c is equal to the number of graphene layers, and, c is the lattice constant along and across the graphite plane.

To split graphite over a layer of thickness R(I), it is necessary to expend energy, which is called adhesion energy and is determined by the Dupre formula [63]:

$$W_{\text{à}} = \gamma_1 + \gamma_2 - \gamma_{12} \approx \gamma_1 + \gamma_2, \quad (4)$$

where γ_1, γ_2 and γ_{12} are the surface energy of the R(I) layer, bulk phase and transition layer, which is negligible.

In [64], we showed that $\gamma_1 \approx 0.3\ \gamma_2$, i.e. the surface energy of the R(I) layer is three times less than the bulk phase. This means that the R(I) layer will more easily move along the cleavage plane. At the boundary of the R(I) layer with the bulk phase, internal stresses arise due to relaxation or reconstruction of the surface [56]. These stresses lead to the formation of nanocracks with dimensions R(I) = L_{nm} [64]. This fact was noticed 100 years ago. In the 20s of the twentieth century, academician A.F. Ioffe conducted a series of experiments with a NaCl crystal and he obtained a fracture of this salt in the amount of 0.4 g/mm^2 instead of 200 g/mm^2 according to Max Born's quatomechanical theory. A.F. Ioffe related this to the existence of microcracks in the surface layer. Then he dipped a NaCl crystal into water and measured the hardness of its surface, which increased as the surface dissolved, approaching the theoretical value [65]. This experiment was called the "Ioffe effect" [66]. Thus, for a NaCl crystal, according to our model, R(I) = 4.6 nm (which is typical for nanostructures) and the number of monolayers n = R(I)/a = 8 (a is the lattice constant). It is not difficult to wash off 8 monolayers of NaCl with water to obtain the Ioffe effect. In the same years, Griffiths examined the change in the energy of a body with a crack L(G) under loading and obtained an energy criterion for destruction, according to which a crack acquires the ability to propagate only when the rate of release of elastic energy σis during growth becomes equal to or exceeds the energy of the newly formed surface.

Internal voltages σis between phases γ_1 and γ_2 can be calculated using the formula [19]:

$$\sigma_{is} = \sqrt{W_a\cdot \text{Å}/R(I)}, \quad (5)$$

where E is Young's modulus of elasticity.

Using equations (1) – (5), we calculate the elastic parameters for graphite.

Table 3.

Elastic parameters of graphite

Graphite	W_{aa}, J/m^2	W_{ac}, J/m^2	σ_{isa}, MPa	σ_{isc}, MPa	E_a, GPa	E_c, GPa
C (ρ = 2,26)	3,613	1,323	5740	1370	7,59	3,48

Next, we will build a theoretical model of graphite, representing it in the form of a cylinder of finite dimensions, and use our modified work [68, 69], supplementing it with homogeneous boundary conditions. In this case, we will calculate the stress gradient in the layer R(I) using standard expressions [70].

The components of thermoelastic stress along the radius r - σr and along the z axis – σz – of the layer R(I) will be assessed using the well-known equations [70]:

$$\sigma_r = -2G\frac{1}{r}\frac{\partial T}{\partial r}. \quad (6)$$

$$\sigma_z = -2G\frac{\partial T}{\partial z}. \quad (7)$$

Here the shear modulus G is determined by the expression:

$$2G = \frac{E}{1+\mu}, \quad (8)$$

where E is Young's modulus, μ is Poisson's ratio.

For graphite E = 8.8 GPa, μ = 0.22, which means 2G = 7.21 GPa.

From equations (6) and (7) we need to determine temperature gradients. To calculate the stress in the layer R(I), when the process of graphite splitting is in progress, we come to a problem with a moving phase boundary, which is called the Stefan problem [45-53] (see above).

In this case, the nonstationary heat equation in a moving cylindrical coordinate system moving according to the law β(t) has the form:

$$\frac{\partial T}{\partial t} = Ä\left[\frac{\partial^2 T}{\partial z^2} + \frac{1}{r}\frac{\partial}{\partial r}\left(r\frac{\partial T}{\partial r}\right)\right], \quad (9)$$

where D is the thermal diffusivity coefficient.

We choose the initial and boundary conditions in general form:

$$T(r, z, t)|_{t=0} = \varphi(r, z),$$
$$T(r, z, t)|_{r=R} = \gamma(z, t),$$
$$T(r, z, t)|_{z=0} = \gamma_1(r, t),$$
$$T(r, z, t)|_{z=\beta(t)} = \gamma_2(r, t).$$

The functions β(t), φ(z, t), γ(z, t), γ1(r, t), γ2(r, t) will be considered continuous. We look for a solution to the problem in the form:

$$T(r, z, t) = \sum_{k=0}^{\infty} \overline{T}_k(z, t) I_0(\lambda_{0k} r), \quad (10)$$

where λ_{0k} are the roots of the equation

$$I_0(\lambda_{ok} R) = 0$$

and $I_0(\lambda_{0k} R)$ is the zeroth order Bessel function satisfying the equation:

$$\frac{1}{r}\frac{d}{dr}\left[r\frac{dI(\lambda_{0k} r)}{dr}\right] + I_0(\lambda_{0k} r) = 0, \quad (11)$$

$$\overline{T}_k(z, t) = \int_0^R T_k(r, z, t) I_0(\lambda_0 r) r dr. \quad (12)$$

The final solution to this problem looks like this:

$$T(r,z,t) = \sum_{\kappa=0}^{\infty} J_0(\lambda_{o\kappa} r)\left\{e^{-Дt}\left[\frac{1}{2Д\sqrt{\pi}}\int_0^t e^{\frac{(z-\xi)^2}{4Дt}} dt\, x\right.\right.$$
$$x\left(\int_0^{\ell} \varphi(r,\xi) I_0(\lambda_{ok} r) r dr\right) d\xi + \frac{R I_1(\lambda_{ok} R)}{2\sqrt{\pi} Д}\int_0^t d\tau \int_0^{\ell} \frac{\gamma(\xi,\tau)}{\sqrt{t-\tau}} e^{-Дt} e^{-\frac{(z-\xi)^2}{4Д(t-\tau)}} d\xi +$$
$$\left.\left. + \frac{1}{4\sqrt{\pi}}\int_0^t \frac{z}{[Ä(t-\tau)]^{3/2}} e^{-\frac{z^2}{4Ä(t-\tau)}} K_1(\tau) d\tau + \frac{1}{4\sqrt{\pi}}\int_0^t \frac{z-\beta(\tau)}{[Ä(t-\tau)]^{3/2}} e^{-\frac{[z-\beta(\tau)]^2}{4Ä(t-\tau)}} K_2(\tau) d\tau\right]\right\}. \quad (13)$$

To use equations (6)-(8), we simplify the general problem (13) by taking homogeneous boundary conditions. In this case:

$$\frac{\partial T}{\partial t} = Ä\left[\frac{\partial^2 T}{\partial z^2} + \frac{1}{r}\frac{\partial}{\partial r}\left(r\frac{\partial T}{\partial r}\right)\right] \quad (14)$$

$$\left.\begin{aligned} &T(r,z,t)|_{t=0} = 0; \\ &T(r,z,t)|_{r=R} = T_0 = \text{const}; \\ &T(r,z,t)|_{z=0} = T_0 = \text{const}; \\ &T(r,z,t)|_{z=\beta(t)} = T_0 = \text{const} \end{aligned}\right\}, \quad (15)$$

where T_0 is the temperature value on the surface of the cylinder and on the moving interface. Then the general solution to the problem will take the form:

$$T(r,z,t) = \sum_{\hat{e}=0}^{\infty} I_0(\lambda_{o\hat{e}} r)\left\{e^{-Ät}\left[\frac{R I_1(\lambda_{o\hat{e}} R)}{2\sqrt{\pi Ä}}\int_0^t d\tau \int_0^H \frac{\tilde{N}_1}{\sqrt{t-\tau}} \times\right.\right.$$
$$\times e^{-Ät} e^{-\frac{(z-\xi)^2}{4Ä(t-\tau)}} d\xi + \frac{1}{4\sqrt{\pi}}\int_0^t \frac{z}{[Ä(t-\tau)]^{3/2}} e^{-\frac{z^2}{4Ä(t-\tau)}} K_1(\tau) d\tau + \quad (16)$$
$$\left.\left. + \frac{1}{4\sqrt{\pi}}\int_0^t \frac{z-\beta(\tau)}{[Ä(t-\tau)]^{3/2}} e^{-\frac{[z-\beta(\tau)]^2}{4Ä(t-\tau)}} K_2(\tau) d\tau\right]\right\}.$$

Limiting ourselves to the first term in sum (16), for stationary temperature we have the following expression:

$$T(r,z,t) = Ò_0 J_0\left(\frac{2r}{R}\right) e^{-Ät}\left\{\frac{e^2 J_0\left(\frac{2r}{R}\right)}{16Ä^{3/2}} \ln t + \frac{L J_1\left(\frac{2r}{R}\right)}{16Ä^{3/2}} e^{-Ät} \ln(t-1) + \right.$$

$$+\left(1-\frac{1}{\sqrt{t}}\right)\left(\frac{Д}{z\pi}+\frac{Д^{3/2}}{\pi^2 z\beta(t)}\right)+\left(1-\frac{1}{\sqrt{t}}\right)\frac{2\sqrt{\partial}}{\sqrt{\pi}}\frac{1}{[z-\beta(t)]}\Bigg\}, \quad (17)$$

When deriving (17), we took into account that the equation $I_0(\lambda_{or})=0$ implies $\lambda_0=2r/R$ and $I_1(2)=1$. In equation (17): $D = \lambda/C_p\,\rho$ - thermal diffusivity coefficient, λ - thermal conductivity, C_p - specific heat capacity, ρ - density. For graphite at T = 300 K: λ = 195 W/m K; C_p = 710 J/kg K; ρ - 1910 kg/m^3; D = 1.44 10-4 m^2/s;

If the time t is very large, then as a result we get:

$$\dot{O}(r,z,t)=\frac{Ä^{3/2}\cdot\dot{O}_0}{\pi^2}J_0\left(\frac{2r}{R}\right)\cdot\frac{t}{z\beta(t)}, \quad (18)$$

Let us use the asymptotic representation of the Bessel functions [71], then we obtain:

$$T(r,z,t)=\frac{D^{3/2}\cdot\dot{O}_0}{\pi^{5/2}}\sqrt{\frac{R}{r}}\cdot\frac{t}{z\cdot\beta(t)}, \quad (19)$$

The radial and axial components of the temperature gradient will be equal:

$$\frac{\partial T}{\partial r}=\frac{2Ä^{3/2}\cdot\dot{O}_9\cdot\sqrt{r\cdot R}}{\pi^2}\cdot\frac{t}{z\beta(t)}, \quad (20)$$

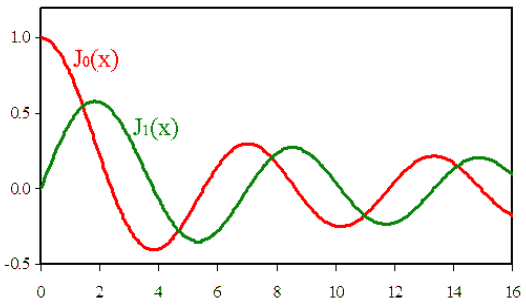

a)

$$\frac{\partial\dot{O}}{\partial z}=\frac{Ä^{3/2}\cdot\dot{O}_0}{\pi^2}J_0\left(\frac{2r}{R}\right)\cdot\frac{2t}{z^2\beta(t)}. \quad (21)$$

We will analyze only the radial component from equation (6), since it leads to a shift of graphite layers and its splitting:

$$\sigma_r=\frac{4Ä^{3/2}\cdot\dot{O}\cdot G\cdot\sqrt{r\cdot R}}{\pi^2\cdot r}\cdot\frac{t}{z\beta(t)}. \quad (22)$$

Let us take r – R, z = β(t), then we get:

$$\beta(t)=\frac{2Ä^{3/4}}{\pi}\cdot\sqrt{\dot{O}}\cdot\sqrt{\frac{G}{\sigma_r}}\cdot\sqrt{t}=\beta_0\cdot\sqrt{t}. \quad (23)$$

Equation (23) mathematically coincides with Stefan's fourth problem, where the freezing of ice is considered, and the movement of phase boundaries $\beta(t) = \beta_0\sqrt{t}$ is called the self-similar law of motion. This issue is discussed in detail in the work of Lyubov B.M. [47].

Solutions (18) will look as shown in Fig. 7a.

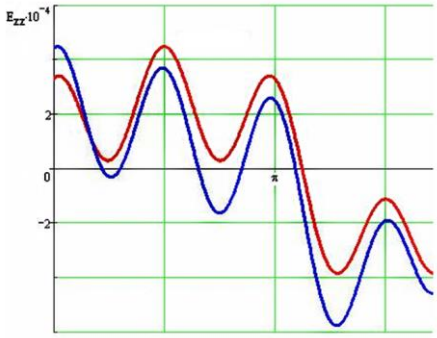

b)

Figure 7. Graphs of Bessel functions (a) and deformation of highly compressed metals (b).

In Fig. 7b shows [72] that a comparison of longitudinal and transverse deformations of highly compressed metals also showed their periodic nature. The experimental and theoretical results we obtained fit into the model of macroscopic localization of plastic flow developed in [73]. This work shows that the localization of plastic flow in solids has a pronounced wave character. Moreover, at the stages of easy sliding, linear and parabolic strain hardening, as well as at the stage of preliminary destruction, the observed localization patterns are different types of wave processes. Analysis of the wave characteristics of such processes made it possible to measure the speed of their propagation (~ 10-4 m/s), wavelength (~ 10-2 m) and establish that the dispersion relation for such waves is quadratic.

Now let's turn to equation (23), where $\beta(t) = \beta_0\sqrt{t}$, $\beta_0 = 0.23\sqrt{T}$.

The components of thermoelastic stresses along the radius r - σr will have the form:

$$\sigma_r=\frac{4Ä^{3/2}\cdot\dot{O}\cdot G\cdot\sqrt{r\cdot R}}{\pi^2\cdot r}\cdot\frac{t}{z\beta(t)}. \quad (24)$$

Let us take r – R, z = β(t), then we get:

$$\sigma_r=\frac{4Ä^{3/2}\cdot\dot{O}\cdot G}{\pi^2}\cdot\frac{t}{\beta(t)^2}=\frac{80Ä^{3/2}\cdot G}{\pi^2}\approx 8Ä^{3/2}\cdot G. \quad (25)$$

Components of thermoelastic stresses for graphite σ_r = 0.24 MPa, which are formed at the interphase boundary separating the R(I) layer from the rest of the volume and associated with relaxation or reconstruction of the graphite surface during its formation. If we compare σr with elastic stresses σisc from table. 3, then their difference is visible by almost three orders of magnitude. This means that it is much easier to obtain graphene mechanically (including ultrasonic splitting, see above) than by changing the temperature gradient.

The components of thermoelastic stresses at the interface are quite difficult to determine. In [74], thermoelastic stresses were calculated in a profiled sapphire single crystal, having the shape of a round rod with a diameter of 10 mm, a length of 100 mm (small parameter ε = 0.05) and grown from a melt using the Stepanov method. Since the given formulas are approximate, the maximum value of this component is σ_r = 1.42 MPa, which is higher than that of graphite. This is due to the fact that graphite's Young's modulus is two orders of magnitude lower than that of sapphire.

According to the principles of thermoelasticity [75], thermoelastic stresses at the interface can be determined by the formula: $\sigma_r = \alpha$ Ec ΔT, α = const. The constant α has not been defined anywhere, so we will determine it using the data from table. 3 and the above value of σ_r. As a result we get:

$$\sigma_r = 10^{-2}\beta^2 \cdot Å_{ñ} \cdot \Delta Ò, \quad (26)$$

where β is the linear expansion coefficient.

Equation (26) shows that it is possible to split graphite using a pulsed picosecond laser ($\beta_2 \sim 10^{-12}$) of the Nd-YAG type for heating. In [76], researchers from the Univ. of Nebraska (USA), together with Chinese scientists, have developed a new approach to producing graphene, based on the exfoliation of crystalline graphite when exposed to laser radiation. A crystal of highly ordered pyrolytic graphite (HOPG) was used as a target, which was placed on a silicon substrate. Graphene synthesis was carried out in an argon atmosphere at a pressure of about 1 Torr. A commercial pulsed Nd:YAG laser with a wavelength of 532 nm, a pulse duration of 7 ns, and a pulse repetition rate of 1 Hz was used as the irradiation source. Laser irradiation provided an energy density on the target in the range from 0.8 to 20 J/cm^2. Carbon particles formed as a result of laser ablation of the graphite surface fell on the Si substrate. When the laser radiation energy density on the target was from 1 to 10 J/cm^2, thin flakes appeared on the HOPG surface, which spontaneously separated from the surface and fell on the surface of the substrate. The resulting graphene samples on a silicon substrate were examined using a scanning electron microscope (SEM), a high-resolution transmission electron microscope (HRTEM), an atomic force microscope (AFM), and a micron-resolution Raman spectrometer (laser wavelength 514 nm). Analysis of Raman spectra indicates that graphene samples consist of several (up to 10) layers. Measurements performed using AFM showed that the thickness of the graphene film is 3.9 nm. TEM images of a graphene film several microns in size indicate its wavy structure (see Fig. 7) and the presence of numerous bends.

In order to study the mechanism of formation of graphene sheets under the action of laser radiation, graphite tablets were used as a target along with HOPG samples. It turned out that irradiation of such tablets at an energy density of 0.8 to 20 J/cm^2 does not lead to the formation of graphene films, but is accompanied by the appearance of nanometer-sized amorphous carbon particles.

In [77], the structural properties and composition of carbon films obtained using pulsed laser evaporation of sublimated carbon tapes were studied. Studies have shown that the resulting films have a graphite-like structure with a low sp3 phase content and can be classified as nanocrystalline defective turbostratic graphite or graphene.

In [78], a study of the process of formation of extended graphitized microstructures in the volume of diamond under the influence of ultrashort and short laser pulses was carried out, as well as a study of the properties, internal structure and prospects for the practical application of these microstructures. Unique features of local laser-induced graphitization, occurring at a considerable distance from the surface of the diamond crystal, have been revealed, which sharply limits the possibility of relaxation of the resulting mechanical stresses (see Table 3) and determines the emergence of a conductive nanostructured heterophase composite, which has also never been observed before. The research carried out laid the scientific foundations for the rapid development of promising technology for laser microstructuring of the volume of diamond crystals.

Conclusion

To split graphite over a layer of thickness R(I), it is necessary to expend energy, which is called adhesion energy and is determined by the Dupre formula. We have shown that $\gamma_1 \approx 0.3\ \gamma_2$, i.e. the surface energy of the R(I) layer is three times less than the bulk phase. This means that the R(I) layer will more easily move along the cleavage plane. Using equations (1) – (5), we calculated the elastic parameters for graphite. To calculate the stress in the layer R(I), when the process of graphite splitting occurs, we come to a problem with a moving phase boundary, which is called the Stefan problem. Our experimental and theoretical results fit into the model of macroscopic localization of plastic flow. The localization of plastic flow in solids has a pronounced wave character. Moreover, at the stages of easy sliding, linear and parabolic strain hardening, as well as at the stage of preliminary destruction, the observed localization patterns are different types of wave processes. Analysis of the wave characteristics of such processes made it possible to measure the speed of their propagation ($\sim 10^{-4}$ m/s), wavelength ($\sim 10^{-2}$ m) and establish that the dispersion relation for such waves is quadratic. According to our proposed model, the components of thermoelastic stresses for graphite are σr = 0.24 MPa, which are formed at the interphase boundary separating the R(I) layer from the rest of the volume and are associated with relaxation or reconstruction of the graphite surface during its formation. If we compare σr with elastic stresses σisc from table. 3, then their difference is visible by almost three orders of magnitude. This means that it is much easier to obtain graphene mechanically (including ultrasonic splitting) than by changing the temperature gradient.

This scientific article was published as part of grant funding for 2024-2026, IRN No. AR32488258 "Development of innovative technology for producing graphene by intercalating graphite with microcluster water and modifying HTSC ceramics with graphene" (the research is funded by the Science Committee of the Ministry of Science and Higher Education of the Republic of Kazakhstan).

References:

1. Stankovich S., Dikin D. A., Dommett G. H. B., Kohlhaas K. M., Zimney E. J., Stach E. A., Piner R. D., Nguyen S. T., Ruoff R. S. Graphene-based composite materials // Nature, 2006, V. 442, № 7100. - P. 282-286.

2. Morozov S.V., Novoselov K.S., Katsnelson M.I., Schedin F., Elias D.C., Jaszczak J.A., Geim A.K.

Giant intrinsic carrier mobilities in graphene and its bilayer // Physical Review Letters, 2008, V. 100, № 1. - P. 4.

3. Lee C., Wei X. D., Kysar J. W., Hone J. Measurement of the elastic properties and intrinsic strength of monolayer graphene // Science, 2008, V. 321, № 5887. - P. 385-388.

4. Balandin A.A., Ghosh S., Bao W.Z., Calizo I., Teweldebrhan D., Miao F., Lau C.N. Superior thermal conductivity of single-layer graphene // Nano Letters, 2008, V. 8, № 3. - P. 902-907.

5. Bonaccorso F., Sun Z., Hasan T., Ferrari A.C. Graphene photonics and optoelectronics // Nature Photonics, 2010, V. 4, № 9. - P. 611-622.

6. Bernhardt T.M., Kaiser B., Rademann K. Formation of superperiodic patterns on highly oriented pyrolytic graphite by manipulation of nanosized graphite sheets with the STM tip // Surface Science, 1998, V. 408, № 1-3. - P. 86-94.

7. Lu X.K., Yu M.F., Huang H., Ruoff R.S. Tailoring graphite with the goal of achieving single sheets // Nanotechnology, 1999, V. 10, № 3. - P. 269-272.

8. Roy H.V., Kallinger C., Marsen B., Sattler K. Manipulation of graphitic sheets using a tunneling microscope // Journal of Applied Physics, 1998, V. 83, № 9. - P. 4695-4699.

9. Novoselov K.S., Geim A.K., Morozov S.V., Jiang D., Zhang Y., Dubonos S.V., Grigorieva I. V., Firsov A.A. Electric field effect in atomically thin carbon films // Science, 2004, V. 306, № 5696. - P. 666-669.

10. Ci L.J., Song L., Jariwala D., Elias A.L., Gao W., Terrones M., Ajayan P.M. Graphene Shape Control by Multistage Cutting and Transfer // Advanced Materials, 2009, V. 21, № 44. - P. 4487-4498.

11. Parvez K., Wu Z. S., Li R.J., Liu X.J., Graf R., Feng X.L., Mullen K. Exfoliation of Graphite into Graphene in Aqueous Solutions of Inorganic Salts // Journal of the American Chemical Society, 2014, V. 136, № 16. - P. 6083-6091.

12. Liang X., Fu Z., Chou S.Y. Graphene transistors fabricated via transfer-printing in device active-areas on large wafer // Nano Letters, 2007, V. 7, № 12. - P. 3840-3844.

13. Brantov S.K. Device for producing thermally split graphite. – Patent of the Republic of Kazakhstan No. 166734. Published 12/10/2016.

14. Van Noorden R. Production: Beyond sticky tape // Nature, 2012, V. 483, № 7389. - P. S32-S33

15. Hernandez Y., Nicolosi V., Lotya M., Blighe F.M., Sun Z.Y., De S., McGovern I.T., Holland B., Byrne M., Gun'ko Y.K., Boland J.J., Niraj P., Duesberg G., Krishnamurthy S., Goodhue R., Hutchison J., Scardaci V., Ferrari A. C. High-yield production of graphene by liquid-phase exfoliation of graphite // Nature Nanotechnology, 2008, V. 3, № 9. - P. 563-568.

16. Lotya M., Hernandez Y., King P.J., Smith R.J., Nicolosi V., Karlsson L.S., Blighe F.M., De S., Wang Z.M., McGovern I.T., Duesberg G.S., Coleman J.N. Liquid Phase Production of Graphene by Exfoliation of Graphite in Surfactant/Water Solutions // Journal of the American Chemical Society, 2009, V. 131, № 10. - P. 3611-3620.

17. Skaltsas T., Ke X.X., Bittencourt C., Tagmatarchis N. Ultrasonication Induces Oxygenated Species and Defects onto Exfoliated Graphene // Journal of Physical Chemistry C., 2013, V. 117, № 44. - P. 23272-23278.

18. Bracamonte M.V., Lacconi G.I., Urreta S.E., Torres L. On the Nature of Defects in Liquid-Phase Exfoliated Graphene // Journal of Physical Chemistry C., 2014, V. 118, № 28. - P. 15455-15459.

19. Denisyuk I.Yu., Logushkova K.Yu., Fokina M.I., Uspenskaya M.V. FT-IR spectra of multilayer graphene and its composition with a surfactant // Optics and Spectroscopy, 2019, vol. 126, issue. 2. – P. 177-179.

20. Rubanik V.V., Savitsky V.O., Rubanik V.V. Jr., Lutsko V.F., Nikiforova I.V., Bui Kh.T., Doan D.F. Preparation of graphene structures and nanopolymers using ultrasonic vibrations // Vector of Science TSU. 2021. No. 3. – P. 74-83.

21. Wu Y.H., Yu T., Shen Z.X. Two-dimensional carbon nanostructures: Fundamental properties, synthesis, characterization, and potential applications // Journal of Applied Physics, 2010, V. 108, № 7, 071301.

22. Hummers Jr.W.S., Offeman R.E. Preparation of graphitic oxide // Journal of the american chemical society, 1958, V. 80, № 6. - P. 1339-1339.

23. Wu J.S., Pisula W., Mullen K. Graphenes as potential material for electronics // Chemical Reviews, 2007, V. 107, № 3. - P. 718-747.

24. Stankovich S., Dikin D. A., Piner R. D., Kohlhaas K. A., Kleinhammes A., Jia Y., Wu Y., Nguyen S.T., Ruoff R.S. Synthesis of graphene-based nanosheets via chemical reduction of exfoliated graphite oxide // Carbon, 2007, V. 45, № 7. - P. 1558-1565.

25. Kroto H.W., Heath J.R., O'Brien S.C., Curl R.F., Smalley R.E. C_{60}: Buckminsterfullerene // Nature, 1985, V. 318. – P. 162-163.

26. Iijima S., Helical microtubules of graphitic carbon // Nature, 1991, V. 354. – P. 56-58.

27. Somani P.R., Somani S.P., Umeno M. Planer nano-graphenes from camphor by CVD // Chemical Physics Letters, 2006, V. 430, № 1-3. - P. 56-59.

28. Obraztsov A.N., Obraztsova E.A., Tyurnina A.V., Zolotukhin A.A. Chemical vapordeposition of thin graphite films of nanometer thickness // Carbon, 2007, V. 45, № 10. - P. 2017-2021.

29. Kim K.S., Zhao Y., Jang H., Lee S.Y., Kim J.M., Kim K.S., Ahn J.H., Kim P., Choi J.Y., Hong B. H. Large-scale pattern growth of graphene films for stretchable transparent electrodes // Nature, 2009, V. 457, № 7230. - P. 706-710.

30. Wang J.J., Zhu M.Y., Outlaw R.A., Zhao X., Manos D.M., Holloway B.C. Synthesis of carbon nanosheets by inductively coupled radio-frequency plasma enhanced chemical vapor deposition // Carbon, 2004, V. 42, № 14. - P. 2867-2872.

31. Berger C., Song Z., Li X., Wu X., Brown N., Naud C., Mayou D., Li T., Hass J., Marchenkov A.N. Electronic confinement and coherence in patterned epitaxial graphene // Science, 2006, V. 312, N. 5777. - P. 1191-1196.

32. Sutter P.W., Flege J.–I., Sutter E.A. Epitaxial graphene on ruthenium // Nature. mater., 2008, V. 7, N. 5. - P. 406-411.

33. Coraux J., N'Diaye A.T., Busse C., Michely T. Structural coherency of graphene on Ir (111) // Nano lett., 2008, V. 8, N. 2. - P. 565-570.

34. Ohta T., Bostwick A., Seyller T. et al. Controlling the electronic structure of bilayer graphene // Science, 2006, Vol. 313, N. 5789. - P.951-954.

35. Virojanadara C., Syvдjarvi M., Yakimova R. et al. Homogeneous large-area graphene layer growth on 6 H -SiC(0001) // Physical Review B., 2008, Vol. 78, N. 24 - P.245403, 1-6.

36. Nikiforov A.A., Kondratenko M.S., Kapitanova O.O., Gallyamov M.O. Electrochemical splitting of graphite in supercritical media // DAN RAS. Chemistry, Materials Science, 2020, Vol. 492–493. - P. 128-133.

37. Lebedev S.P. Preparation of graphene by dissociative evaporation (sublimation) of the SiC surface and study of the properties of graphene/SiC structures. – Dissertation of a candidate in physics and mathematics. Sciences, St. Petersburg, 2021. – 164 p.

38. Kochergin V.K. Platinum-free oxygen reduction catalysts for fuel cells based on plasma-electrochemically split graphite. - Abstract of a candidate of chemical sciences, Moscow, 2022. - 26 p.

39. Yapryntsev A.D. Layered hydroxides of rare earth elements (Y, Eu, Gd, Tb) and materials based on them: synthesis and physicochemical properties. - Dissertation of a candidate of chemical sciences, Moscow, 2021. – 165 p.

40. Gorynin G.L. Method of asymptotic splitting in spatial problems of deformation of layered structures. - Dissertation of Doctor of Physics and Mathematics. Sciences, Novosibirsk, 2006. – 474 p.

41. Vyachkin E.S. Development of methods, algorithms and software for mathematical modeling of layered structures containing volumetrically incompressible layers. - Dissertation of a candidate of technical sciences, Novokuznetsk, 2018. – 112 p.

42. Gorynin G.L., Nemirovsky Yu.V. Spatial problems of bending and torsion of layered structures. Asymptotic splitting method. - Novosibirsk: Science, 2004. - 408 p.

43. Vyachkin E.S., Kaledin V.O., Aulchenko S.M., Bondarenko A.S., Vyachkina E.A. Numerical solution of the problem of deformation of a layered structure with volumetrically incompressible layers // Scientific and Technical Bulletin of the Volga Region. - Kazan, 2016. - No. 6. - P. 117-120.

44. Kolesnikov S.A., Kim L.V., Dudin V.R. Experimental and numerical study of the formation of thermophysical characteristics of carbon composite materials // New Ogneupory, 2019, No. 8 – P. 13-22.

45. Mikhailov V.Yu. Mathematical modeling of the process of foaming oxidized graphite. - Dissertation of the candidate in physics and mathematics. Sciences, Saratov, 2006. – 101 p.

46. Rubinshtein L.I. Stefan's problem. - Riga, 1967. - 457 p.

47. Lyubov B.M. Theory of crystallization in large volumes. - M.: Nauka, 1975. – 256 p.

48. Meirmanov A.M. Stefan's problem. - Novosibirsk: Nauka, 1986. - 239 p.

49. Sigunov Yu.A. Methods for solving the classical Stefan problem. - Surgut: RIO of Surgut State University, 2009. - 140 p.

50. Weinberg A.M. Mathematical modeling of transfer processes. Solution of nonlinear boundary value problems. - Moscow-Jerusalem, 2009. – 210 p.

51. Kot V.A. High-precision polynomial solutions of the classical Stefan problem // Dokl. National acad. Sciences of Belarus, 2017, V. 61, No. 6. - P. 112-122.

52. Vasiliev V.N., Vasilyeva M.V., Stepanov S.N., Sidnyaev N.I., Matveeva O.I., Tseeva A.N. Solution of the two-phase Stefan problem in the enthalpy formulation with smoothing coefficients // Bulletin of MSTU im. N.E. Bauman, 2021, No. 4(97). – P. 4-23.

53. Gupta S.C. The Classical Stefan Problem: Basic Concepts, Modelling and Analysis. - Amsterdam: Elsevier, 2018. - 732 p.

54. Gibbs J.W. Thermodynamic works. - M.: GITTL, 1950. - 303 p.

55. Rusanov A.I. Phase equilibria and surface phenomena. - L.: Chemistry, 1967. -346 p.

56. Oura K., Lifshitz V.G., Saranin A.A., Zotov A.V., Katayama M. Introduction to surface physics. - M.: Nauka, 2006. - 490 p.

57. Mamonova M.V., Prudnikov V.V. Prudnikova I.A. Surface Physics: Theoretical Models and Experimenal Methods. - CRC Press. 2016. - 384 p.

58. Yurov V.M., Guchenko S.A., Laurynas V.Ch. Surface layer thickness, surface energy and atomic volume of an element // Physico-chemical aspects of the study of clusters, nanostructures and nanomaterials, 2018, issue. 10. - P. 691-699.

59. Yurov V.M. The thickness of the surface layer of atomically smooth crystals // Physical and chemical aspects of the study of clusters, nanostructures and nanomaterials, 2019,- Issue. 11. - P. 389-397.

60. Yurov V.M., Goncharenko V.I., Oleshko V.S., Sha Mingun. Anisotropy of the surface of carbon materials // Eurasian Physical Technical Journal, 2021, Vol. 18, No. 3(37). – P. 15-24.

61. Panin V.E., Sergeev V.P., Panin A.V. Nanostructuring of surface layers of structural materials and application of nanostructured coatings. – Tomsk: Publishing house TPU, 2010. - 254 p.

62. Rekhviashvili S.Sh., Kishtikova E.V., Karmokova R.Yu. On the calculation of the Tolman constant // Letters to ZhTF, 2007, V. 33, Issue. 2.-P.1–7.

63. Zimon A.D. Adhesion of films and coatings. - M.: Chemistry, 1977. - 352 p.

64. Yurov V.M., Goncharenko V.I., Oleshko V.S. Study of primary nanocracks in atomically smooth metals // Letters to ZhTP, 2023, vol. 49, issue. 8. - P. 35-38.

65. Ioffe A.F. Report on the work of the Institute of Physics and Technology // UFN, 1936, Vol. XVI, No. 7. – P. 848-871.

66. Frenkel V.Ya. Abram Fedorovich Ioffe (Biographical sketch) // UFN, 1980, Vol. 132, No. 1. - P. 11-45.

67. Griffith A.A. The theory of rupture // In Proc. Ist. Congr. Appl. Mech.-Delft., 1924. - P. 55-63.

68. Yurov V.M., Kuketaev T.A. Crystallization of a cylinder of finite dimensions // Ruk. dep. in VINITI. 1982. No. 6485-82 Dep..

69. Yurov V.M., Platonova E.S., Guchenko S.A. Corrosion and Stefan's problem // Sciences of Europe, 2019, No. 45(2). – P. 48-53.

70. Zarubin V.S., Kuvyrkin G.N. Mathematical models of thermomechanics. - M.: Fizmatlit. 2002. - 168 p.

71. Gavrilov V.S., Denisova N.A., Kalinin A.V. Bessel functions in problems of mathematical physics. - Nizhny Novgorod: Publishing House of Nizhny Novgorod State University, 2014. – 40 p.

72. Opanasyuk A.A. Periodic oscillatory nature of deformation of highly compressed rock samples // Improvement of technology for the construction of mines and underground structures. Sat. scientific works – Donetsk: "Nord-Press", 2006, Vol. No. 12. - P. 79-80.

73. Zuev L.B. Danilov V.I., Barannikova S.A. Physics of macrolocalization of plastic flow. - Novosibirsk: Science, 2008. - 328 p.

74. Bakholdin S.I., Galaktionov E.V., Tropp E.A. Calculation of thermoelastic stresses near the crystallization front for single-crystalline rods of round cross-section grown from a melt // Journal of Technical Physics, 2014, vol. 84, issue. 8. – P. 1-7.

75. Novatsky V. Dynamic problems of thermoelasticity. - M.: Mir, 1979. - 256 p.

76. Min Qian, Yun Shen Zhou, Yang Gao et al. Formation of graphene sheets through laser exfoliation of highly ordered pyrolytic graphite // Appl. Phys. Lett., 2011, V. 98, 173108.

77. Ershov I.V., Prutsakova N.V., Kholodova O.M., Lavrentiev A.A., Mardasova I.V., Zhdanova T.P. Structural properties and composition of graphite-like carbon films obtained by pulsed laser evaporation // Journal of Technical Physics, 2021, vol/ 91, issue. 4. – P. 635-642.

78. Kononenko T.V. Laser-induced graphitized microstructures in the bulk of diamond. - Dissertation of Doctor of Physical and Mathematical Sciences, Moscow, 2022. – 196 p.

ON THE QUESTION OF STONE–WELES DEFECTS IN GRAPHENE

Yurov V.,
Karaganda Technical University, candidate of phys.-mat. sciences, associate professor, Kazakhstan, Karaganda
Zhangozin K.
TSK Vostok LLP, candidate of phys.-mat. sciences, associate professor, Kazakhstan, Ust-Kamenogorsk
https://doi.org/10.5281/zenodo.10492440

Abstract

In this article, we examined the SW defect in graphene and, after a brief review of previous studies, proposed a model for its origin. This model is based on the thickness of the surface layer R(I) of graphene, equal to the length of the nanocrack L_{nm}. Based on this model, elastic parameters for graphite and graphene are calculated. It is shown that large internal stresses between the graphene plane and the air gap lead to warping of the graphene surface, detected experimentally and theoretically. These internal stresses arise due to the relaxation of the graphene surface. For the same reason, SW defects and other defects arise in graphene through the Frank-Read model. We considered the SW defect from the standpoint of: birth → migration → annihilation → destruction of a graphene sheet. We have already considered the birth of the SW defect. This dislocation (nanocrack) has an autowave character. The maximum speed of movement (migration) of a dislocation (nanocrack) for graphene is $V_{max} \approx 10^4$ m/s. The brake on the movement of dislocations in pure graphene can be the Peierls–Nabarro barrier and internal friction. The Peierls–Nabarro barrier is significantly less than the energy of motion of the dislocation $F(I)_{aP\text{-}N} L << m V^2_{max}/2$. The brake on the movement of SW dislocations is terahertz oscillations or plasmons in graphene. Annihilation of edge dislocations of opposite signs occurs with the dipole arm in the range $l > 11.5 – 16$ Å. We have presented all the parameters of graphene for calculating the force, deformation and energy criteria for destruction.

Keywords: *graphene, defect, surface layer, nanocrack, dislocation, birth, migration, annihilation, destruction of a graphene sheet.*

Introduction

In quasi -alarm solids there are topological defects that arise as a result of regrouping of intermediary ties [1]. In Grafen [2] - a crystal with a hexagonal grate - a simple defect of this type is a defect of Stone -Wels (SW) [3]. It is formed when one of the bonds of C-C in the plane of the monofry at an angle of 90° (transformation of Stone -Wels [1]), which leads to the appearance of two seven -angles and two pentagons.

In addition to graphene, graphan [4], graphin [5], graphdin [6], diaman on the SiC (0001), fluorine diamond (F-diaman) on the CuNI substrate (111) [8], as well as quasi-alarmed were synthesized. Composite of polyanilin and oxide graphene [9]. Theoretically proposed a number of stable two-dimensional allotles of carbon: metal R-10 graphene [10]; carbon monoxide 123-E8Y24-1 [11], two sp^2+sp^3 hybridized structures [12]; PHH-graphite [13]. Most recently, theoretically predicted thermodynamically stable single -layer structures - azuratial [14] and Stone - Wales graphene (SWG) [15]. Stone - Wales graphene, in his two-layer modification, was considered in the work [16].

In this article, we will consider SW - defect in graphene, after a brief review of previous studies, from the standpoint of the causes of its origin.

Structure and properties SW - defect

In [17], two types of SW defects are proposed, namely S-W1 and S-W2, which are caused by a rotation of 90° C-C connections in different directions, as shown in Fig. 1.

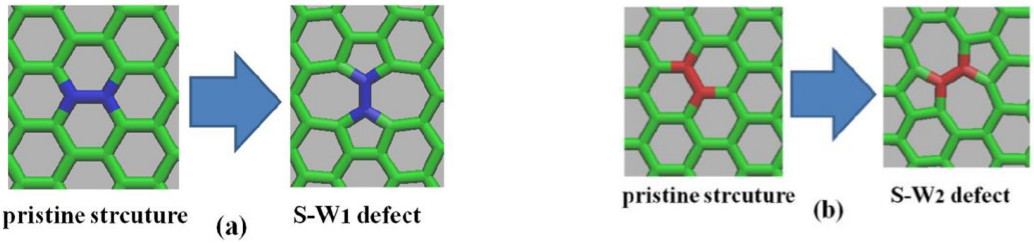

Figure 1. Two types of defects of Stone-Wales: (a) Blue connection CC rotates 90° to the defect S-W1; (b) the red bond CC is rotated 90 ° to the defect of the S-W2 [17].

At the stress of deformation for the graphene sheet ε = 0.0125, the energy barrier for the S-W1 defect is 53.9 EV, which is slightly lower than for the S-W2 61.1 EV defect (Fig. 2). In Fig. 3a shows a change in energy barriers. For the formation of defects S-W1 and S-W2 with an increase in mechanical deformation. Regardless of the level of deformation, the barrier for the S-W1 defect is constantly lower than for S-W2,

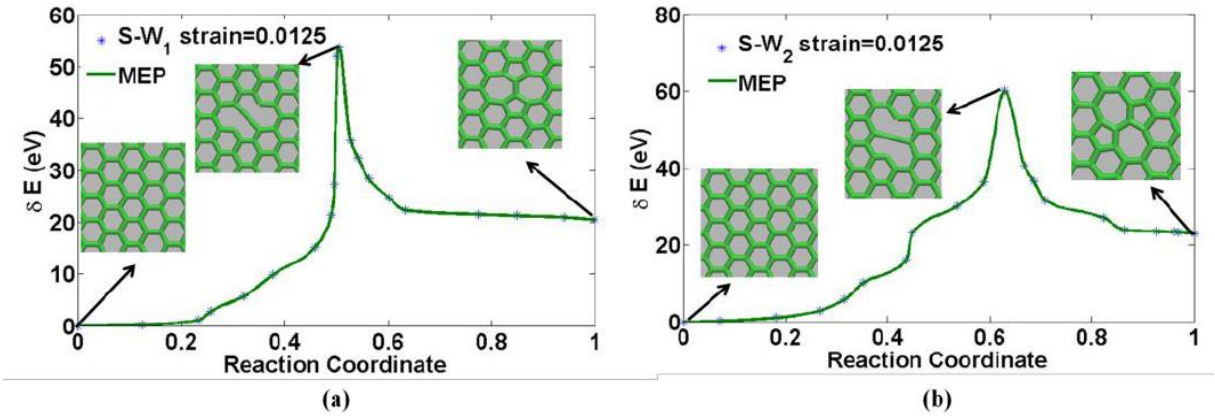

Figure 2. The minimum energy path (MEP) of the emergence of the defect S-W1 (A) and the origin of the defect S-W2 (b) during stretching deformation ε = 0.0125 [17].

This indicates that the S-W1 defect is kinetically more profitable than the S-W2. Obviously, the required energy decreases with an increase in deformation. Energy barriers for generating S-W1 and S-W2 are 16.8 EV and 28.9 EV, respectively. In Fig. 3b shows that the strength of the break is reduced with an increase in temperature. The loss of strength of the S-W2 defect is greater than the S-W1 defect due to its lower energy barrier. In a recent review article [18], it is believed that using the DFT methods, the energy barrier is about 10 EV (compared with work [17]). About the defect of Stone-Weyl (SW), see Fig. 4.

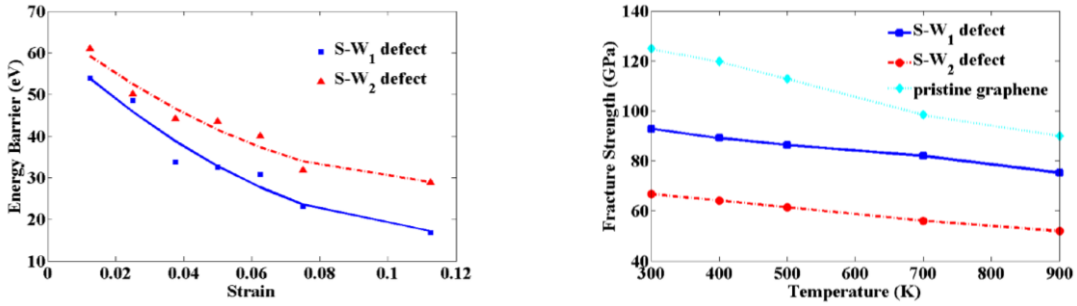

Figure 3. Energy barriers S-W1 (squares) and S-W2 (triangles) depending on the deformation of stretching; The strength for the destruction of the original graphene (green), the defective graphene S-W1 (blue) and defective graphene S-W2 (red) depending on the temperature [17].

Rapid cooling from high temperatures or irradiation with an electron beam can cause SW defects. These results are obtained within the framework of the theory of density functionality using the method of nonequilibrium green functions and in the approximation of local density with various configurations of single -wall graphene nanotubes with SW defects. In this work, the evolution of the passage spectrum with an increase in displacement voltage, states density, voltamper characteristics and the differential conductivity of the puppies under consideration are calculated. Features of the density of electronic states of defective carbon nanotubes were found with energies of ~ 0.5 eV and -1.92 eV above the level of Fermi. It is shown that the nature of the current flowing through defective graphene nanotubes depends on the length of the defects of the SW. It was revealed that the graphene nanotubes with two sequentially connected SW defects with a displacement voltage of ± 2.6 V has a negative differential conductivity -170 μS.

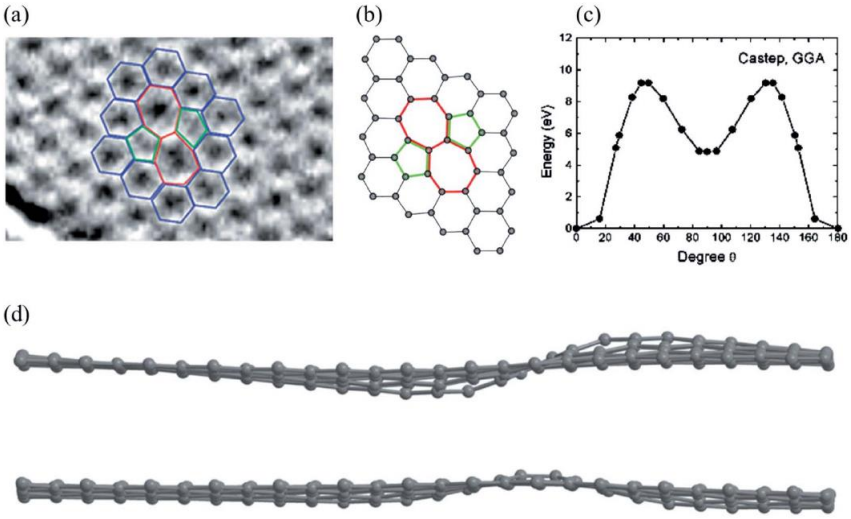

Figure 4. Stone-Wales defect: (a) experimental TEM image; (b) DFT calculated image; (c) energy barrier for bond rotation calculated by DFT; (d) Image of sine and cosine-like configurations calculated by DFT [18].

Molecular dynamics (MD) simulations showed that SW defects significantly reduced the strain failure and intrinsic strength of monolayer graphene sheet. SW defects in graphene can alter its physical properties and alter its chemical properties by acting as active sites for the adsorption of other atoms and molecules, increasing local chemical reactivity. In [19], the formation and movement of SW dislocations in graphene was studied in real time using high-resolution transmission electron microscopy (Fig. 5). SW dislocations move by sliding or crawling at a speed of ~ 0.1 nm/min. Each dislocation creates a deformation field in its vicinity, which extends over a length of ~1 nm.

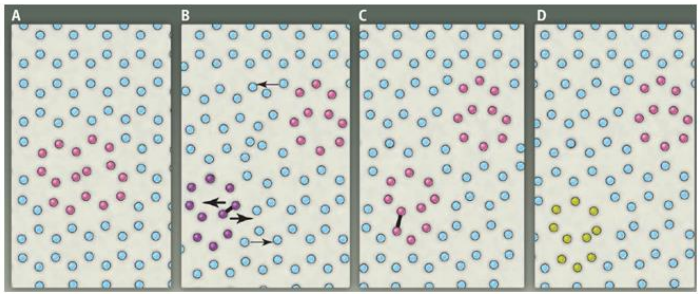

Figure 5. (A) Stone-Wales defect in graphene. (B) Dislocations in graphene. Thin arrows are Burgers vectors. Thick arrows show the directions of displacement of atoms when a dislocation glides to the right. (C) Atomic configuration resulting from sliding. If an electron beam knocks out two labeled atoms, then the dislocation creeps down. (D) Atomic configuration after crawling [19].

Ourmodel of SW – defect (dislocation)

As stated above, SW - defect is formed during rapid cooling from high temperatures or during irradiation with an electron beam. This is not entirely true. In the 20s of the twentieth century, academician A.F. Ioffe conducted a series of experiments with a NaCl crystal and he obtained a fracture of this salt in the amount of 0.4 g/mm2 instead of 200 g/mm2 according to the quantum mechanical theory of Max Born [20]. A.F. Ioffe related this to the existence of microcracks in the surface layer. Then he dipped a NaCl crystal into water and measured the hardness of its surface, which increased as the surface layer dissolved, approaching the theoretical value. This experiment was called the "Ioffe effect" [21]. Only in 2018 did it become clear to us how theoretically it is possible to determine the thickness of the surface layer (see below), where defects are mainly formed [22]. Thus, for a NaCl crystal, according to our model, R(I) = 4.6 nm (which is typical for nanostructures) and the number of monolayers n = R(I)/a = 8 (a is the lattice constant). It is not difficult to wash off 8 monolayers of NaCl with water to obtain the Ioffe effect.

Griffiths [23] in the same 20s of the twentieth century examined the change in the energy of a body with a crack under loading and obtained an energy criterion for destruction, according to which a crack acquires the ability to propagate only when the rate of release of elastic energy during growth becomes equal to or exceeds the energy of the newly formed surfaces.

Frenkel [24] and Schottky [25] proposed their models of defects in solids (Fig. 6). A Frenkel defect is formed when an atom (ion) moves from a crystal lattice site to an interstitial site. A Schottky defect is formed when individual atoms located near the surface, as a result of thermal motion, leave the bulk to the surface, and the resulting vacancy then migrates deep into the crystal [26]. These models laid the foundation for the physics of real crystals.

The fact that defects are formed first in the surface layer (Ioffe effect) is due to the fact that atoms (ions)

on the surface have a different environment than the atoms inside the crystal. The possibility of the appearance of surface states was first predicted by Tamm [27]. Such surface states subsequently became known as Tamm states.

Currently, there are two approaches: the Gibbs approach [28], in which the surface layer is conventionally considered as a geometric surface without thickness; the approach of Van der Wals [29], Guggenheim [30], Rusanov [31], in which the surface layer is considered as a layer of finite thickness. According to modern concepts [32], the surface phase is understood as an ultrathin film (surface layer) that is in equilibrium with a crystalline base (substrate), the properties and structure of which are different from the bulk properties. However, the question of the theoretical "thickness" of this surface layer for various substances remained open until 2018.

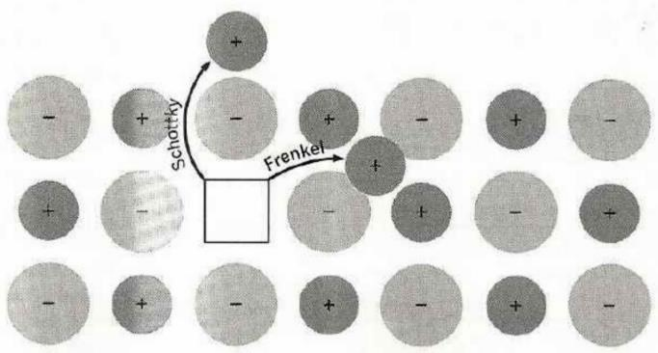

Figure 6. Defects according to Frenkel and Schottky [26].

Only after our work [22, 33] did it become clear how the thickness of the surface layer of a solid, which plays a big role in nanotechnology and mesomechanics, can be theoretically determined [34]. We will consider the thickness of the surface layer of graphite and graphene. The works [22, 33] generalize our proposed model of the surface layer of atomically smooth metals. To determine the thickness of the surface layer of various compounds, the size dependence of the melting temperature $T_m(r)$ was used:

$$\begin{aligned} T_m(r) &= T_m(\infty)\cdot(1-R(I)/r), \qquad r >> R(I), \\ T_m(r) &= T_m(\infty)\cdot(1-R(I)/R(I)+r), \qquad R(0) \le r \le R(I). \end{aligned} \tag{1}$$

Here the first formula coincides with the formula of R. Tolman [35], where R(I) = 2δ, δ is the Tolman parameter, which is not determined experimentally. The second formula is further defined in the region R(0) ≤ r ≤ (R(I), so that at r = 0 the first formula does not go to infinity. The parameter R(I) is related to the surface energy γ by the formula [22]:

$$R(I) = 2\gamma\upsilon/RT\,. \tag{2}$$

Here γ is the surface energy of the massive sample; υ – volume of one mole; R – gas constant; T – temperature. In [36] it is shown that, with an accuracy of up to 3%,:

$$\gamma = 0{,}70\cdot10^{-3}\cdot T_m \ \ [J/m^2], \tag{3}$$

where T_m is the melting temperature of the solid (K). The relationship holds for all metals and for other crystalline compounds. At T = T_m from (2) we obtain:

$$R(I) = L_{nm} = 0{,}17\cdot10^{-9}\cdot\alpha\cdot\upsilon \ \ (m). \tag{4}$$

Here we took into account that, according to our work [37], the thickness of the surface layer is equal to the length of the nanocrack, i.e. R(I) = L_{nm}, and α = 1 m^{-2}, so that the dimensionality of the quantities is respected.

This model is shown schematically in Fig. 7a. Equation (4) shows that the thickness of the surface layer R(I) and the length of nanocracks Lnm are determined by one parameter - the molar (atomic) volume of the element (υ = M/ρ, M is the molar mass (kg/mol), ρ is the density (kg /m3)), which periodically changes in accordance with table D.I. Mendeleev (Fig. 7b). From Fig. 7b shows that carbon is at the beginning of the periodic table next to boron and beryllium. Using equations (1) – (4) we calculate the surface layer R(I) for graphite and graphene.

Table 1.

Parameters of graphite and grapheme

Carbon	ρ, g/sm^3	T_m, K	$R(I)_a=L_{nma}$, nm	$R(I)_c=L_{nmc}$, nm	γ_a, mJ/m^2	γ_c, mJ/m^2
Graphite	2,26	3970	0,90 (3)	2,46 (3)	2779	591
Graphene	2,26	4510	0,246 (1)	-	3157	-

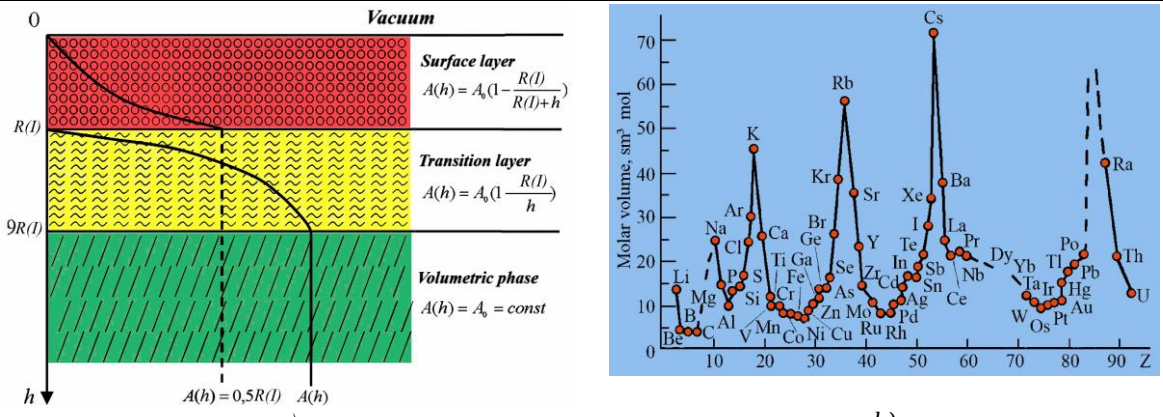

a) *b)*

Figure 7. Schematic representation of the surface layer (a), periodic change atomic volume of elements (b).

Graphite [38] is a thermodynamically stable allotropic modification of carbon - an element of the 4th group of the main subgroup of the 2nd period of the periodic system, serial number 6, atomic mass of a natural mixture of isotopes 12.0107 g/mol. The theoretical density of 2.26 g/cm3 is achieved only in natural graphite. The thickness of the surface layer and the length of graphite nanocracks in the longitudinal direction is $R(I)_a = L_{nma} = 0.90$ nm, and in the perpendicular direction $R(I)_c = L_{nmc} = 2.46$ nm, which is a nanostructure according to Gleiter [39]. The number of graphite monolayers is n = R(I)/a = 3, which makes it easy to obtain graphene from it, even mechanically [2]. Graphene is a two-dimensional allotropic modification of carbon, formed by a layer of carbon atoms one atom thick (R(I) = a = 0.246 nm - lattice constant), which are in a state of sp2 hybridization [2]. Carbon atoms in graphene layers are in a three-coordinated state, i.e. each of them forms covalent bonds with three neighbors. As a result, a network of hexagons is formed, the vertices of which are carbon atoms, carbon-carbon bonds form the corresponding sides. The melting point of graphene is T_m = 4510 K [40]. In the surface layer R(I), relaxation or reconstruction [32] of atomic monolayers occurs (Fig. 8).

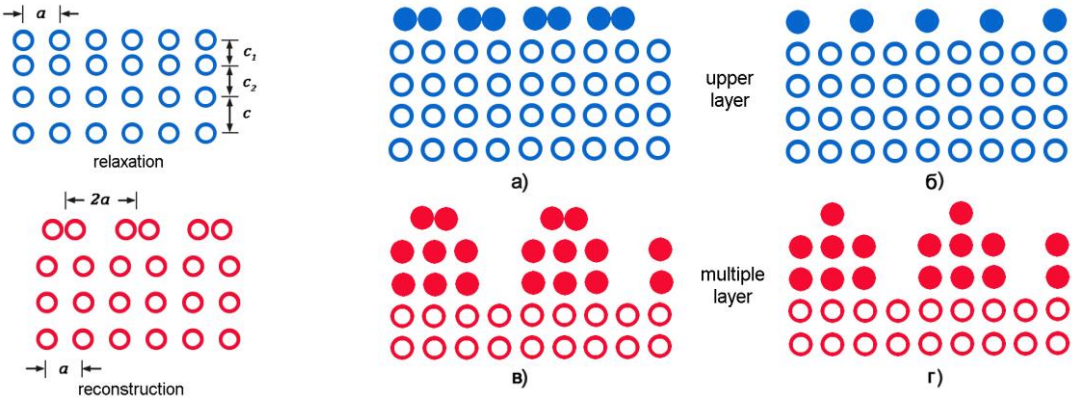

Figure 8. – Transformation of the crystal surface

Size effects in the R(I) layer are determined by the entire collective of atoms in the system (collective processes). Such "quasi-classical" size effects are observed only in nanoparticles and nanostructures [41]. Experimentally, R(I) can be observed on very pure single crystals in high vacuum with grazing incidence of X-ray radiation, when the angle of incidence is equal to or less than the critical angle of total internal reflection [32]. When the angle of incidence becomes less than the critical one, the refracted wave decays exponentially in the volume at a characteristic depth of the order of several nanometers (for example, for silicon this depth is R(I) = 3.2 nm, and for gold R(I) = 1.2 nm) [32].

To separate the R(I) layer from the rest of the crystal, it is necessary to expend energy, which is called adhesion energy [42]:

$$W_a = \gamma_1 + \gamma_2 - \gamma_{12} \approx \gamma_1 + \gamma_2 = 1.3\gamma_2, \quad (5)$$

where γ_{12} is the surface energy at the phase interface, which is negligible due to a second-order phase transition.

Internal voltages σis between phases γ_1 and γ_2 can be calculated using the formula [42]:

$$\sigma_{is} = \sqrt{W_a \cdot Å / R(I)}, \quad (6)$$

where E is Young's modulus of elasticity.

Using equations (5) – (6), we calculate the elastic parameters for graphite and graphene.

Table 2.

Elastic parameters of graphite and grapheme

Carbon	W_{aa}, J/m^2	W_{ac}, J/m^2	σ_{isa}, GPa	σ_{isc}, GPa	E_a, GPa	E_c, GPa
Graphite	3,613	1,323	5,74	1,37	7,59	3,48
Graphene	4,100	-	130,4	-	1020	-

Large internal stresses σis between the graphene plane and the air gap lead to warping of the graphene surface, which was discovered experimentally and theoretically in [43, 44]. According to the authors of [17, 19, 45], a SW defect can be considered as a dislocation dipole (DD), in which two edge dislocations with opposite signs (see Fig. 1) of the Burgers vector are shifted by one lattice period. As a rule, the presence of DD leads to warping of graphene [43, 44].

For SW dislocations to move in graphene, they need to overcome a potential barrier. Today, there are several mechanisms of dislocation braking, which can be divided into two groups. The first group discusses the inhibition of dislocations due to the presence of potential barriers in crystals caused by various structural defects, including the Peierls–Nabarro barrier. The second group discusses the inhibition of dislocations due to the presence of dynamic interaction in crystals. This includes interaction with electrons, phonons, excitons, magnons and other elementary excitations of the crystal lattice. The role of the latter excitations is insignificant for most crystals, but the interaction with phonons is most significant. The Peierls–Nabarro barrier always exists, since it is equal to the force of interatomic interaction in solids [46, 47]. In contrast to the Frenkel–Kontorova model [48], as well as works [49, 50] and others, we will propose a model that can be used to estimate the barrier $F(I)_{P\text{-}N}$ and $\sigma(I)_{P\text{-}N}$ Peierls – Nabarro stress [51]:

$$\begin{aligned} F(I)_{P\text{-}N} &= \gamma \cdot R(I)/n = \gamma \cdot a, \\ \sigma(I)_{P\text{-}N} &= F(I)_{P-N}/S = \gamma/a = E \cdot \varepsilon(I), \end{aligned} \quad (7)$$

where n is the number of layers in layer R(I); a is the lattice constant; S – barrier area (a^2), $\sigma(I)_{P\text{-}N}$, – Peierls–Nabarro stress; E – Young's modulus; ε represents the relative elongation of the lattice parameter in the direction of the external force F.

Relation (7) shows that the Peierls–Nabarro barrier in the R(I) layer is completely determined by experimentally determined values and is presented in Table. 3. You can add the term sin(2πz/a) to equation (7) and show the relief of the Peierls–Nabarro barrier [49-50] (see Fig. 4d).

Table 3.

Barrier F(I) and σ(I) Peierls – Nabarro stress of graphite and grapheme

Carbon	Structure	$F(I)_{aP\text{-}N}$, 10^{-9} N	$F(I)_{cP\text{-}N}$, 10^{-9} N	$\sigma(I)_{aP\text{-}N}$, MPa	$\sigma(I)_{cP\text{-}N}$, MPa
Graphite	$P6_3/mmc$	0,23	0,13	3783	294
Graphene	hexagon.	0,26	-	4268	-

From the table Figure 3 shows that the barrier value F(I) and the Peierls–Nabarro stress σ(I) for graphite and graphene in the longitudinal plane do not differ much, since the thickness of the surface layer is three graphene monolayers. It follows from this that the SW defect is an edge dislocation in graphene that is capable of moving (Fig. 5). More precisely, a SW defect can be considered as a dislocation dipole (DD), in which two edge dislocations with opposite signs (see Fig. 1) of the Burgers vector are shifted by one lattice period [45]. The second conclusion that follows from table. 2 and 3, is that the SW defect does not arise during the rapid cooling of graphene or when it is irradiated with electrons, but due to the formation of a surface and the appearance of internal stresses in it. The length of the edge dislocation (nanocrack) of graphene is L_{nma} = 0.246 nm [52], which after its relaxation becomes equal to $L_{\mu ma}$ = 24.6 nm [53]. Let's look at the table. 2 and consider the question: can internal stresses σis in the R(I) layer become sources of dislocations? Let us consider the Frank-Reed model for graphene, set out in [54]. According to this model, a dislocation behaves like an elastic thread and bends due to internal stresses τ = Gb/L, where G is the shear modulus; b – Burgers vector; L – dislocation length. For graphene G = E/1+ν = 1457 GPa [44], b = 0.24 nm [45], L_{nma} = 0.246 nm [53]. As a result, τ = 1421 GPa instead of σ_{is} = 130.4 GPa from Table. 2, i.e. $\tau > \sigma_{is}$ and this means that the Frank-Reed model can be a source of dislocations for graphene. The dislocation density is $\rho_{nm} = (L_{nma}\, b)^{-1}$ [55] and for graphene $\rho_{nm} = 4.2\ 10^{14}$ cm^{-2}. At such a dislocation density, it turns into a nanocrack [19, 56, 57].

Let us now consider the speed of movement of the nanocrack. The maximum crack propagation speed according to Griffiths theory is [58]:

$$V_C = \beta \cdot V_0 \cdot (1 - \gamma_1 / W_a)^{1/2} \quad (8)$$

and is about 1/3 of the speed of sound V_0 in the material.

After Griffiths, a significant number of works were published in which various models of crack development were analyzed, but we make a choice in work [59], where it became possible to calculate the maximum crack propagation speed Vmax in solid materials for which the main mechanical characteristics are known (E – Young's modulus, ν - Poisson's ratio, ρ - material density):

$$V_{\max} = \frac{dL}{dt} = \sqrt{\frac{1-\nu}{4(1+\nu)[\nu^2 - 3\nu/2 + 7/8)\ln 5{,}2 - 3\nu/8 + 3/32]}} \cdot \sqrt{\frac{E}{\rho}},$$

$$\text{at } \nu = 0{,}25 \quad V_{\max} = 0{,}38 \cdot \sqrt{\frac{E}{\rho}}. \tag{9}$$

Using the values from table. 1 and 2, we calculate V_{max} for graphene: $V_{max} \approx 10^4$ m/s. The calculated speed of sound in graphene was 50334 m/s, which is much higher than the experimental values for graphite (1470 m/s), diamond (12000 - 18350 m/s), single-walled carbon nanotubes (31470 m/s) and graphene (13600 - 21300 m/s) [60-63]. The average value of 1/3 of the speed of sound in graphene is 1.2 10^4 m/s (from experiment), which almost coincides with the Vmax value we calculated using formula (9). This means that the Griffiths formula for the maximum speed of crack propagation is also valid. However, calculating this speed using formula (8) is much more difficult (β, γ_1, W_a) than using formula (9) - (E, ρ).

Let us summarize the above and imagine the SW defect from the standpoint of: birth → migration → annihilation → destruction of a graphene sheet.

Birth (creation) of SW – dislocations (nanocracks) in graphene

SW – dislocation in graphene occurs due to the formation of a surface and the appearance of internal stresses in it. The length of the edge dislocation (nanocrack) of graphene is L_{nma} = 0.246 nm [52], which after its relaxation becomes equal to $L_{\mu ma}$ = 24.6 nm [53]. It was shown above that the Frank-Reed model can be a source of dislocations for graphene. The birth of a dislocation dipole in graphene is taken from [57] and shown in Fig. 9, however, the interpretation of the results in this work is different from that proposed by us. This dislocation (nanocrack) has an autowave character, shown in Fig. 4d and here's why? In open systems of inanimate nature, which constantly receive negative entropy and matter from the external environment, stationary nonequilibrium states with a high degree of order can arise [64, 65]. The processes in which self-organization phenomena occur include autowave processes (AWP) [66-70]. AWP is usually understood as a self-sustaining wave process (including stationary structures) in an active nonlinear medium, which maintains its characteristics constant due to an energy source distributed in the medium [71-73].

These characteristics - period, wavelength (or pulse), propagation speed, amplitude and shape - in a steady state depend only on the local properties of the medium and do not depend on the initial ones, but rather far from the boundaries of the medium and from the boundary conditions.

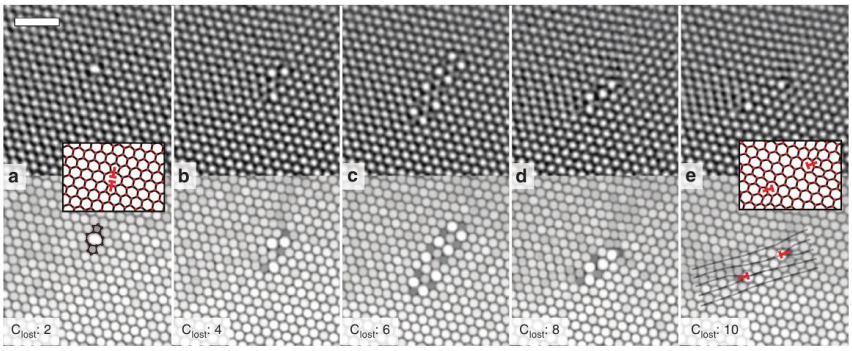

Figure 9. Birth of a dislocation dipole in graphene. The top panels show the original AC-HRTEM images with low-pass Fourier filtering applied, while the bottom panels show frames with maximum filtering applied for better visibility. In panel a, two atoms have been removed, forming a divacancy. In each subsequent panel b–e, two more atoms were removed and the defect underwent significant reorganization. In panel e, after ten missing atoms, the defect structure has reorganized into a dislocation dipole with two edge dislocations at its ends pointing away from each other. The scale bar is 1 nm [57].

Migration of SW – dislocations (nanocracks) in graphene

We showed above that the maximum speed of movement (migration) of a dislocation (nanocrack) for graphene is Vmax ≈ 104 m/s. The brake on the movement of dislocations in pure graphene can be the Peierls–Nabarro barrier and internal friction. The Peierls–Nabarro barrier is significantly less than the energy of motion of the dislocation $F(I)_{aP\text{-}N}$ L << m $V^2_{max}/2$.

A measure of internal friction is the inverse quality factor Q^{-1}, which is equal according to Debye [74]:

$$Q^{-1} = 2Q^{-1}_{\max} \frac{2\pi f\tau}{1 + (2\pi f\tau)^2}, \tag{10}$$

where f is the vibration frequency of the sample, τ is the relaxation time.

The maximum value of internal friction is achieved at 2πfτ = 1. The relaxation time τ can be determined for the layer R(I), knowing the speed of sound in graphene - τ1 = R(I)/υ: τ = 0.246 10^{-9}/13600 = 1.8 10^{-14} s, f = 0.3 1014 = 30 10^{12} Hz = 30 THz. This means that a terahertz oscillation (radiation) is observed for the R(I) layer in graphene (Fig. 10) [75]. In graphene,

the maximum frequency f of low-amplitude phonon vibrations is 46 THz [76, 77], which is in good agreement with our value. This means that the brake on the movement of SW dislocations is terahertz vibrations or plasmons in graphene.

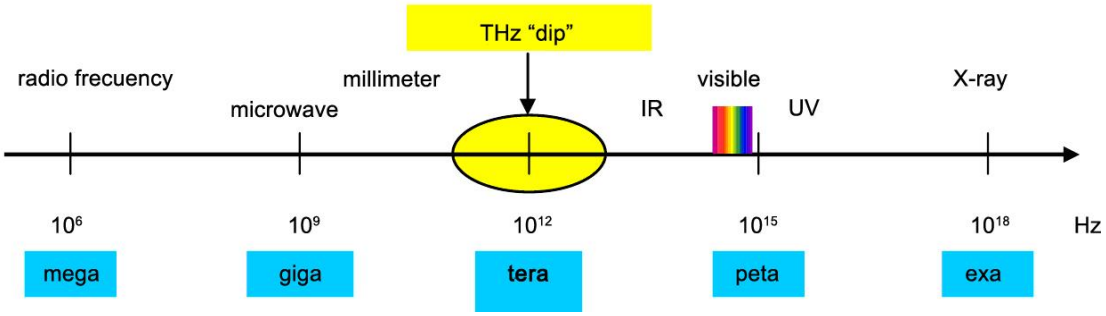

Figure 10. Spectrum of electromagnetic waves and terahertz "dip".

In recent years, a number of both theoretical [78–80] and experimental [81–83] works have appeared devoted to the study of plasmons in graphene. The use of graphene plasmons makes it possible to obtain significantly stronger nonlinear effects in the THz frequency range compared to THz photons. This occurs due to the fact that the group velocity of plasmons in graphene is two to three orders of magnitude lower than the speed of light in vacuum and the plasmon field is highly localized near the graphene layer. This, in turn, leads to significant inhibition of the movement of dislocations.

Annihilation of SW – dislocations (nanocracks) in graphene

The dynamics of SW dislocations and their annihilation were carried out in a number of works [84–86]. These works described the annihilation of a pair of dislocations using a combined DFT and MD method. We will take the most recent work on the motion of dislocations and their annihilation [45, 87–89]. In [87], the time evolution of a pair of dislocations in graphene is studied by performing molecular dynamics simulations on a subnanosecond scale based on the tight coupling density functional method. The simulation shows self-healing of the graphene lattice, leading to complete annihilation of dislocations, that is, to the formation of the pristine graphene structure. Unusual local bond states arise mainly due to the geometric features of the out-of-plane deformation of dislocation structures. Dislocation annihilation was studied by DFTB/MD simulation of graphene containing dislocations on a subnanosecond scale. To approximate the local heating caused by electron beam irradiation and induce structural changes within the available simulation time, the system temperature was between 3000 and 3500 K. In Fig. 11 compares DFTB results with DFT results for paired dislocation structures.

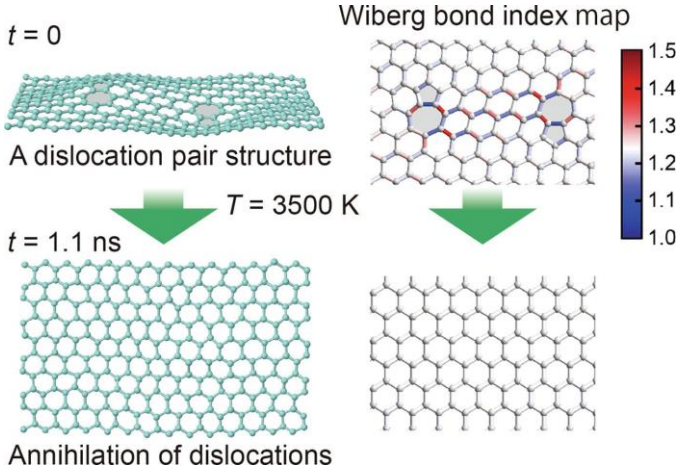

Figure 11. Comparison of DFTB results (left) with DFT results (right) [87].

It was shown in [88] that an arm length of 9.3 Å is close to the equilibrium value at which dislocation annihilation is not observed, and annihilation occurs at an arm length l >11.5 Å. It was established in [89] that annihilation is possible for dislocation dipoles with arm length l >16 Å. Annihilation can easily occur at high temperatures.

Let us turn to the data obtained within the framework of our model. The increase in dislocation density during deformation is caused by the intersection of newly generated and existing dislocations. The average path length of dislocations L with the Burgers vector b and their density ρ depend on the degree of deformation ε as [90]:

$$\varepsilon_{nm} = \rho_{nm} \cdot b \cdot L_{nm} \quad (11)$$

For graphene ρ_{nm} = 4.2 10^{18} m^{-2} b = 0.24 10^{-9} m, L_{nma} = 0.246 10^{-9} m, then it turns out that ε_{nm} = 0.248. In [45], at T = 300 K for dislocations in graphene with a dipole arm l = 15 Å, the value ε_F = 0.24 was obtained. This result was obtained by the MD method and differs slightly from our value of ε_{nm}. The internal stresses can be estimated in the form [90]:

$$\sigma = \tilde{N}_1 \cdot G \cdot b \cdot \rho^{1/2}, \quad (12)$$

where C_1 is a constant of the order of 0.2 and G is the shear modulus.

For graphene ρ_{nm} = 4.2 10^{18} m^{-2} b = 0.24 10^{-9} m, C_1 = 0.2, G = 1457 10^9 Pa, then it turns out that σ = 139.8 GPa, instead of σ = 130.4 GPa (Table 2). The given examples show the consistency of our model.

Let us now estimate the dipole arm in our model for graphene. Annihilation of edge dislocations of opposite signs in the same slip plane can occur even at low temperatures, reducing the dislocation density (Fig. 11). The distance between edge dislocations of opposite signs is equal to $l_\rho = 1/\rho^{1/2}$, where ρ is the dislocation density, which is related to the dislocation shoulder by the expression:

$$I = \alpha \cdot I_\rho = \alpha / \rho^{1/2} \approx 3/\rho^{1/2}, \quad (13)$$

where α = 3, taken from our work [53], where $\alpha = \gamma_2/\gamma_1 \approx 3$.

For graphene ρ = 4.2 10^{18} m^{-2} and according to our model l = 14.6 Å. Annihilation of edge dislocations of opposite signs occurs according to the data of [88, 89] with a dipole shoulder in the range l > 11.5 – 16 Å, which agrees well with our data.

Fracture of a graphene sheet

For the destruction of a solid body, force, deformation and energy failure criteria have been developed. There is the following connection between them [91]:

$$\frac{K_{1\tilde{N}}^2(1-\mu^2)}{E} = 2\delta_{1\tilde{N}}\sigma_B = G_{1\tilde{N}} = J_{1\tilde{N}} = 2\gamma = W_a, \quad (14)$$

where K_{Ic} is the critical stress intensity factor, the force criterion for destruction; E - elastic modulus; μ - Poisson's ratio; δ_{Ic} - critical opening at the crack tip, deformation criterion of destruction; $\sigma_в$ - tensile strength; G_{Ic} - critical intensity of released energy, energy criterion of destruction; J_{Ic} - critical j-integral, energy criterion of destruction; γ – surface energy, W_a – adhesion energy.

Wherein:

$$K_{1\tilde{N}} = \sqrt{EJ_{1\tilde{N}}}\,. \quad (15)$$

In the case of a plate with a crack L_C:

$$\hat{E}_{1\tilde{N}} = \sigma_{is}\sqrt{L_{\tilde{N}}}, \quad \delta_{1\tilde{N}} = K_{1\tilde{N}}^2/\sigma_{is} \cdot E\,. \quad (16)$$

According to our work [51], the length of a nanocrack varies according to the law:

$$L_{nm} \rightarrow L_{\mu m} = 10^2 \cdot L_{nm} \rightarrow L_C = 10^4 \cdot L_{nm} = 0{,}17 \cdot 10^{-5} \cdot M/\rho.. \quad (17)$$

Tables 1-3 show all graphene parameters for calculating force, deformation and energy failure criteria.

Conclusions

The topological Stone–Wales defect we considered is the most important defect in graphene, to which a large number of theoretical and experimental works are devoted and which continue to this day. In this study, we also proposed our own model of a SW defect from the standpoint of: birth → migration → annihilation → destruction of a graphene sheet. In the future, we plan to experimentally test some of the results of the proposed model.

This scientific article was published as part of grant funding for 2024-2026, IRN No. AR32488258 "Development of innovative technology for producing graphene by intercalating graphite with microcluster water and modifying HTSC ceramics with graphene" (the research is funded by the Science Committee of the Ministry of Science and Higher Education of the Republic of Kazakhstan).

References:

1. Stone A.J. and Wales D.J. Theoretical studies of icosahedral C_{60} and some related species // Chem. Phys. Lett., 1986, Vol. 128. – P. 501-503.

2. Novoselov K.S., Geim A.K., Morozov S.V., Jiang D., Zhang Y., Dubonos S.V., Grigorieva I.V., Firsov A.A. Electric field effect in atomically thin carbon films // Science, 2004, V.306, №5696. - P. 666-669.

3. Meyer J.C., Kisielowski C., Erni R., Rossell M.D, Crommie M.F., Zettl A. Direct imaging of lattice atoms and topological defects in graphene membranes // Nano letters, 2008, Vol.8, Issue 11. – P. 3582-3586.

4. Sofo J.O., Chaudhari A.S. and Barber G.D. Graphane: A Two-Dimensional Hydrocarbon // Phys.Rev. B., 2007, V 75, No. 15. 153401.

5. Elias D.C., Nair R.R., Mohiuddin T.M.G., Morozov S.V., Blake P., Halsall M.P., Ferrari A.C., Boukhvalov D.W., Katsnelson M.I., Geim A.K. and Novoselov K.S. Control of Graphene's Properties by Reversible Hydrogenation: Evidence for Graphane // Science, 2009, V.323. P. 610-613.

6. Li Y., Xu L., Liu H. and Li Y. Graphdiyne and graphyne: from theoretical predictions to practical construction // Chem. Soc. Rev., 2014, V.43, Issue 8. – P. 2572-2586.

7. Gao Y., Cao T., Cellini F., Berger C., de Heer W.A., Tosatti E., Riedo E. and Bongiorno A. Ultrahard carbon film from epitaxial two-layer grapheme // Nature nanotechnology, 2018, V.13, Issue 2. – P. 133-138.

8. Bakharev P.V., Huang M., Saxena M., Lee S.W., Joo S.H., Park S.O., Dong J., Camacho-Mojica D., Ji S., Kwon Y., Biswal M., Ding F., Kwak S. K., Lee Z. and Ruoff R.S. Chemically induced transformation of chemical vapour deposition grown bilayer graphene into fluorinated single-layer diamond // Nature nanotechnology, 2020, V. 15, Issue 1. – P. 59-66.

9. de Araujo G.M., Codognoto L. and Simo F.R. Self-assembled electrodes based on polyaniline grafted with reduced graphene oxide and polystyrene sulfonate // Journal of Solid State Electrochemistry, 2020, V. 24. – P. 1857-1866.

10. Lv Zh.-L., Lu Q., Huang D.-H. and Liu F.-T. R10-graphene: a predicted two-dimensional metallic carbon // Diamond and Related Material, 2021, V. 114, 108315.

11. Yan P., Ouyang T., He Ch., Li J., Zhang Ch., Tang Ch., Zhong J. Newly discovered graphyne allotrope with rare and robust Dirac node loop // Nanoscale, 2021, V. 13(6). – P. 3564-3571.

12. Zhang W., Chai C.C., and Yang Y.T. Two-dimensional carbon allotropes with tunable direct band gaps and high carrier mobility // Applied Surface Science, 2021, V.537, 147885.

13. Li J., Li Sh., Ouyang T., Zhang Ch., Tang Ch., He Ch. and Zhong J. Two-dimensional carbon allotropes and nanoribbons based on 2, 6-polyazulene chains: stacking stabilities and electronic properties // J. Phys. Chem. Lett., 2021, V.12(2). – P. 732-738.

14. Liu J.and Lu H. Azugraphene: a new graphene-like hexagonal carbon allotrope with Dirac cones // RSC Adv., 2019, V. 9. – P. 34481-34485.

15. Yin H., Shi X., He C., Martinez-Canales M., Li J., Pickard C.J., Tang C., Ouyang T., Zhang C. and Zhong Stone-Wales graphene: A two-dimensional carbon semimetal with magic stability // J., Phys. Rev. B., 2019, V. 99, 041405.

16. Podlivaev A.I. Double-layer graphene - Stone-Wales graphene: structure, stability and interlayer thermal conductivity // JETP Letters, 2022, vol. 115, issue. 6. - P. 384-391.

17. Wang M.C., Yana C., Ma L., Hu N., Chen M.W. Effect of defects on fracture strength of graphene sheets // Computational Materials Science, 2012, 54(4). - P. 236-239.

18. Bhatt M.D., Kim H. and Kim G. Various defects in graphene: a review // RSC Adv., 2022, V. 12. – P. 21520–21547

19. Warner J.H, Margine E.R., Mukai M., Robertson A.W., Giustino F., Kirkland A.I. Dislocation-driven deformations in grapheme // Science, 2012, Vol. 337. - P. 209-212.

20. Ioffe A.F. Report on the work of the Institute of Physics and Technology // UFN, 1936, Vol. XVI, no. 7. – P. 848-871.

21. Frenkel V.Ya. Abram Fedorovich Ioffe (Biographical sketch) // UFN, 1980, Vol. 132, No. 1. – P. 11-45.

22. Yurov V.M., Guchenko S.A., Laurinas V.Ch. The thickness of the surface layer, surface energy and atomic volume of an element // Physicochemical aspects of studying clusters, nanostructures and nanomaterials, 2018, Issue. 10. - P. 691-699.

23. Griffith A.A. The theory of rupture // In Proc. Ist. Congr. Appl. Mech.-Delft., 1924. - P. 55-63.

24. Frenkel J. Über die Wärmebewegung in festen und flüssigen Körpern // Zeitschrift für Physik, 1926, Tom 35(8). - S. 652-669.

25. Schottky W. Thermodynamik, die Lehre von den Kreisprozessen, den physikalischen und chemischen Veränderungen und Gleichgewichten - J. Springer, 1929. – 619 s.

26. Kittel C. Introduction to Solid State Physics, 4-th edition. - Jonn-Wiley and Sons, 1971. – 766 p.

27. Tamm I.E. Collection of scientific works. Vol.1. – M.: Nauka, 1975. – P. 216.

28. Gibbs J.W. Thermodynamic works. - M.: GITTL, 1950. - 303 p.

29. Van der Waals I.D. Thermodynamische Theorie der Capil-laritat. - Verh. Kon. Acad. - Amsterdam, 1893. - 529 p.

30. Guggenheim B.A. Thermodynamics. - Amsterdam: North-Holland Publishing Co., 1967. - 390 p.

31. Rusanov A.I. Phase equilibria and surface phenomena. - L.: Chemistry, 1967. - 346 p.

32. Oura K., Lifshits V.G., Saranin A.A. and others. Introduction to surface physics. - M.: Nauka, 2006. - 490 p.

33. Yurov V.M. Thickness of the surface layer of atomically smooth crystals // Physico-chemical aspects of studying clusters, nanostructures and nanomaterials. 2019. issue. 11. - P. 389-397.

34. Panin V.E., Sergeev V.P., Panin A.V. Nanostructuring of surface layers of structural materials and application of nanostructured coatings // Tomsk. Publishing house TPU. 2010. - 254 p.

35. Tolman R.C. The effect of droplet size on surface tension // J. Chem. Phys., 1949, Vol. 17, № 2. - P. 333-337.

36. Rekhviashvili S.Sh., Kishtikova E.V., Karmokova R.Yu., Karmokov A.M. To the calculation of Tolman's constant // Technical Physics Letters, 2007, V. 33, no. 2. - P. 1-7.

37. Heimann R.B., Evsyukov S.E., Koga Y. Carbon allotropes: a suggested classification scheme based on valence orbital hybridization // Carbon, 1997, V.35, №10-11. - P. 1654-1663.

38. Zhmurikov E.I., Bubnenkov I.A., Dremov V.V., Samarin S.I., Pokrovsky A.S., Kharkov D.V. Graphite in science and nuclear technology. – Novosibirsk, 2013. – 193 p.

39. Gleiter H. Nanostructured materials: basic concepts and microstructure // Acta mater., 2000, V.48. - P. 1-29.

40. Los J.H., Zakharchenko K.V., Katsnelson M.I. and Fasolino A. Melting temperature of graphene // Phys. Rev., 2015, B91, 045415.

41. Uvarov N.F., Boldyrev V.V. Size effects in the chemistry of heterogeneous systems // Uspekhi khimii, 2001, Vol. 70 (4). – P. 307-329.

42. Zimon A.D. Adhesion of films and coatings. - M.: Chemistry, 1977. – 352 p.

43. Skowron S.T., Lebedeva I.V., Popov A.M., Bichoutskaia E. Energetics of atomic scale structure changes in graphene // Chem. Society Rev., 2015, V.44. - P. 3143-3176.

44. Lazar M. Dislocation field theory in 2D: Application to graphene // Phys. Lett. A, 2013, V. 377, №5. - P. 423-429.

45. Akhunova A.Kh., Baimova Yu.A. The influence of dislocation dipoles with different arms on the deformation behavior of graphene: molecular dynamics // Journal of Technical Physics, 2023, Vol. 93, issue. 4. – P. 445-442.

46. Peierls R. The size of a dislocation // Proc. Phys. Soc. London, 1940, V. 52. - P. 34–37.

47. Nabarro F.R.N. Dislocations in a simple cubic lattice // Proc. Phys. Soc. London, 1947, V. 59. - P. 256–272.

48. Usatenko O.V., Gorbach A.V., Kovalev A.S. Energy and Peierls barrier of the Frenkel–Kontorova dislocation (kink) // FTT, 2001, vol. 43, issue. 7. - P. 1202-1206..

49. Grinberg B.A., Ivanov M.A., Kruglikov N.A., Antonova O.V. On the possibility of self-blocking of dislocations in various materials // Physics and Mathematics,

2009, V. 108, No.1. - P. 93-104..

50. Fan T., Luo L., Ma L., Tang B., Peng L., Ding W. Study of total a-dislocations in pure magnesium based on first principles // PMT, 2014, V. 55, N4. - P. 141-151..

51. Yurov V.M., Goncharenko V.I., Oleshko V.S. Primary nanocracks in nitrides, borides and carbides of refractory metals // Physical and chemical aspects of studying clusters, nanostructures and nanomaterials, 2023, No. 15. - P. 328-337.

52. Vettegren V.I., Ponomarev A.V., Mamalimov R.I., Shcherbakov I.P. Nanocracks during the destruction of oligoclase // Physics of the Earth, 2021, No. 6. - P. 87-92..

53. Yurov V.M., Goncharenko V.I., Oleshko V.S. Study of primary nanocracks in atomically smooth metals // Letters to ZhTP, 2023, vol. 49, issue. 8. P. 35-38.

54. Natsik V.D., Chishko K.A. Effect of impurities on dynamic dragging of dislocations // Crystal Research and Technology, 1984, V. 19, №6. – P. 763-768.

55. Kozlov E.V., Popova N.A., Koneva N.A. Size effect in dislocation substructures of metallic materials // Fundamental problems of modern materials science, 2009, Vol. 6, No. 2. - P. 14-24.

56. Hashimoto, A., Suenaga, K., Gloter, A., Urita, K. & Iijima, S. Direct evidence for atomic defects in graphene layers // Nature, 2004, Vol. 430. – P. 870-873.

57. Lehtinen O., Kurasch S., Krasheninnikov A.V., Kaiser U. Atomic scale study of the life cycle of a dislocation in graphene from birth to annihilation // Nature Communications, 2013, Vol. 4(1), 2098.

58. Griffith A.A. The phenomena of rupture and flow in solids // Philos. Trans. Roy. Soc. London. Ser. A., 1920, V. 221. - P. 163-198.

59. Chekunaev N.I., Kaplan A.M. Limiting speed of crack propagation in elastic materials // Applied mechanics and technical physics, 2009, Vol. 50, No. 4. – P. 158-166.

60. Saito R, Dresselhaus G, Dresselhaus M S Physical Properties of Carbon Nanotubes. - London: Imperial College Press, 2003. – 272 p.

61. Falkovsky L.A. Optical properties of graphene and A4B6 type semiconductors // Uspekhi Fizicheskikh Nauk, 2008, Vol. 178, Issue 9. – P. 923-934.

62. Nika D.L., Pokatilov E.P., Askerov A.S. and Balandin A.A. Phonon thermal conduction in graphene: Role of Umklapp and edge roughness scattering // Phys. Rev. B, 2009, Vol. 79, 155413.

63. Eletsky A.V., Iskanderova I.M., Knizhnik A.A., Krasikov D.N. Graphene: production methods and thermophysical properties // Advances in Physical Sciences, 2011, Vol. 181, No. 3.. – P. 233-268.

64. Loskutov A.Yu., Mikhailov A.S. Fundamentals of the theory of complex systems. – M:.-Izhevsk: Institute of Computer Research, 2007. - 620 p.

65. Zaslavsky G.M. Physics of chaos in Hamiltonian systems. - Moscow-Izhevsk: Institute of Computer Research, 2004. - 288 p.

66. Anishchenko V.S., Vadivasova T.E., Shimansky-Gayer L. Dynamic and statistical description of oscillatory systems. - Moscow-Izhevsk: Institute of Computer Research, 2005. - 156 p.

67. Kahrig E., Beberdich H. Dissipative Structuren. - Leipzig: VEB Georg Thieme, 1977. - 342 p.

68. Davydov V.A., Davydov N.V., Morozov V.G., Stolyarov M.N., Yamaguchi T. () Autowaves in the moving excitable media // Condensed Matter Physics, 2004, Vol. 7, No. 3(39). - P. 565–578.

69. Kolobov A.V., Gubernov V.V. and Polezhaev A.A. () Autowaves in the Model of Infiltrative Tumour Growth with Migration-Proliferation Dichotomy // Math. Model. Nat. Phenom. 2011, Vol. 6, No. 7. - P. 1-12.

70. Yurov V.M., Laurynas V.Ch., Zavatskaya O.N., Guchenko S.A. Autowave processes during the formation of ion-plasma coatings // Bulletin of KarSU. Physics, 2013, No. 1(69). – P. 57-68.

71. Gerasev A.P. Nonequilibrium thermodynamics of autowave processes in the catalyst layer // UFN, 2004, Vol. 174, No. 10. - P. 1061-1087.

72. Elkin Yu.E. Autowave processes // Mathematical biology and bioinformatics, 2006, Vol. 1, No. 1. - P. 27-40.

73. Khishchenko K.V., Tkachenko S.I., Levashov P.R. On the melting wave in a metal during rapid heating by a powerful current pulse // Letters to ZhTP, 2006, Vol. 32, issue. 3. – P. 67-74.

74. Golovin I.S. Internal friction and mechanical spectroscopy of metallic materials. – M.: Publishing house. House of MISiS, 2012. – 247 p.

75. Tsarev M.V. Generation and registration of terahertz radiation by ultrashort laser pulses. - Nizhny Novgorod: Nizhny Novgorod State University, 2011. - 75 p..

76. Zimmermann J., Pavone P., Cuniberti G. Vibrational modes and low-temperature thermal properties of graphene and carbon nanotubes: Minimal force-constant model // . Phys. Rev. B, 2008, Vol. 78, 045410

77. Nika D.L., Balandin A.A. Phonons and thermal transport in graphene and graphene-based materials // Rep. Progr. Phys., 2017, Vol. 80, 036502.

78. Roldan R., Fuchs J.-N., Goerbig M.O. Collective modes of doped graphene and a standard two-dimensional electron gas in a strong magnetic field: Linear magnetoplasmons versus magnetoexcitons // Phys. Rev. B., 2009, vol. 80. – P. 085408.

79. Christensen J., Manjavacas A., Thongrattanasiri S., Koppens F.H.L., Garcia de Abajo F.J. Graphene plasmon waveguiding and hybridization in individual and paired nanoribbons // ACS Nano., 2012, Vol. 6. - P. 431-440.

80. Thongrattanasiri S., Silveiro I., Garcia de Abajo F.J. Plasmons in electrostatically doped graphene // Appl. Phys. Lett., 2012, Vol. 100. - P. 201105.

81. Liu Y., Willis R.F. Plasmon-phonon strongly coupled mode in epitaxial graphene // Phys. Rev. B., 2010, Vol. 81. - P. 081406.

82. Fei Z., Rodin A.S., Basov D.N. et al. Gate-tuning of graphene plasmons revealed by infrared nano-imaging // Nature, 2012, Vol. 487. - P. 82-85.

83. Zhou W., Lee J., Nanda J., Pantelides S.T., Pennycook S.J. and Idrobo J.-C. Atomically localized plasmon enhancement in monolayer graphene // Nature Nanotechnol., 2012, Vol. 7. - P. 161–165.

84. Carpio A., Bonilla L.L., Periodized discrete

elasticity models for defects in graphene // Physical Review B, 2008, Vol. 78(8), 085406.

85. Gomez-Navarro C., Meyer J.C., Sundaram R.S., Chuvilin A., Kurasch S., Burghard M., Kern K., Kaiser U. Atomic structure of reduced grapheme oxide // Nano Letters, 2010, Vol. 10(4). – P. 1144-1148.

86. Gong C., Robertson A.W., He K., Lee G.-D., Yoon E., Allen C.S., Kirkland A.I., Warner J.H. Thermally induced dynamics of dislocations in graphene at atomic resolution, ACS Nano, 2015, Vol. 9(10). - P. 10066-10075.

87. Kawamura Yu., Ohta Ya. Annihilation dynamics of a dislocation pair in graphene: Density-functional tight-binding molecular dynamics simulations and first principles study // Computational Materials Science, 2022, Vol. 205. - P. 111224.

88. Galiakhmetova L., Krylova K., Kosarev I. Dislocation dipole movement in graphene at finite temperatures: Molecular dynamics study // AIP Conf. Proc., 2022, Vol. 2533, 020015.

89. Galiakhmetova L.Kh., Safina L.R., Murzaev R.T., Baimova J.A. Dynamics of dislocation dipoles in graphene at high temperatures // SSRN, 2023, Vol. 10, 4630709.

90. Zaripova R.G. Recrystallization in metals and alloys. - Ufa: UGATU, 2022. – 179 p..

91. Erasov V.S., Oreshko E.I. Reasons for the dependence of the mechanical characteristics of the crack resistance of a material on the size of the sample // Aviation materials and technologies, 2018, No. 3(52). – P. 56-64.

VETERINARY SCIENCES

PARASITISES OF SHEEP

Antipov A.,
candidate of veterinary sciences, associate professor
associate Professor of the Department of Parasitology and Pharmacology
Bilotserk National Agrarian University,
Bila Tserkva, 8/1 Cathedral Square, Ukraine, 09100
Schmaun S.,
candidate of veterinary sciences, associate professor
Associate Professor of the Department of Normal and Pathological Animal Physiology
Belotserk National Agrarian University,
Bila Tserkva, 8/1 Cathedral Square, Ukraine, 09100
Tkachenko I.,
erhiivna a teacher of the highest category
VSP „Company Professional College of Veterinary Medicine
Belotserk National Agrarian University"
Kompaniivka village, st. Parkova, 3, Ukraine, 28400
Tkachenko S.,
a teacher of the highest category
VSP „Company Professional College of Veterinary Medicine
Belotserk National Agrarian University"
Kompaniivka village, st. Parkova, 3, Ukraine, 28400
Palienko S.
teacher of special disciplines
VSP „Zolotonosha Professional College of Veterinary Medicine
Belotserk National Agrarian University"
Zolotonosha, st. Sadovy proezd, 1 Ukraina, 19700

ПАРАЗИТОЗИ ОВЕЦЬ

Антіпов А.А.
кандидат ветеринарних наук, доцент
доцент кафедри паразитології та фармакології
Білоцерківський національний аграрний університет,
м. Біла Церква, Соборна площа 8/1, Україна, 09100
Шмаюн С.С.
кандидат ветеринарних наук, доцент
доцент кафедри нормальної та патологічної фізіології тварин
Білоцерківський національний аграрний університет,
м. Біла Церква, Соборна площа 8/1, Україна, 09100
Ткаченко І.С.
викладач вищої категорії
ВСП „Компаніївський фаховий коледж ветеринарної медицини
Білоцерківського національного аграрного університету"
смт Компаніївка, вул. Паркова, 3 Україна, 28400
Ткаченко С.М.
викладач вищої категорії
ВСП „Компаніївський фаховий коледж ветеринарної медицини
Білоцерківського національного аграрного університету"
смт Компаніївка, вул. Паркова, 3 Україна, 28400
Палієнко С.О.
викладач спеціальних дисциплін
ВСП „Золотоніський фаховий коледж ветеринарної медицини
Білоцерківського національного аграрного університету "
м. Золотоноша, вул. Садовий проїзд, 1 Україна, 19700
https://doi.org/10.5281/zenodo.10492780

Abstract

Our research established that during the study of 254 sheep, 142 were affected by parasitosis (EI was 55.91%), and 112 were free from parasitosis, which was 44.09%. According to the morphological characteristics of eggs isolated from the feces of sick animals, eggs of the order Strongylida, Trichurida, Rhabditida, as well as oocysts of protozoa belonging to the order Sossidiida were found. It was recorded that most often (36.62%) the causative agents of strongyloidosis of the alimentary canal were registered, to a somewhat lesser extent - the causative agents of trichurosis (26.76%), and the least affected by Strongyloides (17.61%) and oocysts of protozoa (19.01%).

Ovoscopic studies showed that parasitosis of the alimentary canal of sheep in farm conditions occurred both as part of mixed invasions (81.69%) and as monoinvasions (18.31%). In sheep, the associated course of parasitosis of the digestive tract was most often recorded. Thus, two- and three-component mixed infections were observed in 76.09 and 21.74%, respectively. To a lesser extent (2.17%) combinations of parasitosis with four types of parasites were recorded.

Анотація

Нашими дослідженнями встановлено, що при дослідженні 254 голів овець паразитозами було уражено 142 голови (ЕІ склала 55,91 %), а вільних від паразитозів було 112 голів, що становило 44,09 %. За морфологічними ознаками яєць виділених із фекалій хворих тварин, були виявлені яйця ряду Strongylida, Trichurida, Rhabditida, а також ооцисти найпростіших, які відносилися до ряду Coccidiida. Зареєстровано, що найчастіше (36,62 %) реєстрували збудників стронгілідозів травного каналу, дещо меншою мірою – збудників трихурозу (26,76 %), а найменшою відмічали ураженість стронгілоїдесами (17,61 %) та ооцистами найпростіших (19,01 %).

Овоскопічні дослідження показали, що паразитози травного каналу овець в умовах господарства перебігали як у складі мікстінвазій (81,69 %) так і у вигляді моноінвазії (18,31 %). У овець найчастіше реєстрували асоційований перебіг паразитозів травного тракту. Так, дво- і трикомпонентні мікстінвазії спостерігали у 76,09 та 21,74 % відповідно. Меншою мірою (2,17 %) реєстрували комбінації паразитозів з чотирма видами паразитів.

Keywords: *sheep, Strongyloides, strongylids, Trichuris, Eimeria oocysts, extensiveness of invasion, , monoinvasion, polyinvasion.*

Ключові слова: *вівці, стронгілоїдеси, стронгіліди, трихуриси, ооцисти еймерій, екстенсивність інвазії, , моноінвазія, поліінвазія.*

Актуальність теми. Вівчарство як галузь тваринництва займають важливе місце в народному господарстві країни. Молоко та м'ясо від овець є додатковим джерелом продовольства. Велике народногосподарське значення має вовна, пух, шкури овець. Другорядна продукція вівчарства має застосування. З рогів виробляють гребінки й інші вироби, з ратиць варять клей, кишки використовуються в ковбасному виробництві [1, 2, 3].

Поряд з позитивними моментами у ведені вівчарства, появились і негативні – захворювання незаразної, інфекційної і паразитарної етіології. Особливої уваги заслуговують паразитарні хвороби овець, частина із яких мають прихований перебіг, такі як нематодози травного каналу [4, 5].

В численних публікаціях приводяться дані про видовий склад збудників нематодозів в органах травного каналу овець як в Україні, так і різних країнах світу і представлений збудниками стронгілятозів, трихурозу, стронгілоїдозу і капіляріозу [6].

В.С. Шеховцов проводячи дослідження в Харківській, Кіровоградській, Полтавській, Херсонській, Хмельницькій, Львівській областях ідентифікував 12 видів нематод стронгілят [7]. О.О. Бойко [8] повідомляє, що на території Дніпропетровської області встановлено збудники стронгілід з родини Trichostrongylidae: Nematodirus sp. та Haemonchus contortus, серед яких домінував вид H. contortus. О.А. Власенко, В.В. Стибель [9] повідомляють, що у Сумській області згідно паразитологічного дослідження овець виявлено збудників стронгілідозів травного каналу 7 родів, а саме: Trichostrongylus, Nematodirus, Ostertagia, Chabertia, Oesophagostomum, Bunostomum.

В.О. Євстаф'єва, А.О Гришко, О.В. Перебийніс [10] повідомляють, що у Полтавській області зареєстровано наявність нематод Nematodirus spathiger.

Таким чином можна зробити висновок, що при аналізі літературних джерел основою прогнозування неблагополуччя овець щодо хвороб паразитарної етіології є дослідження та вивчення видового складу гельмінтів.

Мета дослідження. Метою роботи було вивчити поширення та видовий склад паразитозів травного каналу овець в умовах науково-виробничого центру (НВЦ) Білоцерківського національного аграрного університету (БНАУ).

Матеріал і методи дослідження. Дослідження проводили на протязі 2023 року на базі наукової лабораторії кафедри паразитології та фармакології БНАУ, а також в умовах НВЦ БНАУ. З цією метою проводили відбір проб фекалій індивідуально з прямої кишки тварин в ранковий час. Дослідження проводили один раз на квартал на вівцях віком від 6 місяців до 4 років, спонтанно інвазованих паразитозами травного каналу. Всього було досліджено 254 проби фекалій від овець.

Основним критерієм зараженості були екстенсивність та інтенсивність інвазії (ЕІ, %; та ІІ, кількість яєць у 1 г фекалій, ЯГФ). Визначення видової належності яєць гельмінтів проводили за атласами диференційної діагностики В.В. Мельничука [11], В.Ф. Галата та ін. [12], О.Ф. Манжоса та ін. [13].

Гельмінтоовоскопію проб фекалій досліджували з використанням лічильної камери для овоскопічних досліджень [14]. Експериментальна частина роботи проводилась з урахуванням „Загальних етичних принципів експериментів на тваринах", схвалених на Національному конгресі з біоетики [15] із дотриманням міжнародних вимог Європейської конвенції „Про захист хребетних тварин, що використовуються для дослідних та інших наукових цілей" [16].

Результати дослідження. У результаті овоскопічних досліджень нами встановлено значне розповсюдження паразитозів травного каналу. Так, з 254 обстежених голів овець паразитозами було вражено 142 голови. Екстенсивність інвазії становила 55,91 %. Тварин вільних від паразитозів 112 голів, що становило 44,09 %.

За морфологічними ознаками яєць та ооцист виділених із фекалій хворих тварин, були виявлені яйця стронгілідного типу, трихурисів, стронгілоїдесів, а також ооцисти найпростіших. Таким чином, у овець нами було встановлено паразитування нематод, які відносяться до трьох рядів, а саме: *Strongylida, Trichurida, Rhabditida* та ооцисти найпростіших, які відносяться до ряду *Coccidiida*.

Нами зареєстровано, що найчастіше (36,62 %) у овець господарства реєстрували збудників стронгілятозів травного каналу (табл. 1), дещо меншою мірою – збудника трихурозу (26,76 %) і найменшою – стронгілоїдозу (17,61 %) та ураженість ооцистами найпростіших (19,01 %).

Таблиця 1

Поширення паразитозів травного каналу овець у господарстві

Кількість обстежених тварин, гол	Кількість вільних від паразитів тварин, гол	Кількість уражених паразитами тварин, гол	в тому числі			
			Strongylida	*Trichurida*	*Rhabditida*	*Coccidiida*
254	112	142	52	38	25	27
100	44,09	55,91	36,62	26,76	17,61	19,01

Гельмінтоовоскопічні дослідження показали, що паразитози травного каналу овець в умовах господарства перебігали як у складі мікстінвазій 116 голів (81,69 %), так і у вигляді моноінвазії 26 голів (18,31 %) (табл. 2).

Таблиця 2

Паразитози травного каналу у складі моноінвазії та мікстінвазії

Асоціація паразитів	Кількість уражених тварин, голів	В процентах до уражених тварин
Моноінвазія	26	81,69
Мікстінвазія	116	18,31
Всього	142	100

Нашими дослідженнями доведено, що серед моноінвазій в умовах господарства вівці більшою мірою уражені збудниками стронгілідозів травного каналу – 50,00 % (табл. 3). Меншою мірою у овець реєстрували стронгілоїдоз (26,76 %), а найменше були уражені вівці трихурисами (15,38 %) та ооцистами еймерій (7,69 %).

Таблиця 3

Паразитози травного каналу у складі моноінвазії

Види паразитів	Кількість уражених тварин, голів	В процентах до уражених тварин
Стронгіляти (S)	13	50,00
Трихуриси (T)	4	15,38
Стронгілоїдеси (R)	7	26,92
Еймерії (C)	2	7,69
Всього уражено тварин, голів	26	100

Слід звернути увагу на той факт, що у овець найчастіше реєстрували асоційований перебіг паразитозів травного тракту (табл. 4). Таким чином двокомпонентну мікстінвазію спостерігали у 84 тварин (76,09 та 21,74 % відповідно. Меншою мірою (2,17 %) у господарстві реєстрували комбінації паразитозів з чотирма видами паразитів.

Таблиця 4

Поширення паразитозів травного каналу овець у складі мікстінвазій

Асоціації паразитів	Уражено тварин, голів	У процентах
Двокомпонентні	84	72,41
Трикомпонентні	24	20,69
Чотирикомпонентні	8	6,90
Всього	116	100

Всього нами нами зафіксовано 9 різних комбінацій збудників паразитів. Із двокомпонентних асоціацій нами зареєстровано 5 різновидів комбінацій. Загалом, із виділених чотирьоз видів збудників мікстінвазій в умовах вівцегосподарства збудників інвазійних захворювань (84 випадки від загальної кількості хворих на мікстінвазії овець). Найбільш поширеною виявилася асоціація паразитів, яка представлена збудниками стронгілят та трихурисів, що склало 51,55 % від загальної кількості хворих на двокомпонентну асоціацію) (рис. 1, рис. 2).

Асоціації паразитів, компонентами яких були: стронгіліди й стронгілоїдеси (5,95 %); стронгіліди й еймерії (10,71 %) (рис. 3); трихуриси й стронгілоїдеси (3,57 %); трихуриси й еймерії (7,14 %) (рис. 4), а також стронгілоїдеси й еймерії (1,20 %).

Трикомпонентні асоціації паразитів реєстрували у меншій мірі (24 випадки від загальної кількості хворих на мікстінвазії тварин. Зафіксовано 4 різновиди комбінацій збудників. Слід акцентувати, що найбільший процент уражених тварин був у комбінації стронгіліди+стронгілоїдеси+еймерії (рис. 5) (12,50 %).

Чотирикомпонентну асоціацію паразитів (стронгіліди, трихуриси, стронгілоїдеси та ооцисти еймерій) реєстрували у однієї тварини (рис. 6) і складало 2,17 %.

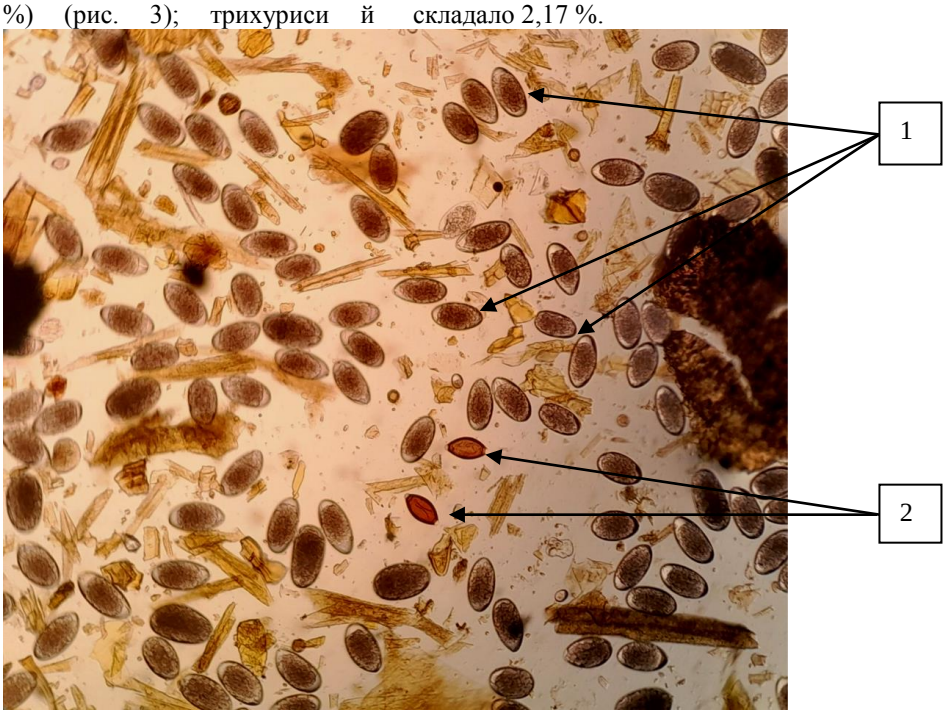

Рис. 1 – Зовнішній вигляд: 1 – яєць стронгілід, 2 – яєць трихурисів.

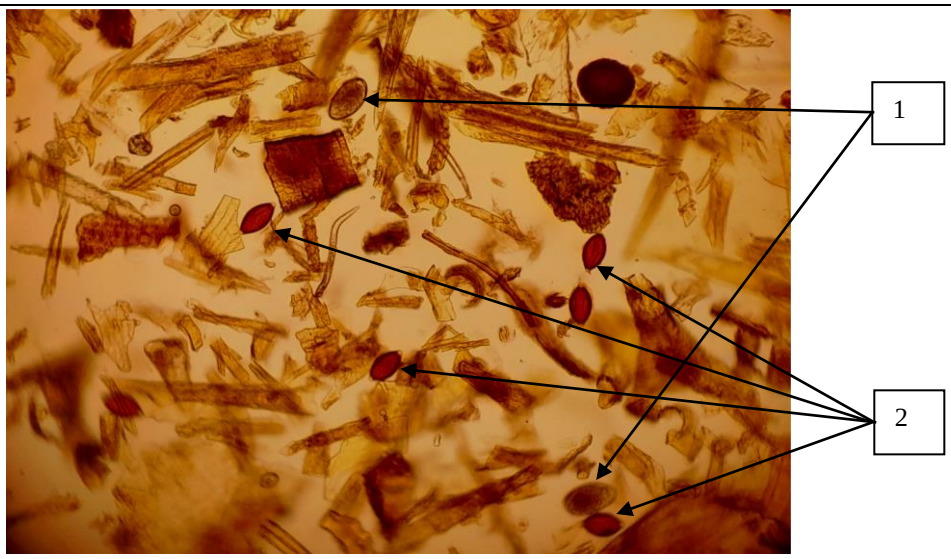

Рис. 2 – Зовнішній вигляд: 1 – яєць стронгілід, 2 – яєць трихурисів.

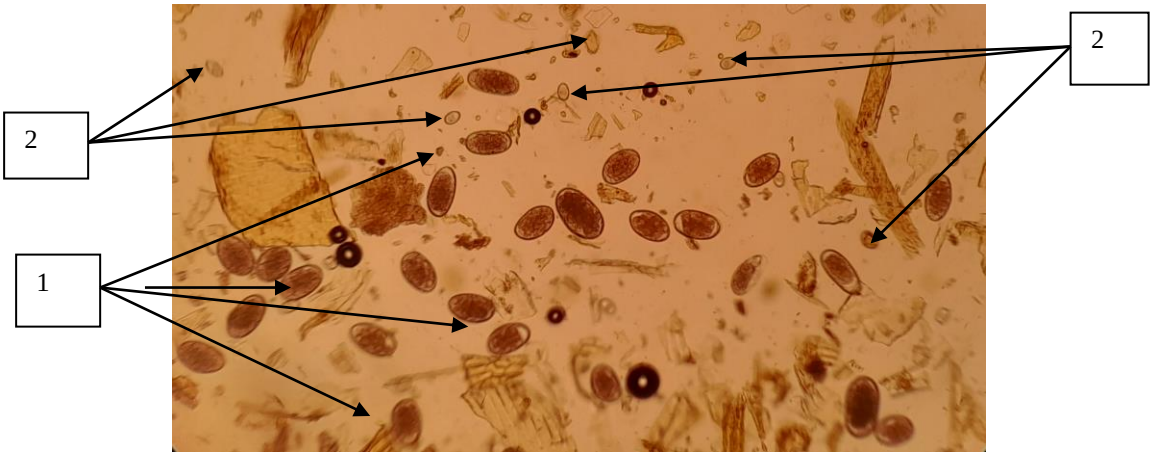

Рис. 3 – Зовнішній вигляд: 1 – яєць стронгілід, 2 – ооцист найпростіших.

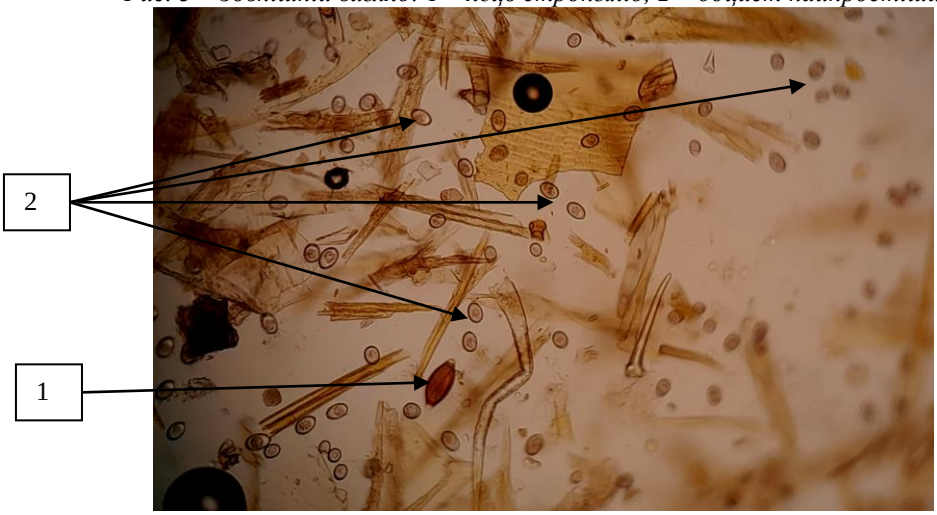

Рис. 4 – Зовнішній вигляд: 1 – яєць трихурисів, 2 – ооцист найпростіших

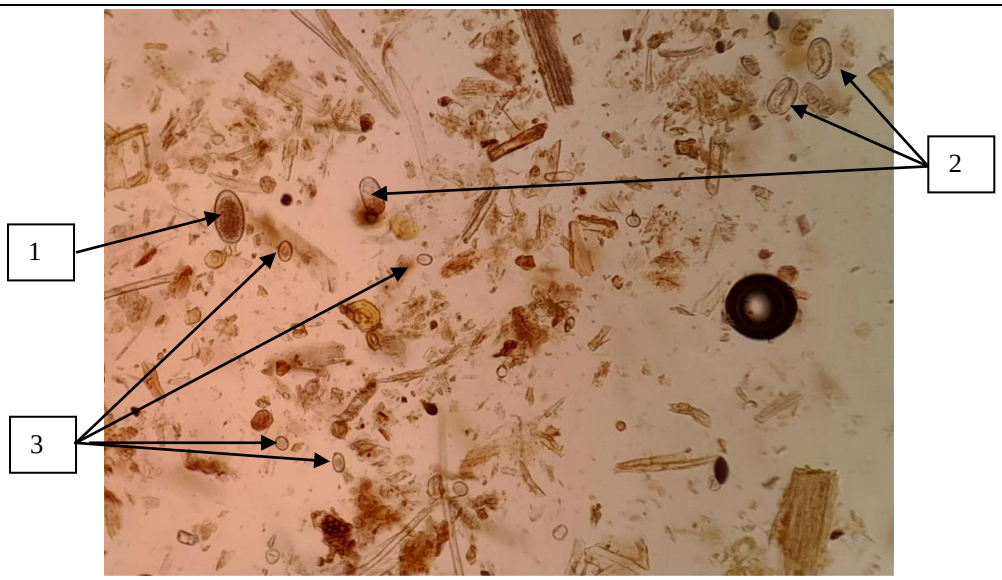

Рис. 5 – Зовнішній вигляд: 1 – яєць стронгілід,
2 – яєць стронгілїдесів, 3 – ооцист найпростіших

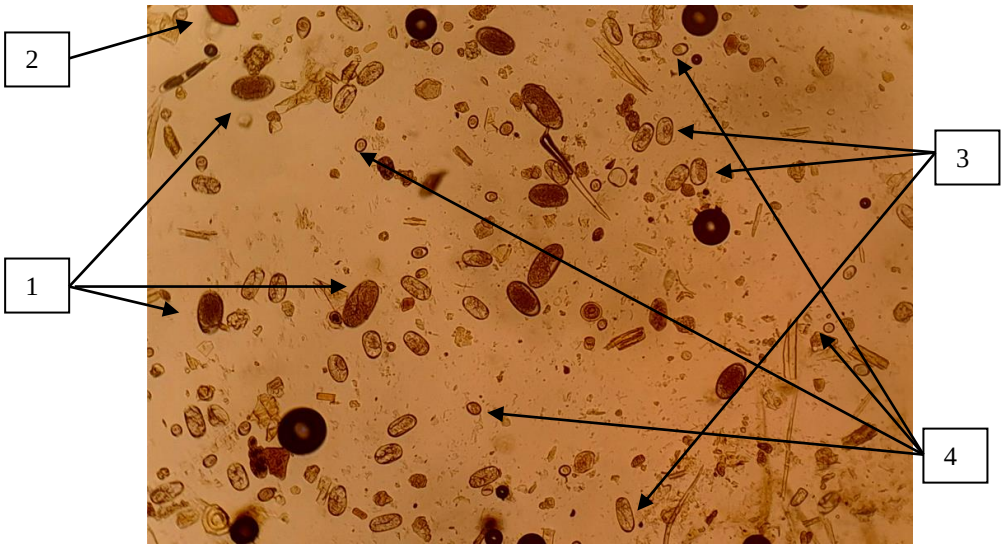

Рис. 6 – Зовнішній вигляд: 1 – яєць стронгілід, 2 – яєць трихурисів,
3 – яєць стронгілїдесів, 4 – ооцист найпростіших

Отже, із отриманих даних видно, що паразитози травного каналу овець (стронгіліди, стронгілоїдеси, трихуриси та еймерії) перебігають як у складі моно та мікстінвазій.

Обговорення отриманих результатів. Сьогодні вівчарство набуває вагомого соціально-економічного значення. Це універсальна галузь, яка дає баранину, субпродукти, молоко і вовну, займає третє місце у світі за статистичними показниками [4, 6].

Однією з причин, які в певній мірі стримують розвиток галузі вівчарства, є інвазійні хвороби. Дослідники у своїх працях вказують на широке розповсюдження паразитозів серед овець, у тому числі й нематодозів травного каналу, що узгоджується з отриманими нами даними. За морфологічними ознаками яєць, виділених з фекалій хворих тварин, встановлено паразитування нематод стронгілід, трихурід, стронгілоїдесів, а також найпростіших одного.

За результатами проведених копроовоскопічних досліджень нами встановлено, що паразитози травного каналу овець є поширеними інвазіями у овець на території господарства. Необхідно відмітити, що із 254 досліджених тварин, паразитозами було уражено 142 голови (ЕІ склала 55,91 %). Овець вільних від паразитозів було 112 голів, що становило 44,09 %.

Отримані у результаті проведених нами досліджень дані певною мірою узгоджуються з даними науковців, які проводили свої дослідження на території нашої держави [1, 4, 7, 9].

Нами встановлено що паразитози травного каналу овець часто перебігають як у складі мікстінвазій (81,69 %), так і у вигляді моноінвазії (18,31 %).

Нашими дослідженнями доведено, що серед моноінвазій в умовах господарства вівці більшою мірою уражені збудниками стронгілідозів травного каналу – 50,00 %. Меншою мірою у овець реєстрували стронгілоїдоз (26,76 %), а найменше

були уражені вівці трихурисами (15,38 %) та ооцистами еймерій (7,69 %).

Слід звернути увагу на той факт, що у овець найчастіше реєстрували асоційований перебіг паразитозів травного тракту. Так, дво- і трикомпонентні мікстінвазії спостерігали у 76,09 та 21,74 % відповідно. Меншою мірою (2,17 %) у господарстві реєстрували комбінації паразитозів з чотирма видами паразитів.

Із двокомпонентних асоціацій нами зареєстровано 5 різновидів комбінацій. Загалом, із виділених чотирьоз видів збудників мікстінвазій в умовах вівцегосподарства збудників інвазійних захворювань (84 випадки від загальної кількості хворих на мікстінвазії овець). Найбільш поширеною виявилася асоціація паразитів, яка представлена збудниками стронгілят та трихурисів, що склало 51,55 % від загальної кількості хворих на двокомпонентну асоціацію).

Трикомпонентні асоціації паразитів реєстрували у меншій мірі (24 випадки від загальної кількості хворих на мікстінвазії тварин. Зафіксовано 4 різновиди комбінацій збудників. Слід акцентувати, що найбільший процент уражених тварин був у комбінації стронгіліди+стронгілоїдеси+еймерії (12,50 %). Отримані в дослідах дані мають важливе теоретичне й практичне значення при плануванні та проведенні заходів з профілактики паразитозів овець.

ВИСНОВКИ.

1. Встановлено, що на території господарства вівці уражені збудниками нематодозів травного каналу, що належать до 3 рядів: Strongylida, Rhabditida, Trichurida, а також ооцисти найпростіших, які відносилися до ряду Coccidiida.

2. Із 254 досліджених тварин, паразитозами було уражено 142 голови (ЕІ склала 55,91 %), а вільних від паразитозів було 112 голів (44,09 %).

3. Паразитози травного каналу овець часто перебігають як у складі мікстінвазій (81,69 %), так і у вигляді моноінвазії (18,31 %).

4. Серед моноінвазій в умовах господарства вівці більшою мірою уражені збудниками стронгілідозів травного каналу – 36,62 %. Меншою мірою у овець реєстрували трихурисів (26,76 %), а найменше реєстрували у овець стронгілоїдесів (17,61 %) та ооцисти еймерій (19,01 %).

5. У овець найчастіше реєстрували асоційований перебіг паразитозів травного тракту. Так, дво- і трикомпонентні мікстінвазії спостерігали у 76,09 та 21,74 % відповідно. Меншою мірою (2,17 %) у господарстві реєстрували комбінації паразитозів з чотирма видами паразитів.

Список література:

1. Мельничук В.В. Епізоотична ситуація та особливості перебігу нематодозів травного каналу овець в умовах господарств Київської області / В.В. Мельничук, А.А. Антіпов // Наук. вісник вет. медицини: зб-к наук. праць. - Біла Церква: БНАУ, 2019. - № 1. - С.75-84.

2. Розповсюдження та вікова динаміка трихурозної інвазії у овець / А.А. Антіпов, В.П. Гончаренко, Н.В. Авраменко та ін. // Scientific Collection «InterConf», (168): with the Proceedings of the 9th International Scientific and Practical Conference «Science, Education, Innovation: Topical Issues and Modern Aspects» (August 26-28, 2023; Tallinn, Estonia) / comp. by LLC SPC «InterConf». Tallinn: Ühingu Teadus juhatus, 2023. P. 115-119 p.

3. Мазанний О.В., Приходько Ю.О., Бирка В.І., Мазанна М.Г. Особливості поширення гельмінтозів овець на сході України. Проблеми зооінженерії та ветеринарної медицини: зб. наукових праць. 2012. Вип. 25, Ч. 2. С. 301–303.

4. Богач М. В., Бондаренко Л. В. Епізоотологія стронгілятозів травного тракту овець і кіз в господарствах Одеської області. Аграрний вісник Причорномор'я: зб. наук. праць. 2017. Вип. 83. С. 17–20.

5. Антигельмінтна ефективність препаратів за трихурозної інвазії у овець / А. Антіпов, В.П. Гончаренко, І.П. Селих та ін. // Scientific Collection «InterConf», (166): with the Proceedings of the 3rd International Scientific and Practical Conference «Science in the Environment of Rapid Changes» (August 16-18, 2023; Brussels, Belgium) / comp. by LLC SPC «InterConf». Brussels: De Boeck, 2023. Pp. 220–227.

6. Мельничук В.В. Епізоотична ситуація щодо нематодозів травного каналу овець в умовах Центрального та Південно-східного регіонів України. Сучасні аспекти лікування і профілактики хвороб тварин. Матеріали IV Всеукраїнської науково-практичної Інтернет-конференції (15–16 жовтня, 2020, м. Полтава). Полтава, 2020. С. 263–265

7. Шеховцов В.С. Система профилактики желудочно-кишечных стронгилятозов овец на Украине: автореф. дис. ... доктора вет. наук: 03.00.20. Москва, 1990. 50 с.

8. Бойко О. О. Гельмінтофауна овець і кіз. Вісник Дніпропетровського університету. Біологія, медицина. 2015. № 6 (2). С. 87-92.

9. Власенко О.А., Стибель В.В. Епізоотологічна ситуація щодо інвазійних захворювань овець у господарствах Сумської області. Науковий вісник ЛНІВМ та БТ ім. С.З. Гжицького. 2012. Т. 14, № 2 (52). С. 44–48.

10. Євстаф'єва В.О., Гришко А.О., Перебийніс О.В. Нематодіроз у складі мікстінвазій травного каналу овець в умовах господарств Полтавської області. Проблеми зооінженерії та ветеринарної медицини: зб. наук. праць. 2016. Вип. 33, Ч. 2. С. 131–134.

11. Мельничук В. В. Морфологічні та метричні особливості нематод Haemonchus contortus (Rudolphi 1803) Cobb 1898, виділених від овець (Ovis aries Linnaeus, 1758). Вісник Полтавської державної аграрної академії. 2018. № 1. С. 126–131. doi: 10.31210/visnyk2018.01.24

12. Галат В.Ф., Євстаф'єва В.О., Галат М.В. Морфологія гельмінтів тварин (атлас). Полтава, 2009. 100 с.

13. Манжос О.Ф. Ветеринарна протозоологія: Навчальний посібник - 2-ге вид., переробл. та допов. / О.Ф.Манжос, І.І.Панікар, А.А. Антіпов, І.В. Пивоварова. Біла Церква: ТОВ „Білоцерківдрук”, 2018. 191 с

14. Лічильна камера для овоскопічних досліджень: патент на корисну модель № 150605, МПК А61Д 99/00 (2022.01) / А.А. Антіпов, С.В. Рубленко, І.В. Сайченко та ін. - заявл. 21.07.2021, опублік. 09.03.2022; Бюл. № 10. 4 с.

15. Рєзников О.Г. Загальні етичні принципи експериментів на тваринах. Ендокринологія. 2003. Т. 8, № 1. С. 142–145.

16. European Convention for the protection of vertebrate animals used for experimental and other scientific purposes / Council of Europe. Strasbourg : Council of Europe, Publications and Documents Division, 1986. 51 p.

№58 2024
International independent scientific journal

ISSN 3547-2340

Frequency: 12 times a year – every month.
The journal is intended for researches, teachers, students and other members of the scientific community. The journal has formed a competent audience that is constantly growing.

All articles are independently reviewed by leading experts, and then a decision is made on publication of articles or the need to revise them considering comments made by reviewers.

***

Editor in chief – Jacob Skovronsky (The Jagiellonian University, Poland)

Częstotliwość: 12 razy w roku – co miesiąc.
Czasopismo skierowane jest do pracowników instytucji naukowo-badawczych, nauczycieli i studentów, zainteresowanych działaczy naukowych. Czasopismo ma wzrastającą kompetentną publiczność.

Artykuły podlegają niezależnym recenzjom z udziałem czołowych ekspertów, na podstawie których podejmowana jest decyzja o publikacji artykułów lub konieczności ich dopracowania z uwzględnieniem uwag recenzentów.

***

Redaktor naczelny – Jacob Skovronsky (Uniwersytet Jagielloński, Poland)

1000 copies
International independent scientific journal
Kazimierza Wielkiego 34, Kraków, Rzeczpospolita Polska, 30-074
email: info@iis-journal.com
site: http://www.iis-journal.com